# EFFECTS OF SEVERING THE CORPUS CALLOSUM ON COHERENT ELECTRICAL AND HEMODYNAMIC INTERHEMISPHERIC OSCILLATIONS INTRINSIC TO FUNCTIONAL BRAIN NETWORKS

A Dissertation
Presented to
The Academic Faculty

By

Matthew Evan Magnuson

In Partial Fulfillment
Of the Requirements for the Degree
Doctor of Philosophy in Biomedical Engineering

Georgia Institute of Technology
and Emory University

May 2013

**Effects of Severing the Corpus Callosum on Coherent Electrical and Hemodynamic Interhemispheric Oscillations Intrinsic to Functional Brain Networks**

Approved by:

Dr. Shella D. Keilholz, Advisor
Department of Biomedical Engineering
*Georgia Institute of Technology and Emory University*

Dr. John Oshinski
Department of Biomedical Engineering
*Georgia Institute of Technology and Emory University*

Dr. Xiaoping Hu
School of Biomedical Engineering
*Georgia Institute of Technology and Emory University*

Dr. Donald Rainnie
Department of Psychiatry and Behavioral Science
*Georgia Institute of Technology and Emory University*

Dr. Dieter Jaeger
Department of Biology
*Emory University*

Date Approved: March 27th, 2013

# ACKOWLEDGEMENTS

Getting a PhD requires years of lab work, years of data processing, years of paper writing, and years of classes; there is no chance that I would have gotten through all of this without a strong support structure. The core of that structure was found at the desks just adjacent to me. Garth Thompson and Waqas Majeed were absolute rocks of friendship and scientific collaboration throughout my time at Emory and Georgia Tech. I cannot thank them enough for the roles they played in my educational process; they will be my friends for life. I would also like to thank Wenju Pan, Jacob Billings, Katie Williams, Mac Merritt, Josh Grooms, and Rae Tang for your friendship, scientific discussions, and material contributions.

Shella Keilholz, my mentor, supported me when I needed support, gave me guidance when I needed guidance, believed in me when I didn't believe in myself, and shaped me into a fine scientist. She was able to keep me motivated, without ever looking over my shoulder. I could not have dreamed up a more perfect advisor; thank you Shella!

I would like to thank my thesis committee (Dieter Jaeger, Donald Rainnie, John Oshinski, and Xiaoping Hu) for their guidance and prodding throughout the process which resulted in a robust body of work that benefitted greatly from their input. I would specifically like to thank Dieter Jaeger for the use of his lab space and equipment. Jeremy Edgerton and Elizabeth Awad from Dieter's lab provided excellent guidance for generalized surgical and electrophysiological methods as well as the subsequent histology. I would also like to thank Tiejun Zhou (MRI scanner training), Steven Harris

(presentation and qualification guidance), and Lei Zhou (fixing my broken stuff) from Xiaoping Hu's lab.

Melike Shaloman pioneered procedures for the rodent callosotomy model and gave me excellent insight for the callosotomy paradigm; thank you Melike for taking the time to answer my questions and for sending me much needed information regarding the procedure. I would also like to thank Sebastien Thomas who provided information regarding his callosotomy surgical plan.

Other friends and colleagues I would like to thank include David Gutman (multiple successful collaborations), Orion Keifer (rodent autopsy, scientific conversation, and collaborations), Lani King, Kirl Staikov, and Christina Nemmeth (each of the final three for their scientific discussions and idea sharing).

The administrators at both Georgia Tech and Emory were amazingly helpful. I would like to thank Shannon Sullivan for pushing me to complete the doctorate despite the difficult road ahead. I would also like to thank Sandra Wilson, Penelope Pollard, Leita Young, and Katrina Gourdet.

Finally, I would like to thank my lovely family who believed in my ability and instilled a strong work ethic since I can remember. I love you mom, dad, Kristen, Laura, and Jagger! I DID IT!

.

# TABLE OF CONENTS

# LIST OF TABLES

# LIST OF FIGURES

# LIST OF SYMBOLS AND ABBREVIATIONS

| | |
|---|---|
| fMRI | Functional magnetic resonance imaging |
| fcMRI | Functional connectivity magnetic resonance imaging |
| rsMRI | Resting state magnetic resonance imaging |
| BOLD | Blood oxygen level dependent |
| CBV | Cerebral blood volume |
| CBF | Cerebral blood flow |
| TR | Repetition time |
| TE | Echo time |
| USPIO | Ultra-small iron oxide particles |
| SEM | Squared error of mean |
| SI | Primary somatosensory cortex |
| SIFL | Primary somatosensory fore-limb |
| SII | Secondary somatosensory cortex |
| CP | Caudate-putamen complex |
| LFF | Low-frequency fluctuation |
| LFP | Local field potential |
| PIC | Phase insensitive coherence |
| ROI | Region of interest |
| ICA | Independent component analysis |
| FIR | Finite impulse response |
| RF | Radio frequency |

| | |
|---|---|
| SAR | Specific absorption rate |
| SNR | Signal to noise ratio |
| FOV | Field of view |
| EPI | Echo planar imaging |
| RARE | Rapid acquisition with relaxation enhancement |
| BLP | Band limited power |
| ECoG | Electrocorticography |

# SUMMARY

Large scale functional brain networks, defined by synchronized spontaneous oscillations between spatially distinct anatomical regions, are essential to brain function and have been implicated in disease states, cognitive capacity, and many sensing and motor processes. The electrical and hemodynamic functional signatures that represent these networks have been well characterized; however, the physiological origins, drivers, and mediators responsible for network behavior remain mysterious. In this work, we sever the corpus callosum in the rodent model, providing a unique platform to determine if structural connectivity (specifically the primary interhemispheric pathway) organizes and influences bilateral neural connectivity, bilateral hemodynamic connectivity, and brain-wide spatiotemporal dynamic activity patterns.

Prior to the callosotomy work, resting state fMRI networks were evaluated using blood oxygen level dependent (BOLD) and cerebral blood volume (CBV) contrast mechanisms to determine if either method offered unique or advantageous functional insights. CBV contrast has indicated increased sensitivity to micro-vascular activity and reduced influences to large draining veins as compared to BOLD in task-based studies, suggesting increased spatial localization of spontaneous low frequency oscillations may be possible using CBV contrast. The fMRI contrast experiments revealed that BOLD and CBV provide highly similar spatial maps of functional connectivity; however, the amplitude of BOLD connectivity was stronger. We also demonstrated that propagating spatiotemporal dynamic waves previously observed only in BOLD data were

reproducible in CBV-weighted imaging. This finding suggests that dynamics are a general hemodynamic phenomenon and not limited to BOLD sensitive contrast.

Due to long surgical periods required for the split brain paradigm, the effects of extended durations of isoflurane and dexmedetomidine on functional network integrity were also evaluated. We found that extended isoflurane anesthetic periods prior to the switch to dexmedetomidine attenuate functional activity for a longer duration as compared to a shorter isoflurane paradigm. We also observed a significant evolution of functional metrics as a result of long durations of dexmedetomidine use under the currently accepted and refined dexmedetomidine sedation paradigm.

A novel tool was developed, building on a on a spatiotemporal pattern finding algorithm previously developed in our lab. One shortcoming of the original spatiotemporal output was its inability to be quantified based on its continuous nature. A statistical threshold generated using a randomization paradigm was applied to the dynamic templates, resulting in only statistically significant voxels that could be counted and otherwise quantified. Interestingly, the dynamic quantitative output shared a linear relationship with traditional seed based functional connectivity.

Taking these previous findings into account, we moved forward with the callosotomy study. There are two primary hypotheses that explain the organization of functional networks: 1.) Bilateral correlation is driven directly by interhemispheric interactions or 2.) Subcortical driving inputs are responsible for the bilateral synchrony. To address the validity of these models, two experimental groups were evaluated, a full callosotomy model in which the corpus callosum was completely sectioned and a sham callosotomy group in which the gray matter was sectioned but the corpus callosum

remained intact. Results indicated a significant reduction in bilateral connectivity in the full callosotomy group as compared to the sham group across all evaluated fMRI seed regions. Similarly electrophysiology revealed significantly reduced bilateral connectivity in delta, theta, low beta, high beta, and gamma band limited power correlation as well as filtered broadband data in the full callosotomy group as compared to the sham group. Spatiotemporal dynamic analysis revealed bilaterally symmetric propagating waves in the sham data, but none were present in the full callosotomy data; however, the emergence of unilateral spatiotemporal patterns became prominent following the callosotomy. This finding suggests that the corpus callosum could be largely responsible for maintaining bilateral network integrity, but non-bilaterally symmetric propagating waves occur after the severance of the corpus callosum, suggesting a possible subcortical driver of the dynamic patterns.

This work represents a robust finding indicating the corpus callosum's influence on maintaining integrity in bilateral functional networks; furthermore, the decrease in functional connectivity amplitude as a result of a full callostomy versus a sham callosotomy is highly similar for fMRI and electrophysiology suggesting the linked nature of these two functional signals.

# CHAPTER 1

# INTRODUCTION

## Functional MRI

In 1990 a Japanese scientist, Seiji Ogawa, introduced the techniques underlying functional magnetic resonance imaging (fMRI) (Ogawa, Lee et al. 1990). fMRI is a functional imaging modality capable of localizing neural activity in the brain with high spatial and temporal resolution. The premise of Ogawa's ingenious work was the ability of the MRI machine, paired with an optimized pulse sequence, to detect small changes in the local levels of blood oxygenation. This change in signal is derived from the intrinsic contrast agent in blood, hemoglobin. Oxygenated hemoglobin is diamagnetic and deoxygenated hemoglobin is paramagnetic. When neural activity occurs, oxygen is consumed from the local blood in surrounding vasculature, and as a compensation for this loss of blood oxygen, the brain routes oxygenated blood to the 'active area' far exceeding the current demand. When diamagnetic oxygenated hemoglobin arrives (specifically when the fraction of oxygenated/deoxygenated hemoglobin increases), magnetic field inhomogeneities are decreased, which leads to a subsequent increase in the measured signal. In fMRI a surrogate signal of neural activity is measured (not a direct measure of neural activity), so it is essential to understand the complex relationship between neural activity and blood oxygen level dependent (BOLD) changes. Ogawa's work opened the proverbial door to a limitless amount of research focused on understanding activity in the

human brain in a non-invasive manner and how this activity relates to brain organization, behavior, genetics, and disease states.

In fMRI, a series of images of the same physical volume are collected over a period of seconds to minutes. Each image represents a snapshot of functional activation occurring within a specific area, manifesting as a change in the signal intensity of a voxel. Functional images are typically acquired in a train using either gradient or spin echo planar image (EPI). Analysis of this train of images allows a clinician to determine the local neuronal activation state over time based on fluctuations in voxel signal intensity. Traditionally fMRI experiments have been conducted utilizing a task-based paradigm where there are periods where task is performed and periods where the subject performs no task. The researcher then compares the two brain states and subsequently determines the amount of 'activity' in response to a given task. These fMRI experiments have been central in mapping the functional architecture of the brain; however, there is abundant functional information to be obtained from the human brain that is not directly related to a task. Other MRI methods have also been used to measure functional activity including cerebral blood volume (CBV) (Zhao, Wang et al. 2005) weighted imaging (increased spatial localization of functional changes, less susceptibility to physiological noise [specifically less single from draining veins that don't necessarily represent local neural activity]) and cerebral blood flow (CBF) (Ostergaard, Weisskoff et al. 1996) weighted imaging (ability to measure blood inflow activity).

The direct relationship between local changes in blood oxygenation and neural activity has been researched extensively. In 2001, Logothetis et al. simultaneously measured local electrical activity using invasive electrodes and the blood oxygen level

dependent (BOLD) signal using MRI in the non-human primate model during visual stimulation (Logothetis, Pauls et al. 2001). This paper garnered the universal acceptance that the signals measured in fMRI are a directly related to neural activity (specifically local field potentials), at least in cases where the input to induce brain activation is carefully controlled. The hemodynamic delay between the onset of neural activity and the peak of the measured BOLD signal was determined to be 4-6 seconds in humans and can be mathematically modeled using the hemodynamic response function (Buxton, Wong et al. 1998). It is often difficult to quantify spontaneous (non-task driven) fluctuations using the BOLD signal because of signal to noise issues. The inability to average multiple repetitions of a functional response because there is no specific time locked stimuli to use as a functional marker also makes it difficult to obtain definitive information regarding spontaneous fluctuations.

**Spontaneous Low Frequency Fluctuations (LFFs) and Functional Connectivity**

In the early days of standard event-related fMRI paradigms, oscillations in the fMRI signal not directly related to the task were disregarded as noise. Cortical low frequency oscillations of < 0.2 Hz were hypothesized to reflect inherent periodic vascular dynamics, breathing/head motion, or some other form of global noise; however, in 1995, Biswal et al. (Biswal, Yetkin et al. 1995) demonstrated that this low frequency "noise" was highly correlated in bilaterally symmetric regions of the previously established motor network. Biswal hypothesized that these synchronous low frequency oscillations were a reflection of coordinated neural activity, termed "functional connectivity", as opposed to simply unimportant physiological noise. This unexpected finding of synchrony in slow

wave oscillations has since been reproduced in several other known networks including the default mode, visual, auditory, memory, and language networks (Belger and Banich 1998; Cordes, Haughton et al. 2000; Raichle, MacLeod et al. 2001; Hampson, Peterson et al. 2002; Fox, Corbetta et al. 2006).

When Biswal first published his work there was some question as to how much physiological noise and inherent vascular dynamics contributed to the coordinated signal. In human fMRI scans, repetition time (TR) values are conventionally around 1-4 seconds allowing for aliasing of the physiological components from breathing and heart rate; both of these sources were suggested as a source of coherent low frequency oscillations. In recent fMRI studies, particularly in animals, high powered, fast switching gradients allow for much shorter (< 500 ms) TRs while maintaining high signal to noise ratios. Shorter TRs allow for sampling of major physiological components and removal during the analysis process. From these studies it was determined that heart rate or breathing rate was not solely responsible for bilateral cortical coherence although both contribute to coherence found between other regions.

Functional connectivity studies are focused on finding areas of the brain with synchronized spontaneous activity. There are several methods commonly used for exploring these functional networks. The simplest and most commonly used technique involves choosing a region of interest in the brain (typically a region known to be involved in a functional network) and obtaining a time course of the activity in that region. The acquired time course is then cross correlated with the time courses of all other voxels in the image. Maps showing the spatial localization of cross correlation are often called functional connectivity maps. These maps show regions of the brain highly

correlated with the "seed" time course can which be used to pinpoint functionally connected brain regions. Higher cross correlation values represent stronger connectivity. Independent component analysis (ICA) is another commonly used functional connectivity analysis technique (Lu, Zuo et al. 2007). ICA separates the complex signal into a number of "independent components" that make up the primary signal. The purpose of this method is to find the independent contributing signals, theoretically suggesting individual neural sources. A shared component spread throughout anatomically distinct brain regions would suggest functional similarity in these regions, possibly representing a functional network. The problem with both seed based analysis and ICA analysis is that they only provide steady-state information, with the assumption that functionally connected areas maintain their connectivity strength over the length of the scan. As it turns out activity within functional networks can vary greatly even within the length of one resting state scan, and that variance can contain highly relevant information to the current functional brain state.

## Spatiotemporal Dynamics

Recently Majeed et al. proposed a method of detecting functionally connected networks based on visual inspection of low frequency power localization over space and time (Majeed, Magnuson et al. 2009; Majeed, Magnuson et al. 2011). Incorporating pattern recognition algorithms allows for the visualization of propagating patterns of spatiotemporal activity that only become apparent using averaging of repeating patterns. This technique provides a unique method of locating spontaneous and coherent events that are simultaneously occurring in the spatial and temporal domain. Majeed's dynamic

technique has since been used in other published work (Magnuson, Majeed et al. 2010). Other recent works have now focused on investigating the dynamic behavior of resting state networks (Chang and Glover 2010; Hutchison, Womelsdorf et al. 2012; Liu and Duyn 2013). The results of these works illustrate the functional connectivity is not only occurring staticly, and it is useful to evaluate the networks from a dynamic perspective.

Using this spatiotemporal dynamic detection method, visualization of both static and dynamic connectivity within the brain is possible. Traditional functional connectivity analysis only allows visualization of networks which maintain strong coherence throughout the duration of the functional scan (6-10 minutes). When brain state changes occur during the scan, the strength of connectivity within functionally connected networks may significantly decrease or even cease to exist; simultaneously another network may significantly increase its strength of connectivity. In the case of static analysis, it is likely that neither of these transient networks would be located.

Brain state changes occur on the order of seconds; static type (region of interest [ROI] and ICA) analysis is unable to distinguish these shorter than scan length state-changes. Furthermore coherence between two regions of the brain may be phase delayed but otherwise coherent. Static analysis would show these two regions as being uncorrelated, when in reality they are highly correlated with a slight phase delay. Spatiotemporal dynamic analysis will allow us to visualize dynamic functional network activation including phase delayed coherent regions allowing us to derive entirely different inferences from the same data sets that were originally analyzed using traditional static analysis techniques.

Using the proposed spatiotemporal dynamic analysis technique will offer researchers a plethora of additional information regarding dynamic events that are not available from static based functional network evaluation. We believe this analysis technique will be vital to understanding the functional significance of coherent neural activity. The long term goal of these findings is to be able to use signatures of resting state functional connectivity data sets for clinical diagnostic and treatment purposes.

## Significance of Low Frequency Fluctuations in the Human Brain

Large scale functional brain networks are defined by synchronous spontaneous oscillations between structurally and functionally connected brain regions. The apparent importance of these brain networks cannot be understated as functional variations in the coordination of these networks have been implicated in countless disease states (Grady, Furey et al. 2001; Lowe, Phillips et al. 2002; Villalobos, Mizuno et al. 2005; Garrity, Pearlson et al. 2007; Greicius, Flores et al. 2007; Liu, Yu et al. 2007); the ability to perform the most common daily tasks including speaking (Tomasi and Volkow 2012), visually perceiving and discriminating our environment (Fairhall, Indovina et al. 2009), or recalling memories and planning (Alnajjar, Yamashita et al. 2013); and recently in defining gradations of cognitive ability in healthy individuals (Weissman, Roberts et al. 2006; Boly, Balteau et al. 2007; Seeley, Menon et al. 2007; Eichele, Debener et al. 2008; Hesselmann, Kell et al. 2008; Kelly, Uddin et al. 2008; Sadaghiani, Hesselmann et al. 2009; van den Heuvel, Stam et al. 2009; Thompson, Magnuson et al. 2012). Scientists have developed a robust picture of the centrality of functional networks as they relate to brain function and the resulting cognitive and behavioral outputs; however, the

underlying physiological components modulating these networks remain largely undetermined.

While functional connectivity analysis is not currently approved as a diagnostic tool, alteration in coherence occurs in the measured FC signal as a function of the progression of certain neuro-degenerative diseases. Researchers have observed altered functional connectivity in patients with Alzheimer's disease, multiple sclerosis, schizophrenia, depression, Parkinson's disease, attention deficit hyperactivity disorder, epilepsy and blindness (Grady, Furey et al. 2001; Lowe, Phillips et al. 2002; Garrity, Pearlson et al. 2007; Greicius, Flores et al. 2007; Liu, Yu et al. 2007).

Most of the energy used by the human brain is consumed when the brain is not performing any specific task (Raichle and Mintun 2006), in a brain state termed the "resting state" mode. Spontaneous low frequency fluctuations are responsible for consuming a large portion of this energy. Although it is not yet clear what the functional purpose of these spontaneous oscillations are, but we can infer from the coordinated nature of the fluctuations and the general efficiency of the brain that it is a necessary process. LFFs have been implicated as playing a critical role in sensory perception, motor integration (Huber, Tian et al. 2008), and memory consolidation during sleep (Haider and McCormick 2009). Other studies insist that this slow-wave activity reflects processing within local circuits and the subsequent "broadcasting" to bilaterally symmetric brain regions (Mohajerani, McVea et al. 2010).

While researchers have a basic understanding of the physiological implications of hemodynamic functional connectivity, a direct relationship between the neural signals

and the physiological underpinnings has not been established. In order for functional connectivity to have relevance as a diagnostic tool, we must first determine the nodes, sources, and mediators responsible for driving functional connectivity, and we also must further explore the functional purpose of coherent activity.

In order to understand the relationship between fMRI LFFs and neural activity, a series of studies have been conducted in animal models that combine fMRI and electrophysiology (He, Snyder et al. 2008; Nir, Mukamel et al. 2008; Shmuel and Leopold 2008). Low frequency oscillations in the fMRI signal have been shown to be highly correlated with low frequency fluctuations of power within the gamma band (40 - 80 Hz) of local field potential (LFP) activity from one electrode (Shmuel and Leopold 2008). This work provides a further understanding of the relationship between hemodynamic and electrical activity but the findings do not provide any insight into to the physiological origin of functional connectivity. LFPs are typically measured by inserting needle electrodes directly into the extracellular matrix of regions of interest in the brain. Further details of electrophysiological recordings will be discussed in the next major section.

Work in our lab suggests that coherence in low frequency oscillations of the gamma band power from electrodes placed in bilaterally symmetric areas of a functional network correlates with a decrease in the functional coherence of low frequency BOLD data as a function of anesthetic depth (Pan, Thompson et al. 2011). An increase of coherence in low frequency power oscillations of theta and delta band electrophysiological activity correlates with increase low frequency BOLD coherence. One hypothesis from our lab suggests that low frequency fluctuations of electrical and

hemodynamic activity are driven by a subcortical source, are largely mediated by intra- and inter-hemispheric cortical components and result in the modulation of low frequency gamma power oscillations. There is much work to be done in order to fully understand the complex relationship between spontaneous neural activity, neural coordination, brain condition, and the hemodynamic response.

The most advantageous model for studying this relationship exists in the rat model. Human subjects exhibit variability in amplitude measures of functional connectivity on different scan dates. This variability is likely due to inherent differences in the individual's neural activity, neurovascular coupling, and general brain activity which can be influenced by chemicals (caffeine, cocaine), stress, and even oxygenation levels (Biswal, Hudetz et al. 1997; Li, Biswal et al. 2000). Lab rodents on the other hand are genetically identical, do not ingest stimulants, and are largely exposed to an identical environment day after day. Animal models also allow for invasive recording resulting in highly specific neural information that cannot be obtained from analogous non-invasive experiments in humans. Finally functional network studies in humans often probe aberrant networks, as a means to understand network structure, in patients with clinical abnormalities such as callosal agenesis, Alzheimer's, epilepsy, or depression. In each of these cases abnormal networks exist prior to network evaluation which makes it difficult to draw conclusions regarding functional changes.

## Generalized fMRI Methods

The experiments in the following chapters each contain an fMRI recording paradigm; however, slightly different parameters are used for each experiment. Here we will briefly discuss imaging procedures and preprocessing. Specific methods will be discussed in the relevant chapters for each experiment.

All images are collected on a 9.4 Tesla / 20cm bore Bruker Biospec MRI machine (Bruker, Billerica, MA). This machine is interfaced with an AVANCE console (Bruker, Billerica, MA) that runs ParaVision software (Bruker, Billerica, MA). The magnet is equipped with an actively shielded gradient coil that creates a known magnetic strength modulation across the primary magnetic field, allowing for spatial localization of recorded signals. These gradients are capable of producing a 20 gauss/cm field strength with a rise time of 120μs. A two-coil actively decoupled imaging setup was used. A 7 cm diameter volume coil was used to transmit a radio frequency (RF) pulse into the imaged object to excite the protons such that they are no longer aligned with the primary magnetic field; a 2 cm surface coil was used to receive the signal generated from the protons returning to alignment with the primary magnetic field.

When the animal or imaged object is introduced into the scanner, the local magnetic field is slightly disturbed. This disturbance must be accounted for to ensure maximal signal to noise ratio (SNR) in the resulting images; in order to alleviate this problem local shims are modulated from the console to create the most homogenous field possible considering the presence of the imaged object. A FASTMAP (Bruker, Billerica, MA) sequence is used to automatically perform this shimming function typically over a 6 x 6 x 6 mm region in the central portion of the imaged object.

Resting state scans are commonly performed in this thesis work and are made of a series of functional images that are sensitive to changes in local blood oxygenation. A single 2mm thick coronal imaging slice is collected with a 2.56 x 2.56cm field of view (FOV) and a 64x64 voxel matrix representation resulting in 400μM spatial resolution. These scans last approximately 8 minutes and are acquired using a gradient echo planar imaging (EPI) sequence. 1000-1200 volume acquisitions are performed with 300 – 500ms between images; the time between scans is known as the repetition time (TR). An echo time (TE) of 15ms is used for all resting state scans in this work which represents the time of data acquisition following the initial RF excitation.

Once the resting state data set is collected, data must be preprocessed before further analysis is performed. MATLAB (MathWorks, Natick, MA) is the programming tool used for all data processing. First all voxel timecourses are demeaned (the mean value of a timecourse is subtracted from all time points, creating a signal oscillating around zero on the y-axis. Positive amplitudes represent an over average activity state while negative amplitudes will represent a less than average activity state. Trends are often found in functional timecourses which represent general scanner instabilities or other non-functionally relevant oscillations of very low frequency (<0.01 Hz). These trends are removed by performing quadratic detrending which removes the aberrant drifts. Following detrending, data is normalized between zero and one by subtracting the minimum value from all data point and dividing by the maximum value in a timecourse. Variations in amplitude of the functional signal are then expressed as percent change from the mean. Following these steps, comparisons can be made between voxels and between subjects.

An additional preprocessing step is necessary for evaluating functional networks. These networks organize in the low frequency range (~0.01 Hz – 0.3 Hz). All voxel timecouses are filtered into this frequency range using a finite impulse response filter with a 100 second window length (1 / minimum evaluated frequency). Data was once again normalized following filtering to remove any additional anomalies attributed filtering. Calculations of functionally relevant information and network activity can now be performed on this preprocessed data.

**Corpus Callosum and Resting State Functional Connectivity**

The corpus callosum has been implicated as a primary mediator of bilateral functionally coherent networks (Nielsen, Montplaisir et al. 1993). Studying the role of the corpus callosum in interhemispheric coherence has been partially investigated, but conclusive findings on the corpus callosum's role in mediating functional connectivity have not been determined. From previous work we expect that the corpus callosum plays a significant role in mediating the interhemispheric coherence of the fMRI and electrophysiological signal as it is the primary interhemispheric neural connection (Nielsen, Montplaisir et al. 1993; Corsi-Cabrera, Trias et al. 1995). Further studying the role of the corpus callosum could provide several important pieces of additional information. 1) Does the corpus callosum mediate electrophysiological and fMRI functional connectivity? 2) Does the corpus callosum similarly influence the electrical and hemodynamic coherence (provides additional information about the coupling of the two signals)? 3) Is the corpus callosum responsible for 'driving' bilaterally symmetric

waves of activity, does it serve to maintain bilateral coherence of the waves, or do the waves cease to exist following callosal sectioning?

Studies focused on the role of the corpus callosum in mediating bilateral functional coherence have produced many conflicting and inconclusive results. Interhemispheric EEG coherence was shown to decrease with increased agenesis of the corpus callosum; however, intra-hemispheric coherence was not altered (Nielsen, Montplaisir et al. 1993). A study by Corsi and Cabrera determined that interhemispheric coherence was unaffected by a lesion of the corpus callosum (only one human patient with untreatable epilepsy) (Corsi-Cabrera, Trias et al. 1995). Similarly, in animal studies of surgically callostomized cats, results have not been conclusive; two groups reported no change in interhemispheric coherence after a full surgical callosotomy while two other groups performing a similar experiment concluded there was a slight decrease in EEG coherence after callosotomy (Leocani and Comi 1999). A more recent study on the role of the corpus callosum was conducted on a 6 year old girl with intractable epilepsy (Johnston, Vaishnavi et al. 2008). Johnston et al. used resting state fMRI to investigate changes in functional connectivity before and after complete severing of the corpus callosum. fMRI scans conducted before and after a complete section of the corpus callosum resulted in a "striking loss" of interhemispheric low frequency BOLD correlations. A limitation of this study is that the results are based on data from only one patient.

In 2010 Mohajerani et al. published a paper imaging normal and acallosal mice using voltage sensitive dyes (VSDs) (Mohajerani, McVea et al. 2010). Spontaneous activity was less synchronized in the acallosal mice as compared to normal mice although

the composition of the frequency distribution of the raw signals was not altered. Some synchrony was maintained, and the authors suggested that subcortical bi-hemispheric structures (thalamus and hippocampus) are responsible for the remaining correlation. The results obtained from the acallosal mice may be different than those taken from an acute sectioning of the callosum; these mice have had to adapt to life without a corpus callosum which likely led to plastic brain changes.

Further evidence of the corpus callosum's likely role in functional network integrity lie in the interrelationship between structural connectivity and functional connectivity (Honey, Sporns et al. 2009); however, it has also been revealed that direct structural connectivity was not necessary for strong functional connectivity to exist (Damoiseaux and Greicius 2009; Honey, Sporns et al. 2009). While the neuroanatomical framework provides the platform on which functional networks are activated, networks are highly adaptive within that substrate to respond to the brain's current processing needs. While structural connectivity plays a central role in functional connectivity it is not the only source driving these networks.

There is a substantial body of work evaluating the role of the corpus callosum in modulating functionally connected networks; however, all of these studies have been performed in human patients with epilepsy (Montplaisir, Nielsen et al. 1990; Corsi-Cabrera, Trias et al. 1995; Brazdil, Brichta et al. 1997; Corsi-Cabrera, Ondarza et al. 2006; Johnston, Vaishnavi et al. 2008; Uddin, Mooshagian et al. 2008; Pizoli, Shah et al. 2011). Functional network integrity is disrupted after a callostomy in some patients while surprisingly increasing functional network integrity in other patients; obtaining a consistent result regarding the influence of the corpus callosum has been elusive. Several

factors may contribute to these non-uniform findings. Callosal surgical parameters are specific to the patients and their conditions effectively resulting in a non-homogenous model. Pre-surgical networks in patients are highly variable and dependent on the severity, classification, and locus of the epileptic seizures. Many patients take drugs that effectively altering functional brain activity prior to and post callosotomy, and similarly anesthesia was used during the imaging/scanning protocols in several of the patients which likely affect functional brain networks. The timing of functional evaluation in these patient models was highly variable, occurring within hours of the surgery or up to decades follow surgery, functional restructuring is highly likely in the latter case. Finally many of these studies only evaluated a single patient and anomalies are possible.

Based on the inhomogeneity of the human subjects, there is a clear need for a controlled, reproducible study of functional connectivity in a population of split-brain animal models. While confounding variables are highly reduced in the current work using the rodent model; the paradigm is not without constraints. While care was taken to avoid large vessels, vascular damage was inevitable as a result of the callosotomy procedure; however, the sham callosotomy group was subject to identical vascular influences which would preserve the integrity of remaining variability between the final connectivity values found in the groups.

While several researchers have investigated the role of the corpus callosum in functional networks; the results have been highly inconclusive with some studies suggesting that the corpus callosum is vital in mediating BOLD functional coherence (Montplaisir, Nielsen et al. 1990; Johnston, Vaishnavi et al. 2008) while other groups say that severing of the corpus callosum does not influence functional coherence (Corsi-

Cabrera, Trias et al. 1995; Pizoli, Shah et al. 2011). In each of the previous studies there have been inconsistencies in the acquired data and acquisition methods, which we largely remedied with this thesis work. We collected BOLD fMRI data and electrophysiological data from a homogenous group of experimental rats and confirmed the findings using careful controls. The methods used to analyze the data included spatiotemporal analysis which we believe provided insight into the functional origin of spontaneous coherent activity. It is possible that while functional coherence is decreased after a callosotomy, relationships still exists between functionally connected regions of the left and right hemispheres; however the phase locked synchrony will be lost.

## Electrophysiology

Our lab is pioneering work focused on recording spontaneous BOLD activity during rest using MRI while simultaneously using electrophysiology to directly measure neural activity in areas of interest. This work will partially focus on determining the relationship between the two signals. Electrophysiology is the measurement of electrical activity originating from cells. For the purpose of the thesis work presented here, we recorded current derived from neurons using electrodes inserted directly into brain regions of interest. Spiking activity and local field potentials (LFPs) generated by the combined activity of many neurons near the tip of the electrode placed in the primary somatosensory cortex were obtained. Multi-unit activity (MUA) is a measurement of the spiking activity of a group of neurons in a given cortical region and reflects the output activity from a cortical region. LFPs are a measurement of the local electrical environment which is influenced by synaptic transmission and inward and outward

currents of the action potential; this measurement is thought to reflect the synchronized input into the region. LFPs are recorded using low impedance electrodes positioned in extracellular brain tissue.

Papers published in the last ten years have focused on combining electrophysiological recording and fMRI recordings in hopes of identifying the neural origin of fMRI signals. Initially simultaneous electrophysiology and fMRI focused on determining the electrical response and the resulting hemodynamic response due to a known input stimulus (Logothetis, Pauls et al. 2001). This work successfully determined the relationship between the electrical activity and resulting hemodynamic activity in response to a stimulus. Logothetis concluded that the LFP and MUA signals were both correlated to the fMRI response, but the LFP was a more accurate predictor of the subsequent response. This finding is consistent with the known bioenergetics underlying the fMRI signal, LFPs account for the consumption of local energy metabolism and energy metabolism is tightly coupled with neural activity (Logothetis, Pauls et al. 2001).

Understanding the relationship between the global fMRI LFFs and the underlying neural activity is understandably more complex than measuring the fMRI and neural activity in response to a stimulus. Instead of focusing on a specific area of the brain which is known to be activated in response to a stimulus, information must be obtained from the entire brain with no known driving source or physiological basis. Early work attempting to understand connectivity in the brain focused primarily measuring coordinated electrical activity using either EEG or inserted electrodes. In 1999 Leocani et al. explored the relationship between coherence in the low frequency EEG activity and pathological conditions (Leocani and Comi 1999). Decreased coherence proved to be a

useful indicator of damaged, disrupted, or deteriorated structural connections in the brain as a result of disease. While this study made it clear that functional networks can be disturbed, the functional significance of this altered activity remained elusive. In another attempt to understand the basis of this neural coherence a 2008 paper by Nir et al. simultaneously combined EEG recordings with local field potential recordings in the human sensory cortex (Nir, Mukamel et al. 2008). Nir's work concluded that spontaneous modulations in the neural firing rate and power modulations in broad band (40 Hz – 100 Hz) gamma LFP power were the most likely correlated to low frequency spontaneous fMRI fluctuations.

The problem with studying only electrical activity is that it is not easily translatable to clinically relevant studies. For diagnostic purposes, fMRI scans are useful because they provide full brain coverage with high spatial resolution and full brain coverage with minimal invasiveness. While EEG data is useful, the data obtained only contains information from the superficial layers of brain, and the information is relatively noisy and has poor spatial resolution. Deep brain electrophysiological recordings have poor spatial coverage and are almost never done in healthy humans due to their invasive nature. An understanding of how the coherent electrical data relates to the coherent slow wave fMRI data is essential.

More recently research groups have explored the underlying electrophysiological basis of functional connectivity in the brain by simultaneously combining resting state fMRI and electrophysiological recording. This research is vital, because it provides a direct link between spontaneous neural activity and a surrogate response, BOLD activity, which provides potential answers two key pieces to the puzzle that is functional

connectivity. 1) What is the neural correlate of low frequency coherent BOLD activity? 2) What is the relationship between the non-invasively measured 'surrogate' of neural activity (BOLD) and direct, invasively measured neural activity.

In order to address the first question posed above, Shmuel and Leopold recorded electrical activity in the monkey's visual cortex while simultaneously obtaining high resolution gradient echo BOLD scans (Shmuel and Leopold 2008). A direct comparison is conducted between the temporal and spatial dynamics of oscillations in BOLD and electrophysiological data. Shmuel determined that the low frequency spontaneous fMRI signal was tightly correlated with gamma band power modulation recorded from one region of the cortex at a time lag of 6 second. Interestingly the 6 second time needed for the highest correlation between electrophysiological gamma power oscillations and the fMRI signal is similar to the traditionally accepted hemodynamic delay reported previously by Logothetis (Logothetis, Pauls et al. 2001). While LF BOLD activity may be correlated with low frequency power oscillations in gamma band electrical activity it is not yet clear whether the neural activity is 'driving' the hemodynamic oscillations or if they are both driven by some other source.

He et al. sequentially recorded electrocorticography (ECoG) data and BOLD fMRI data in humans (He, Snyder et al. 2008). Electrocorticography (electrodes placed directly on the exposed brain) data was collected from bilateral sensorimotor areas; correlation values were calculated between low frequency (<0.5 Hz) timecourses generated from these two electrodes. Correlation values were also obtained from bilateral sensorimotor low frequency BOLD fMRI data. Values obtained from the ECoG data were plotted versus fMRI correlation data. This process was repeated for data obtained

during awake periods, slow-wave sleep, and rapid-eye-movement (REM) sleep. Highly significant correlations were found between the ECoG and fcMRI data across all three arousal state demonstrating the tight correspondence between these two signals. Similar to previous studies, He's work suggests that spontaneous slow wave cortical potential and low frequency BOLD signal fluctuations most likely reflect endogenous fluctuations of cortical excitability within functional relevant systems.

A 2010 paper by Schölvinck et al. expanded on this work (Scholvinck, Maier et al. 2010). She determined that modulations in the gamma band electrophysiological activity measured from a single cortical site in the monkey brain exhibit positive correlation with 6s – 8s lagged fMRI LFFs over the entire brain. Coherence measures in the fMRI LFFs (<0.1 Hz) and low frequency power modulations in the gamma band were similarly influenced based on the monkey's behavioral state further suggesting a tight coupling of fMRI LFFs and neural activity.

While these combination electrophysiology/functional connectivity MRI (fcMRI) studies provide vital insight into the neural correlates of BOLD functional connectivity, we are a long way from truly understanding complex functional networks. In this work we focused on elucidating possible mediators of coherent spontaneous BOLD activity. The corpus callosum serves as the primary anatomical connection between the brain's hemispheres, and disturbing this primary interhemispheric connection should disturb normal function. This model will provide a unique evaluation of the existence of coherence and general low frequency spontaneous oscillations and the role of the corpus callosum in mediating this activity.

## Use of Animal Models

Animals have become the go to model when probing the origins of functional connectivity. Functional networks that are very similar to those found in humans have been observed in rats and monkeys (Vincent, Patel et al. 2007; Pawela, Biswal et al. 2008; Williams, Magnuson et al. 2010). The rat model is ideal for fMRI functional connectivity scans for several reasons:

1) One major problem with human subjects is the lack of consistency between data obtained from one subject on multiple scan days. There are even greater inconsistencies in the data collected between patients (Xiong, Rao et al. 2000). Human brain anatomy is highly variable between human subjects; this makes ROI type analysis and functional region comparisons very difficult (Brett, Johnsrude et al. 2002). This data variability problem is ameliorated using rats that are bred to be consistently genetically identical.

2) Because less stringent guidelines are placed on the gradient strength, primary magnetic field, and the amount of radio frequency (RF) a patient experiences (Specific absorption rate [SAR] limits) in animal scans as compared to human scans (Carmichael, Thornton et al. 2010), high field scanners (7T – 16T) with ultra-fast gradient sets are often used for animals. In the rodent model, our lab use a 9.4 T scanner (Bruker, Biosepec) to obtain fMRI images with spatial resolution of 200 μM in plane and temporal resolution of 100 ms. The high temporal resolution allows us to sample physiological noise and remove the contributing components, while the high spatial resolution compensates for the much smaller rodent brain as compared to human brain.

3) Rodents and humans are ~ 90% genetically similar, but more importantly for our research, functional connectivity studies conducted in rodents have resulted in similar functional networks, spatiotemporal patterns, and connectivity strengths as found in humans (Majeed, Magnuson et al. 2009; Williams, Magnuson et al. 2010).

4) The ability to perform invasive procedures in rats that cannot be performed in humans provides the necessary motivation for using the rodent model. Surgical lesions, deep brain electrophysiological recording, chronically implanted electrodes, long scans, and histology are all procedures that can be performed in rats but not in humans. Each of these invasive procedures was necessary for my thesis work, and could be a critical tool for understanding the functional basis and the mechanisms underlying coherent LFFs in the brain.

Lesioning of anatomical connections in a known functional network are only performed in humans in rare circumstances where it is necessary for disease treatment purposes. Humans with severe epilepsy sometimes undergo callosotomies as a treatment (Kim, Wang et al. 2008); however, it is difficult to find patients in this condition receiving this particular treatment that is willing to undergo research related scans before and after their procedure while dealing with a life threatening condition. Furthermore a patient with chronic seizures could hardly be considered a "normal" subject prior to the callosotomy, and it is unclear how the underlying disease would influence connectivity. In the rodent we will begin collecting data on a healthy animal, we will then sever a connection known to be central to functional connectivity, and we will collect data from this specific model. Simultaneously we can record the non-invasive fMRI signal and the functional origin of this signal, neural activity, and then compare the information.

# CHAPTER 2

# FCMRI CONTRAST MODALITIES: BOLD VS. CBV

In this chapter we explore functional insights obtained from BOLD and CBV resting state functional connectivity by evaluating the similarities in seed based functional connectivity maps, spectral information, and resulting spatiotemporal dynamic templates. We will use information garnered from the work in this chapter to determine which fMRI contrast would be ideal for the split-brain callosotomy experiment that will be the central focus of this work. The results of this chapter are also independently significant to the fMRI research field as they elucidate the physiological origins of spontaneous fluctuations by evaluating a more spatially sensitive contrast mechanism and comparing the findings to standard BOLD contrast. Much of the content in this chapter comes from my work presented in journal of Magnetic Resonance Imaging in 2010 (Magnuson, Majeed et al. 2010).

Clinical interest in mapping functional connectivity with MRI continues to grow as the technique has demonstrated the ability to detect alterations in patients with disorders such as Alzheimer's (Wang, Liang et al. 2007), schizophrenia (Hoptman, D'Angelo et al. 2010), and depression (Cullen, Gee et al. 2009). Despite this promising evidence of sensitivity to clinically relevant changes, the interpretation of functional connectivity data remains limited by our incomplete understanding of the interactions between the local changes in neural activity, metabolism, and hemodynamics that lead to the low frequency BOLD fluctuations.

To elucidate the origins of functional connectivity, several groups have turned to animal models (Lu, Scholl et al. 2007; Pawela, Biswal et al. 2008; Shmuel and Leopold 2008; Zhao, Zhao et al. 2008; Williams, Magnuson et al. 2010). Their work has demonstrated that functional connectivity similar to that observed in awake humans can be detected in other species such as rodents, even though anesthesia is typically required to facilitate imaging. These animal models provide a platform for investigations of the relationship between spontaneous neural activity, local metabolic changes, variations in blood flow, and MRI signal fluctuations (Logothetis, Pauls et al. 2001; Shmuel A 2007). The rodent brain in particular has been well-characterized by neuroscientists through electrophysiological recordings, selective lesioning, and behavioral studies, providing an extensive framework for the design and interpretation of functional connectivity experiments. Rodent models also offer the advantage of high inter-subject homogeneity, and the use of high-field dedicated small animal MRI systems provides excellent spatial and temporal resolution.

In humans, functional connectivity studies are performed almost exclusively with BOLD contrast (Biswal, Yetkin et al. 1995; Lowe, Mock et al. 1998; Cordes, Haughton et al. 2000; Hampson, Peterson et al. 2002). In animal models, however, both BOLD and cerebral blood volume (CBV) weighting have been used to map correlated signal fluctuations (Lu, Scholl et al. 2007; Zhao, Zhao et al. 2008; Williams, Magnuson et al. 2010), raising the issue of whether BOLD and CBV-weighted studies supply comparable measurements of functional connectivity. The BOLD signal comprises a complicated combination of several hemodynamic and metabolic properties including CBV, cerebral blood flow (CBF), and the local rate of oxygen consumption (CMRO2). It is not yet

clear if spontaneous fluctuations in each of these parameters are equally linked to spontaneous fluctuations in neural activity. For example, 0.1 Hz oscillations in CBF and CBV have been observed with multiple modalities and are often attributed to vasomotion, and some studies have not found a clear link between these oscillations and electrical activity (Golanov, Yamamoto et al. 1994; Mayhew, Askew et al. 1996; Vern, Leheta et al. 1997). By measuring hemodynamic parameters that contribute to the BOLD signal, such as CBV, it may be possible to determine if particular contrasts were more closely related to neural activity than others.

Previous work with stimulus-induced activation suggests that CBV-weighted imaging may offer enhanced sensitivity and increased functional localization compared to BOLD (van Bruggen, Busch et al. 1998; Mandeville and Marota 1999), partially due to reduced contributions from large vessels. It is possible that this same property will improve localization in functional connectivity studies. In this study, BOLD and CBV-weighted data were acquired sequentially from the same rat to determine the relative sensitivity and specificity of the two techniques.

In addition to examining the steady-state characteristics of the BOLD and CBV functional connectivity maps, this study also compares the spatiotemporal dynamics of the signal fluctuations. Functional connectivity scans are conventionally analyzed using seed region-based cross-correlation techniques (Biswal, Yetkin et al. 1995; Lowe, Mock et al. 1998; Xiong, Parsons et al. 1999; Cordes, Haughton et al. 2000); however, a recent article by Majeed et al. (Majeed, Magnuson et al. 2009) describes a method for visualizing the spatiotemporal dynamics of the low frequency fluctuations. The data presented by Majeed et al. challenges standard interpretations of functional connectivity

maps acquired in the anesthetized rodent, as waves of BOLD signal propagate along the cortex, connecting areas that exhibit little correlation in their time courses.

Dynamic spatiotemporal analysis of resting state functional connectivity (RSFC) scans has only been conducted using the BOLD signal to date. At short TRs, the BOLD signal is heavily weighted toward CBF due to inflow effects, which could be partially responsible for the spatiotemporal dynamics observed in Majeed's work (Majeed, Magnuson et al. 2009). CBV-weighted imaging, using ultra-small paramagnetic iron oxide (USPIO) particles to provide contrast, is not typically susceptible to inflow effects because the signal from the blood is diminished due to the presence of iron oxide, so the presence of propagating waves in the CBV-weighted signal would suggest that they are not primarily due to inflow effects.

The purpose of this study is twofold; first, to determine whether measurements of BOLD and CBV RSFC provide comparable information for functional connectivity mapping and second, to provide insight into the relative contribution of CBV information to the BOLD signal. BOLD and CBV-weighted data from the same rats were examined using spectral analysis, traditional cross correlation analysis, and dynamic spatiotemporal visualization. The results of this study show that BOLD and CBV provide similar maps of functional connectivity and demonstrate that the propagating waves previously observed in the BOLD signal can be detected with CBV-weighted imaging, suggesting that these dynamics are a general hemodynamic phenomenon widely observed in anesthetized rodents.

## Materials and Methods

### Animal Preparation and Monitoring

All experiments were performed in compliance with guidelines set by the Institutional Animal Care and Use Committee (IACUC) at Emory University. Ten male Sprague-Dawley rats weighing 200-300g were initially anesthetized with 2.5% isoflurane (mixed with 1:1 oxygen and room air) and maintained at 1.5% isoflurane throughout the experimental setup. Heart rate and blood oxygen saturation were recorded with a pulse oximeter placed on the hind paw. Body temperature was monitored with a rectal thermometer and maintained at 36º C - 38º C using an adjustable temperature water circulating pad. The respiratory rate was monitored using a pressure sensitive balloon placed under the rat's chest. To provide forepaw stimulation for activation studies, two needle electrodes were inserted underneath the skin of the rat's left forepaw between digits 2 and 3 and digits 3 and 4. The rat's tail vein was catheterized to allow for injection of iron oxide contrast agent later in the experiment. Finally the rat was placed in the MRI cradle and the head was secured with a bite bar and ear bars.

Once experimental setup was complete, the rat was given a subcutaneous bolus injection of 0.05 mg/kg medetomidine (Domitor, Pfizer, Karlsruhe, Germany). Three minutes after the medetomidine bolus, isoflurane was discontinued. Fifteen minutes post bolus, subcutaneous infusion of 0.1 mg/kg/hr medetomidine was initiated to maintain anesthetic depth for the duration of the experiment (Weber, Ramos-Cabrer et al. 2006).

**fMRI**

Images were acquired on a 9.4 T / 20 cm horizontal bore Bruker BioSpec magnet interfaced with an AVANCE (Bruker, Billerica, MA) console. The magnet was equipped with an actively shielded gradient coil capable of producing a maximum gradient strength of 20 G/cm with a rise time of 120μs. A two-coil actively decoupled imaging setup was used (2cm surface coil for reception and 7 cm diameter volume coil for transmission; Bruker, Billerica, MA) to achieve maximal signal to noise ratio (SNR) over the cortical areas of interest. Shimming, to obtain homogeneity in the local magnetic field, was initially performed on a 6 mm x 6 mm x 6 mm region visually centered over the primary somatosensory cortex using FASTMAP (Gruetter 1993). A single-shot, multi-slice gradient echo planar imaging (EPI) sequence (TR=1500ms, echo time [TE] = 15ms, field of view [FOV] = 2.56 cm x 2.56 cm, matrix size = 64 x 64, slice thickness = 2 mm, effective bandwidth = 200kHz, flip angle = 31º) was used to acquire a time series of 180 BOLD weighted images for the duration of a forepaw stimulation paradigm (A.M.P.I. Master-8 Stimulator; 4mA, 0.3ms duration, 9 Hz; 30 imaging volumes off - 20 on - 30 off - 20 on - 30 off - 20 on - 30 off).

Activated voxels in the primary somatosensory cortex were identified using STIMULATE (Strupp 1996) which correlates the timecourses of voxels in the acquired image set with a box car function representing on and off times for stimulation. Following the forepaw stimulation scan, a BOLD weighted dataset was acquired without stimulation with the following parameters: TR = 300ms, TE = 15ms, number of repetitions = 1200, FOV = 2.56 cm x 2.56 cm, matrix size = 64 x 64, slice thickness = 2mm, 1 slice centered over the forepaw regions of the primary somatosensory cortex

(located using data from the preceding stimulation scan). Manual shimming was then performed on the single slice to remove any local field inhomogeneities. The same imaging setup was repeated two more times to obtain a total of three sets of BOLD weighted image series. After BOLD scans, 2% isoflurane was administered to further sedate the rat to allow for tail vein infusion of 5 mg/kg of USPIO particles (Molday Ions, BioPal, Worcester, MA) over a period of ~1 minute. Isoflurane was discontinued after USPIO infusion was completed. Thirty minutes after USPIO injection, three sets (1 stimulation scan and 1 resting state scan) of images were acquired with identical parameters to the resting state BOLD images but with cerebral blood volume (CBV) weighting due to USPIO particles.

**Preprocessing**

All data processing was performed using MATLAB (MathWorks, Natick, MA). Each time course used for analysis was de-meaned (mean value of timecourse subtracted from each data point), quadratically detrended (removing baseline drifts in the signal), and normalized by converting the data to percentage difference relative to mean voxel intensity. Image signal to noise ratio (mean brain signal / standard deviation of the background noise), temporal variation (variance of demeaned and detrended timecourse from the primary somatosensory cortex [SI]), and activation percent changes were calculated for the CBV and BOLD data sets. The primary somatosensory cortex was localized by cross-correlating time courses from the forepaw stimulation scan with a box car reference function representing stimulus on and off times. A seed region for cross correlation analysis of the resting state data was constructed from the nine voxels which were most highly correlated with the stimulus reference function.

**Connectivity Analysis**

Additional 3x3 voxel ROIs were selected based on anatomy in the secondary somatosensory cortex (SII) and the caudate/putamen (CP) complex directly from the EPI images (no visible distortion was apparent in the EPI images which would negatively affect the manual selection of ROIs; Figure 2 contains the actual EPI images with locations of seed ROIs) for further cross-correlation analysis (ROIs were chosen in accordance with the Paxinos and Watson rat brain anatomical atlas (Paxinos G 2005)). A 6x6 average correlation matrix representing data from all rats was calculated from the average time courses from six seed regions (left and right SI, SII, and CP) in order to visualize the strength of connectivity between the regions.

**Spectral Information**

Power spectra were obtained for the time courses of selected ROIs by using the Welch method (8 sections with 50% overlap, Hamming window). Visual inspection of the power spectra revealed that peak power was shifted to higher frequencies for CBV data as compared to BOLD. Time courses were bandpass filtered based on initial inspection of the power spectra using a $3^{rd}$ order butterworth filter to retain contributions from a 0.2 Hz frequency window (0.05 Hz-0.25 Hz for BOLD, 0.1 Hz-0.3 Hz for CBV). The window was shifted higher by 0.05 Hz for CBV data to prevent attenuation of the peak typically seen at 0.2 Hz. Nine voxels in SI activated by forepaw stimulation were used as the seed region for cross-correlation analysis of resting state data. The average time course representing the voxels in the selected ROI was correlated with the time course from voxels throughout the image and a correlation map was obtained.

### Spatiotemporal Dynamics

Spatiotemporal dynamics of the low frequency signal fluctuations were analyzed using image by image visualization of data normalized and filtered to contain only low frequencies (Majeed, Magnuson et al. 2009). The resulting images were displayed as a movie in order to locate visually detectable spatiotemporal patterns or events. If spatiotemporal patterns in the BOLD and CBV signals contain similar time and spatial signatures this would suggest that the BOLD and CBV MRI signals are affected similarly by coordinated neural activity.

## Results

### SNR, Temporal Variance, and Signal Change During Stimulation

SNR, temporal variance, and average percent change in signal during stimulation were calculated for CBV and BOLD (Table I). The use of USPIOs to create CBV contrast leads to dose dependent (USPIO dose) decreases in image signal-to-noise ratio and a dose dependent increase in the absolute value of the signal percent change during activation (Lu, Scholl et al. 2007). As expected in this study SNR decreased significantly with the addition of USPIOs ($p<0.01$). The absolute value of the average percent change during stimulation was found to be significantly greater for BOLD as compared to CBV ($p<0.01$). The average temporal variance for time courses representing spontaneous activity in SI was similar for CBV and BOLD ($p = 0.36$); however the difference in temporal variance between CBV and BOLD was significant in the SII and CP regions ($p <0.01$). The USPIO concentration of 5 mg/kg used in this experiment was chosen based

on preliminary experiments to approximately match absolute maximum signal percentage change ( ~2% from baseline) observed in the BOLD images during forepaw stimulation.

**Table 1:** BOLD and CBV temporal variance, SNR, and percentage signal change during forepaw simulation calculated using data obtained from ten rats.

| | BOLD | CBV | P-Vals |
|---|---|---|---|
| **Temporal Variance** | | | |
| **SI** | 0.72% ± 0.32% | 0.78% ± 0.39% | 0.36 |
| **SII** | 1.19% ± 0.42% | 1.48% ± 0.62% | < 0.01 |
| **CP** | 0.72% ± 0.29% | 1.26% ± 0.45% | < 0.01 |
| **Spatial SNR** | 55.25 ± 16.58 | 46.09 ± 13.25 | < 0.01 |
| **Activation % Change** | 1.91% ± 0.59% | -1.41% ± 0.39% | < 0.01 |

## Spectral Analysis

Figure 1 shows the individual power spectra for two rats and the average power spectra of all ten rats for time courses from the SI for BOLD and CBV resting state scans. The power spectra from the BOLD scans had maximum power in the very low frequency range with a broad distribution of power across the low frequencies (< 0.3 Hz). There was less power in the very low frequency range in the CBV scans, and the distribution of power was more localized than in the BOLD scans, with a distinct peak often appearing near 0.2 Hz. The center of mass for the low frequency power (< 0.3Hz) for BOLD occurred at 0.13 Hz. The center of mass for all low frequency power (< 0.3 Hz) in the CBV scans was localized to 0.16 Hz. For both CBV and BOLD power spectra, just before 0.3 Hz power was reduced abruptly to a baseline level (low power noise at all frequencies) in a nearly identical pattern.

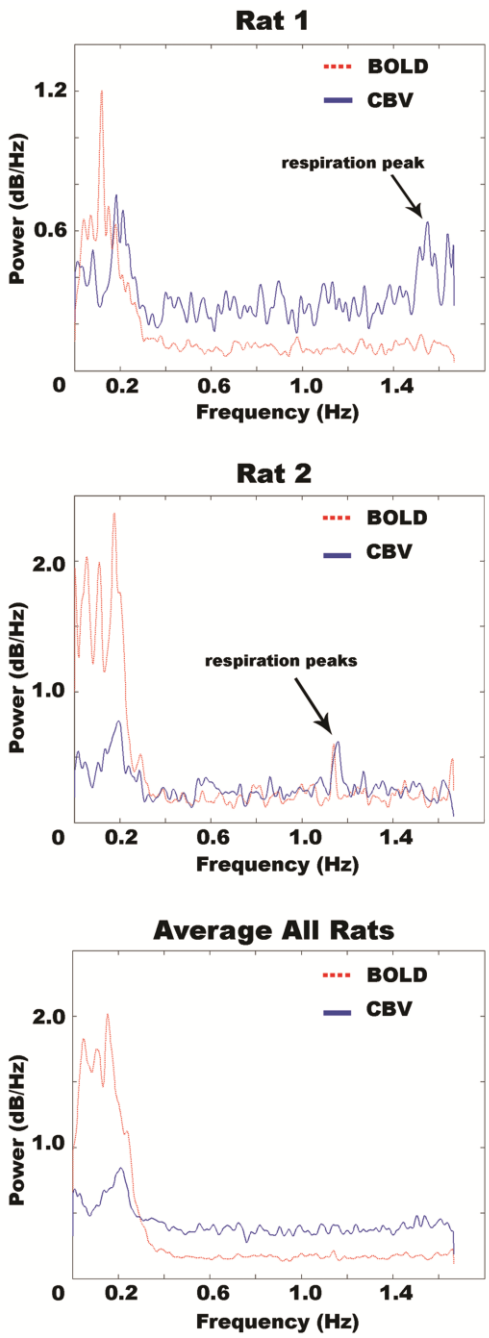


**Figure 1:** Average CBV and BOLD power spectra for two representative rats. The average BOLD and CBV power spectra for all ten rats is shown in the bottom plot. BOLD data exhibits higher power in the very low frequencies (less than 0.1 Hz) and a broader distribution of power throughout the low frequency range, while the CBV data often exhibits a distinct peak localized near 0.2 Hz. The respiratory contribution to the resting state data set is visible in the BOLD and CBV power spectra (clearly evident in Rat 1 and 2) around 1.6 Hz and 1.1 Hz respectively (95 and 65 breaths per minute).

**Seed-based Correlation Analysis**

Representative cross-correlation maps of CBV and BOLD for all three seed regions (SI, SII, and CP) are shown in Figure 2. CBV cross correlation was significantly more localized than BOLD in the cortex contralateral to the seed region in band passed (0.05 – 0.25 Hz BOLD; 0.1 – 0.03 Hz CBV) SI and SII data (for the SI region). BOLD connectivity based on a seed region in the left SI resulted in an average of 45 ± 17 voxels exceeding half of the maximum cross correlation value in the bilaterally symmetric area as compared to 26 ± 13 for CBV ($p<0.01$).The average cross correlation value (of voxels greater than half of the maximum correlation value) for voxels in the SI BOLD data was 0.50 ± 0.15 in the 3x3 region bilaterally symmetric to the ROI while the average cross correlation in the SI CBV data was 0.25 ± 0.08 ($p< 0.01$). Connectivity and extent values for SI, SII, and CP are located in Table 2.

**Table 2:** BOLD and CBV functional connectivity statistics calculated from data obtained in ten rats.

| | BOLD | CBV | P-Vals |
|---|---|---|---|
| **Mean CC > Half Max** | | | |
| **SI** | 0.50 ± 0.15 | 0.25 ± 0.08 | < 0.01 |
| **SII** | 0.45 ± 0.13 | 0.23 ± 0.10 | < 0.01 |
| **CP** | 0.31 ± 0.10 | 0.17 ± 0.03 | < 0.01 |
| **Number of Pixels > Half Max** | | | |
| **SI** | 45 ± 17 pixels | 26 ± 13 pixels | < 0.01 |
| **SII** | 27 ± 9 pixels | 17 ± 11 pixels | < 0.01 |
| **CP** | 30 ± 13 pixels | 13 ± 6 pixels | < 0.01 |

To determine whether the 0.2 Hz peak observed in the CBV data had different properties from the lower frequency range typically used in functional connectivity studies, connectivity maps were created using only the low frequency range (< 0.1 Hz)

for CBV and BOLD (Figure 2; first column) in SI. BOLD and CBV connectivity strength for the lower frequency data resulted in an increase in average connectivity values (0.55 ± 0.12 and 0.34 ± .14 respectively) which was significant ($p = 0.04$ and $p < 0.01$ respectively). The spatial extent of connectivity in the contralateral cortex was reduced slightly for BOLD (voxels greater than half max connected to seed = 43 ± 18) and increased slightly for CBV (voxels greater than half max connected to seed region = 26 ± 15); the change was not significant for BOLD ($p = 0.57$) or for CBV ($p = 0. 84$). Although the spatial extent of connectivity in the contralateral cortex does not change significantly, the number of voxels connected to the seed region outside of the contralateral cortex greatly increases for CBV weighted scans. The low pass filter images in Figure 2 show increased connectivity in subcortical brain regions for CBV weighted images while the low pass BOLD connectivity maps look almost identical to the band pass maps. The low pass CBV images also contain several voxels located in the skull weakly connected to the seed region. Low frequency connectivity in CBV scans based on a seed region in SI resulted in widespread, but relatively weak cross correlation throughout cortical and subcortical areas which was not seen in the higher frequency (0.1 Hz – 0.3 Hz) cross correlation analysis. Low frequency BOLD correlation did not exhibit the widespread connectivity pattern seen in the CBV scans (Figure 2).

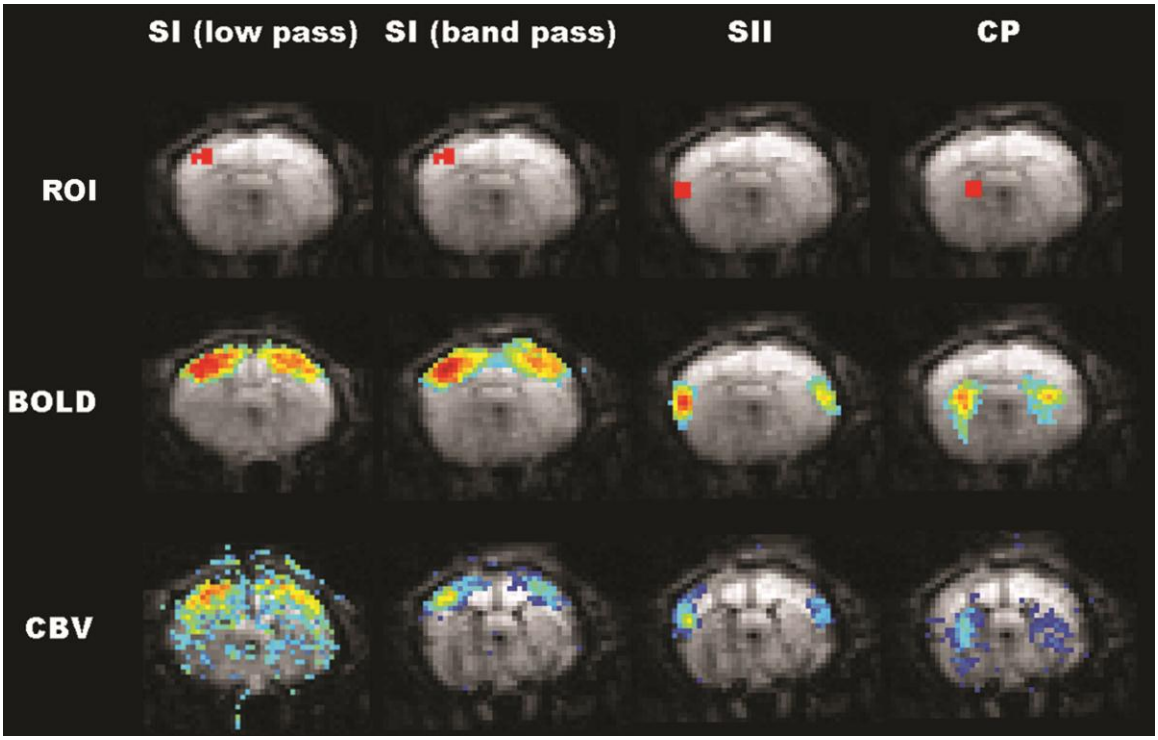


**Figure 2:** Cross correlation maps for CBV and BOLD resting state scans. Correlation maps from a typical rat are overlaid on the EPI image used to create the map. Locations of the seed regions are shown in the first row. Bilateral connectivity is evident for BOLD and CBV for all three seed regions, though the strength of the correlation is weaker for CBV-weighted scans. The first column, labeled SI 'low pass', shows cross correlation maps for spontaneous fluctuation < 0.1 Hz; the remaining three columns are based on frequencies between 0.05 Hz - 0.25 Hz for BOLD and 0.1 Hz – 0.3 Hz for CBV. The BOLD functional connectivity maps exhibit little dependence on the frequency range used, while the cross correlation in the CBV maps created with the low pass filter appears less localized.

Averaged cross correlation matrices (all ten rats) showing the connectivity between averaged time courses in six regions of interest (right SI, SII, CP and left SI, SII, and CP) are shown in Figure 3. The pattern of connectivity between contralateral analogues is similar for BOLD and CBV (highest for SI and lowest for CP); however, the correlation values for BOLD scans is significantly higher for all regions. The average value of correlation between left and right SI was 0.66 for BOLD and 0.31 for CBV.

Anatomically selected seed regions in the SII region resulted in average bilateral correlation values of 0.58 for BOLD and 0.22 for CBV, and seed regions selected in the CP resulted in average bilateral cross correlation strength of 0.37 for BOLD and 0.12 for CBV. Weak correlation is observed between non-analogous areas for both contrast mechanisms.

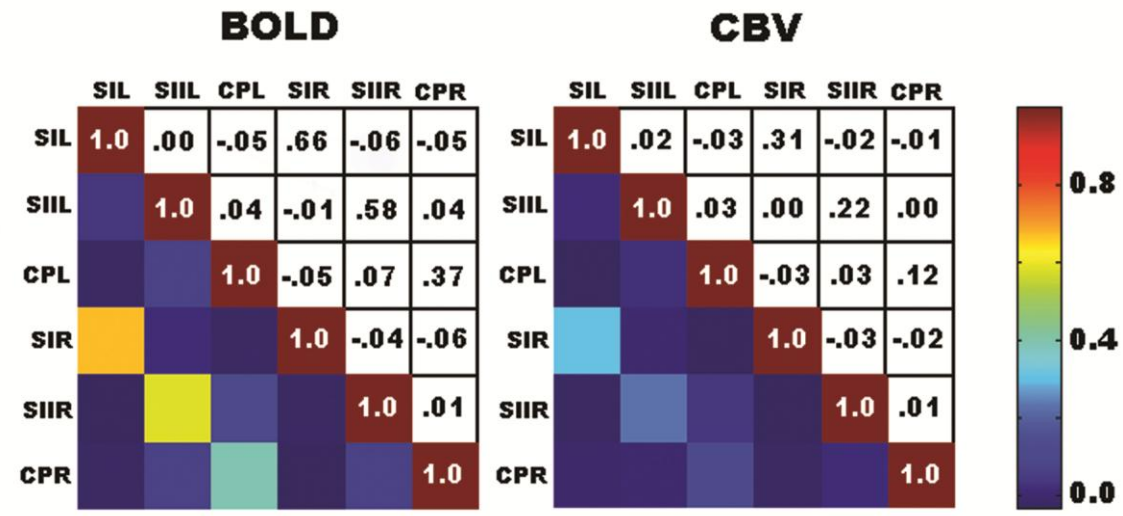


**Figure 3:** Average cross correlation matrix showing the strength of connectivity between six areas (left and right SI, SII, and CP) for CBV and BOLD. For both contrast mechanisms, the highest correlation values are between left and right SI, followed by left and right SII and left and right CP. Little correlation is observed between adjacent ipsilateral areas or non-analogous areas in contralateral hemispheres.

**Spatiotemporal Dynamics**

Spatiotemporal analysis was conducted using image to image visualization of low frequency fluctuations in the filtered, normalized BOLD and CBV resting state data sets following the method described by Majeed et al. (Majeed, Magnuson et al. 2009). Both

data sets showed well organized bilateral waves of increased signal in the optimal frequency range (BOLD - 0.05 Hz – 0.25 Hz; CBV - 0.1 Hz to 0.3 Hz) that propagated along the cortex from SII towards the primary motor cortex (MI) (Figure 4). These waves occurred often within each 6 minute resting state data set. The very low frequency range for BOLD and CBV (<0.1Hz) was also analyzed for propagating waves. Propagating waves in this low frequency range were seen sparsely for BOLD and never for CBV.

The waves occurred spontaneously and typically occurred in groups of two or three repeating waves before ceasing for several seconds or several minutes. The time from the increased signal inception in SII to its disappearance in MI is defined as the wave propagation time. Propagation of the waves from SII to MI took approximately four seconds for the 0.05 Hz – 0.25 Hz BOLD data and approximately three seconds for the 0.1 Hz – 0.3 Hz CBV data. The increased signal intensity moved toward MI and eventually fades away (Figure 4; last frame for BOLD and CBV). These propagation times are similar to those measured by Majeed et al. in the α-chloralose anesthetized rat (Majeed, Magnuson et al. 2009).

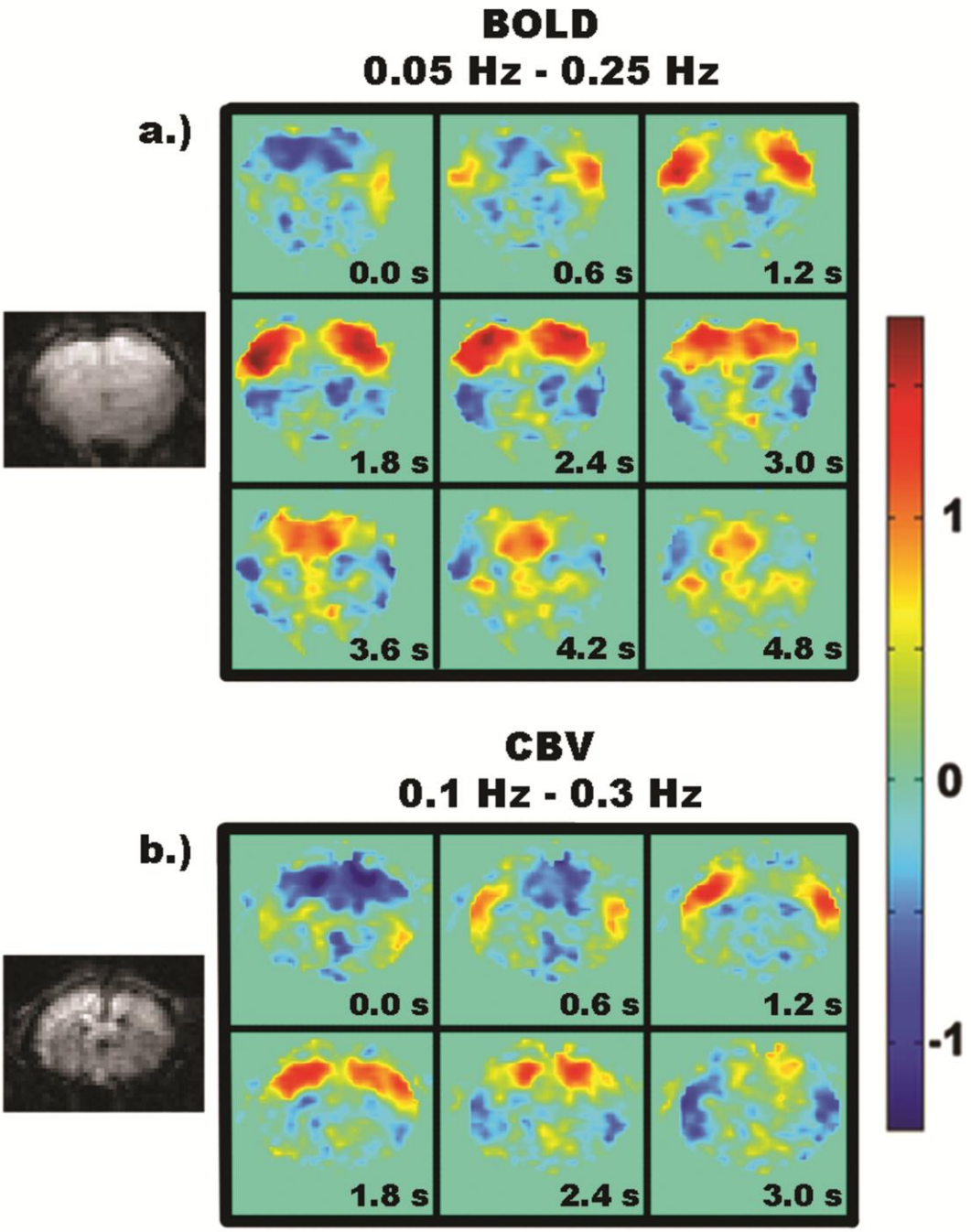


**Figure 4:** Propagating waves of activity from SII towards MI in BOLD and CBV resting state scans. a.) 0.05 Hz – 0.25 Hz filtered BOLD scan. Propagation from SII to MI takes approximately four seconds. b.) 0.1 Hz – 0.3 Hz filtered CBV scan. Propagation from SII to MI occurs in approximately three seconds.

## Summary of Results and Discussion

The work described here directly compares two types of contrast (BOLD and CBV) used in previous functional connectivity rodent studies. Spontaneous fluctuations of the BOLD signal arise from increasing and decreasing metabolic demand as a function of local neural activity. The vasculature responds to this metabolic demand by increasing the volume (CBV) and flow (CBF) of blood to an area. Changes in oxygen metabolism (CMRO2), CBV, and CBF can be measured independently with MRI, and much research has focused on how changes in these parameters in response to stimulation give rise to the task-related BOLD signal. However, the relationship between the recorded BOLD and CBV signals in the absence of a task has not been explored.

### Comparison with Previous Functional Connectivity Studies in Rodents

The functional connectivity maps obtained with BOLD and CBV weighted imaging in this study are similar to those reported in previous rodent studies. BOLD studies performed by Pawela and Zhou also found strong connectivity between bilaterally symmetric SI, SII, and CP regions (Pawela, Biswal et al. 2008; Zhao, Zhao et al. 2008). Lu et al. observed similar connectivity between bilaterally symmetric SI regions using CBV (Lu, Scholl et al. 2007). While these functional connectivity studies were performed with a longer TR (1 – 1.5 s) and no correction for physiological noise, the results were similar to those obtained in this study, suggesting that respiratory noise may not have a significant impact on functional connectivity in rodent models. Majeed et al. utilized a TR of 100 ms, short enough to resolve the primary cardiac contribution as well as the primary respiratory peak (Majeed, Magnuson et al. 2009). The functional connectivity maps were similar to those presented here suggesting that cardiac noise contamination

does not alter correlation patterns in rodents; however, Majeed's rats were anesthetized with alpha-chloralose and were mechanically ventilated. We have mapped the location of contributions from the respiratory signal in the freely breathing medetomidine anesthetized rats from this study (Figure 5). It does not appear that respiratory noise corrupts the functional connectivity data because of its localization to the base and edges of the brain for both BOLD and CBV. At the TR used in this study (300ms), we are unable to resolve the contributing signal from cardiac noise.

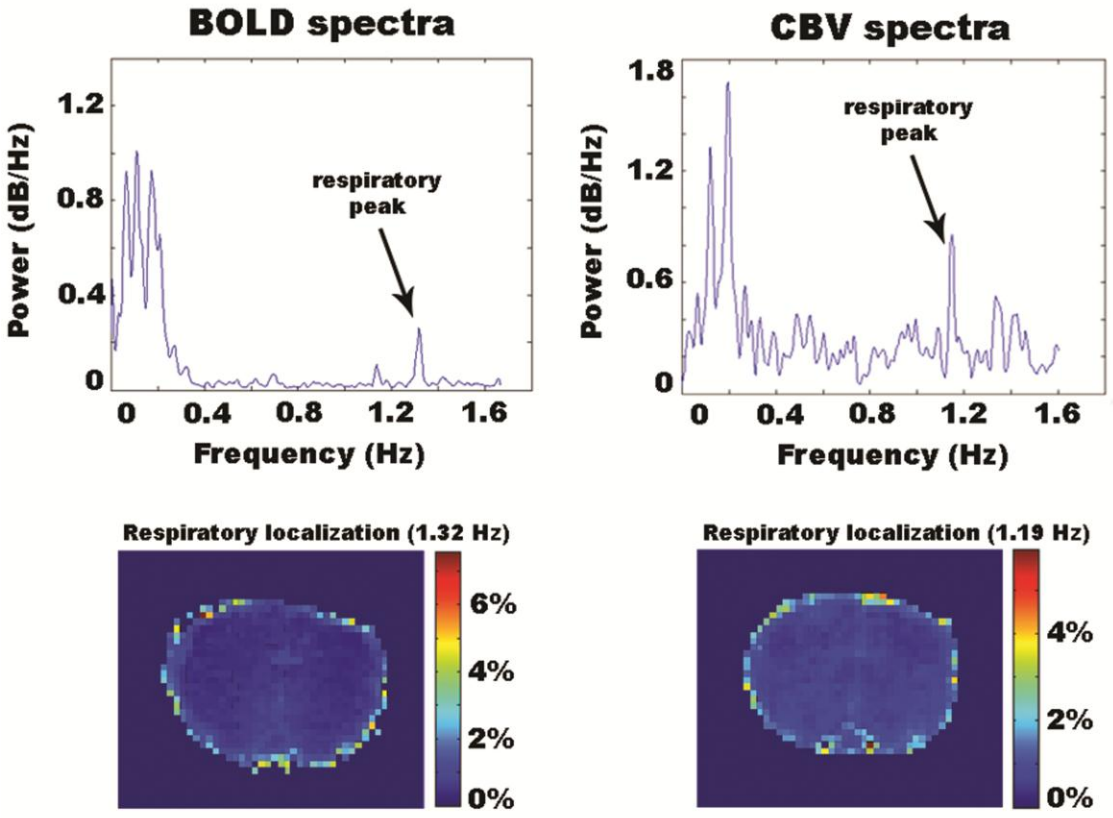


**Figure 5:** Map of peak in power spectrum repesenting respiratory noise. The majority of the noise is localized to the base and edge of the brain. This should not influence functional connectivity mapping.

Most functional imaging studies conducted in rodent models are performed in anesthetized animals, and the choice of anesthesia can impact the results. α-chloralose has traditionally been the primary anesthesia for functional imaging in the rat, but it requires intubation and mechanical ventilation, cannulation of the femoral artery for blood gas monitoring, and subsequent sacrificing of the animal at the end of the experiment (Keilholz, Silva et al. 2004; Keilholz, Silva et al. 2006; Lu, Zuo et al. 2007). In this experiment a continuous infusion of medetomidine anesthesia is used, which allows for longitudinal studies (Weber, Ramos-Cabrer et al. 2006). The results are similar to functional connectivity experiments carried out in animals anesthetized with α-chloralose (Lu, Zuo et al. 2007; Majeed, Magnuson et al. 2009).

Isoflurane was administered to each rat for ~2 minutes during tail vein injection of the USPIOs for CBV imaging. Isoflurane could potentially alter the vascular response and could be partially responsible for the change in the LFFs. Two control rats were imaged to ensure that the brief administration of isoflurane nor the injection process was responsible for the change in the power spectrum observed between BOLD and CBV scans. Each of the control rats were administered isoflurane while injecting a dose of saline equal to the dose of USPIOs they would have otherwise received. Neither control rat exhibited a change in functional connectivity, power spectra, or SI activation to a forepaw stimulation as compared to the previous BOLD scans after administration of the isoflurane and saline.

**BOLD vs CBV Weighting for Functional Connectivity Mapping**

Similar spatial patterns of connectivity were observed for both BOLD and CBV-weighted data using seed regions in SI, SII, and CP. The strongest correlation was

observed between bilaterally symmetric regions, with very little correlation between non-analogous regions in either the ipsilateral or contralateral hemisphere. These findings are in agreement with previous studies of functional connectivity in the rodent, which predominantly found bilateral patterns of correlation (Pawela, Biswal et al. 2008; Zhao, Zhao et al. 2008; Williams, Magnuson et al. 2010).

Cross correlation analysis conducted with the lower frequency spontaneous fluctuations (< 0.1 Hz) resulted in a global increase in the number of voxels connected to the seed region for CBV scans; however, there was very little change in the connectivity patterns for the BOLD data. The widespread connectivity in the low frequency CBV data is not unexpected considering there is less power located in the low frequency (< 0.1 Hz) portion of the spectra as compared to the BOLD spectra. Correlation of the seed region with such a widespread group of voxels including several voxels in the skull (Figure 2; CBV - low pass) suggests an increased contribution from noise sources as opposed to correlated CBV signals. The high power in the low frequency BOLD signal may represent other physiological processes, such as metabolic fluctuations that are also tied to neural activity, so the functional connectivity maps appear unchanged.

We chose the dose of USPIOs (5mg/kg) based upon preliminary experiments so that approximately equivalent temporal variance and percent signal change during stimulation were obtained in the BOLD and CBV-weighted scans. Similar temporal variance was considered a priority since it provides some measurement of the relative amplitude of the spontaneous signal fluctuations. While the temporal variance was well-matched for BOLD and CBV scans in this study, the absolute percent change during activation was significantly higher for the BOLD scans ($p<0.01$). This may indicate that

the fluctuations in the CBV-weighted scans contained relatively lower contributions from hemodynamic processes and relatively stronger influences from system noise, in agreement with the observation that SNR was reduced in CBV weighted images. This reduction in SNR may account for the lower correlation values observed in the CBV data.

A USPIO concentration of 5 mg/kg was used for CBV scans. In order to optimize dosing for functional connectivity studies, several combinations of USPIO concentrations and TRs were tested in preliminary experiments. USPIO doses between 1 mg/kg and 15 mg/kg were tested with TRs ranging from 100 ms to 1000 ms. A TR of 300 ms was chosen to allow the sampling and removal of the primary respiratory component while maintaining acceptable SNR. With this TR, a USPIO concentration of 5mg/kg provided approximately the same percentage change during stimulation and level of temporal variance observed in BOLD studies. The ideal dose of iron oxide for functional connectivity studies may be different from the dose used for functional studies, particularly when the available SNR is limited due to the use of a short TR. Higher percent changes during stimulation in CBV-weighted scans can be achieved by using higher doses of USPIO (Keilholz, Silva et al. 2006; Lu, Zuo et al. 2007), but the resulting signal loss may degrade the quality of functional connectivity maps. Previous CBV functional connectivity studies in rodents employed larger doses of USPIO than were used in the present study, but cross-correlation values were higher in our study.

The high degree of similarity between the functional connectivity maps created with BOLD and CBV suggests that results from studies using different contrast mechanisms should be readily comparable. Because CBV-weighted scans have a lower SNR, BOLD is potentially a better choice for studies with high temporal resolution and

limited SNR. The use of BOLD contrast also eliminates the need for exogenous contrast agent.

**Spectral Differences Between BOLD and CBV**

Recent work in the α-chloralose-anesthetized rat reported two low frequency peaks with different characteristics (Majeed, Magnuson et al. 2009), motivating the further exploration of frequency-dependent differences in BOLD and CBV data in this study. Resting state data collected in the rat model using the BOLD signal reveals LFFs with relatively uniform power within a frequency range of 0.01 Hz - 0.30 Hz, with one or two localized low frequency peaks, similar to previous experiments in α-chloralose-anesthetized rats (Lu, Scholl et al. 2007; Majeed, Magnuson et al. 2009; Williams, Magnuson et al. 2010). CBV weighted data collected from the same animals exhibit different spectral properties, with a strongly localized peak at ~ 0.2 Hz. The differences in the two power spectra are related to the frequency signatures of the components contributing to the measured signal. The BOLD spectrum is derived from a combination of several signals (CBF, CBV, $CMRO_2$) with independent frequency contributions which results in a relatively uniform power band between 0.0 Hz – 0.3 Hz. The CBV spectrum ideally contains only one signal, blood volume changes, which oscillate at approximately 0.2 Hz during resting state. Despite the differences in the power spectra obtained with CBV and BOLD weighting, the resulting connectivity maps are very similar, suggesting that the processes contributing to different frequency bands share a common origin.

In addition to fluctuations arising from spontaneous variations in neural activity, low frequency oscillations in these signals may also arise from sources that may or may not be closely tied to neural activity. Oscillations of approximately 0.1 Hz have been

observed in CBF using laser-Doppler flowmetry (Golanov, Yamamoto et al. 1994), and in combination CBV, CBF, and oxygen saturation data using reflective light imaging (Mayhew, Askew et al. 1996). While some studies report a relationship between these oscillations and neural activity (Golanov, Yamamoto et al. 1994), others do not (Vern, Leheta et al. 1997). It appears that these fluctuations can be decoupled from neural activity, as they have also been observed in isolated arteries (Osol and Halpern 1988). It is therefore possible that particular hemodynamic processes exhibit slow oscillations that are partially related to neural activity and partially due to other factors. If so, it may be possible to identify frequency ranges and/or hemodynamic contrasts that are more specific to neural activity than the broadband BOLD signal typically used. Combined with Majeed et al.'s study showing that low and high frequency peaks in the BOLD signal from α-chloralose-anesthetized rats have different spatiotemporal dynamics, our finding that the CBV power spectra exhibits a localized peak in the higher frequencies as compared to the broader BOLD signal suggests that perhaps the higher frequency fluctuations are linked to ongoing regulatory processes. In support of this idea, the patterns of spatiotemporal dynamics linked to the higher peak in both types of scans are highly reproducible, both within and across animals. The regulatory processes could be vascular, neural, or a combination of both. An intriguing possibility is that functional connectivity is mediated by both a low frequency regulatory 'driver', possibly in the brainstem (Drew, Duyn et al. 2008) and by communication between strongly connected areas, which may preferentially contribute to different frequency ranges of the BOLD fluctuations. However, in this study little difference was observed between functional connectivity mapped with BOLD as compared to CBV. This would suggest that the

regulatory processes either dominate the fluctuations used to map functional connectivity in the anesthetized rodent, or that any vasoregulatory processes are tightly tied to neural activity and provide nearly identical information about functional connectivity. Further work in human subjects or unanesthetized animals would assist in addressing these issues.

**Spatiotemporal Dynamics**

The detection of a spatiotemporal pattern of propagation from lateral to medial cortical areas reproduces the results recently reported by Majeed et al., but at a lower field strength (9.4 T rather than 11.7 T) and using a different anesthetic (medetomidine instead of alpha-chloralose). The number of occurrences of the waves in this study was lower than that previously observed under alpha-choloralose, possibly due to a change in magnetic field strength or an effect of altered vascular response, neuro-vascular coupling, or alterations in the underlying neural triggers in response to the anesthesia being used. These waves of signal were also observed in CBV-weighted images for the first time. These findings demonstrate that the patterns of spatiotemporal propagation are common to multiple contrast mechanisms and anesthetics in the anesthetized rat.

In the previous work by Majeed et al., a TR of 100 ms was used, making the images sensitive to the effects of inflowing blood (and thus CBF fluctuations). This study also utilized a relatively short TR (300 ms; chosen to maximize signal while allowing the primary contribution from respiration to be removed by filtering), but the use of USPIO should reduce or eliminate the signal from the inflowing blood, suppressing inflow effects. Nevertheless, a well-defined peak at 0.2 Hz was observed, and the spatiotemporal dynamics of the CBV fluctuations were similar to those observed in the previous study

with BOLD, suggesting that inflow effects are not the primary source of the spatiotemporal waves observed in the cortex.

The presence of propagating waves in the cortex illustrates the limitations of traditional functional connectivity studies. In both BOLD and CBV data, little correlation is observed between SI and SII even though some type of connectivity is present, since the signal waves clearly move between the two areas. The lack of correlation is likely due to the time lag (2-3 s) between the two areas, rather than a lack of relationship between their time courses.

It is important to further explore the relationship between neural activity and the physiological processes (CBF, CBV, and $CMRO_2$) with low frequency components contributing to the BOLD resting state signal. We have imaged the CBV signal, one contributor to the BOLD signal, independently to determine its contribution to the overall BOLD signal. The results show that while the power spectrum of the CBV signal is different from that of the BOLD signal, both connectivity maps and spatiotemporal dynamics are similar for the two modalities. This may indicate that functional connectivity (FC) is primarily reflective of coordinated fluctuations within the vasculature which may be fully or partially driven by neural activity. The links between neural activity and vasomotion are still unclear and further experiments will be necessary to better understand the origin of the spontaneous MRI signal oscillations (Sirotin and Das 2009).

# CHAPTER 3

# ISOFLURANE AND DEXMEDETOMIDINE'S TIME DEPENDENT EFFECT ON FUNCTIONAL CONNECTIVITY

## Introduction

Animal models are a powerful tool, allowing for the detailed and often invasive investigation into analogues of human disease, structure, and function. Animal models have provided an ideal platform to study the origin and functions of the BOLD signal and functional connectivity in fMRI; however, one complication is that anesthesia is commonly required to prevent movement and alleviate pain or anxiety (Keilholz, Silva et al. 2004; Keilholz, Silva et al. 2006; Weber, Ramos-Cabrer et al. 2006). Anesthetic agents introduce confounding influences to the function of the neural and vascular architecture of the brain (Zhao, Zhao et al. 2008; Pawela, Biswal et al. 2009; Magnuson, Majeed et al. 2010; Williams, Magnuson et al. 2010; Pan, Thompson et al. 2011; Pan 2013). Anesthesia directly affects basal neuronal activity as well as the coupling between neurons and the vasculature (Nakao, Itoh et al. 2001); understanding an anesthesia's effect on neural activity and BOLD data is vital for interpreting functional data.

In 2005 Austin, et al. published data indicating that the BOLD response to a fixed stimulus was variable as a function of time under α–chloralose anesthesia (following halothane induction); specifically, the spatial extent and peak amplitude response to the stimulus both increased several hours post α–chloralose induction (Austin, Blamire et al. 2005). Austin, et al. suggest that changes in the BOLD response under α–chloralose was

a product of combined effects of halothane and α–chloralose on neuronal activity or changes in vascular response and neurovascular coupling as a result of anesthesia. If the changes observed are related to changes in vascular tone, then variations in the BOLD response over time should theoretically manifest in the spontaneous BOLD signal as well.

Slow fluctuations in the BOLD signal (presumed to be linked to spontaneous neural activity) have been used to map functional connectivity, a term used to describe spectrally and temporally coherent activity arising in different areas of the brain (Biswal, Yetkin et al. 1995; Bullmore, Rabe-Hesketh et al. 1996; Zhao, Zhao et al. 2008; Magnuson, Majeed et al. 2010; Williams, Magnuson et al. 2010). The frequency of the fluctuations depends on the type of contrast (Magnuson, Majeed et al. 2010) and the anesthetic agent (Majeed, Magnuson et al. 2009). Spatiotemporal dynamic analysis reveals patterns of quasi-periodic, often bilaterally symmetric, spatially propagating patterns of functional activity observed both in humans (Grigg and Grady 2010; Majeed, Magnuson et al. 2011) and in the anesthetized rat (Majeed, Magnuson et al. 2009; Majeed, Magnuson et al. 2011). In the work presented here, we evaluate the time-sensitive effects of dexmedetomidine anesthesia (following initial administration of isoflurane anesthesia) on traditional functional connectivity MRI, the frequency specific signatures of the BOLD fluctuations, and the occurrence of spatiotemporal dynamics.

Isoflurane is commonly used to induce anesthesia, perform surgical procedures, and maintain a deep level of unconsciousness in rodents during setup for fMRI (Weber, Ramos-Cabrer et al. 2006; Pawela, Biswal et al. 2008; Zhao, Zhao et al. 2008; Pawela, Biswal et al. 2009; Williams, Magnuson et al. 2010). Anesthesia is typically switched to

an agent that is less suppressive of neural activity for the imaging portion of the experiment, although isoflurane has been used during imaging as well (Liu, Zhu et al. 2012; Guilfoyle, Gerum et al. 2013; Kalthoff, Po et al. 2013). Isoflurane's anesthetic mechanism is not well understood, but it is known that is acts on GABA receptors, potassium channels, and the GLT1/EAAT2 glial glutamate transporter, all resulting in complex interrelationships producing the desired anesthetic state (Ferron, Kroeger et al. 2009). At high isoflurane doses (>1.8%) widespread cortical neural burst suppression results in reduced cortical excitation (Antunes, Golledge et al. 2003; Ferron, Kroeger et al. 2009) and reduced spatial sensitivity of functional connectivity (Liu, Zhu et al. 2012), while at lower dosages (<1.5%) functional activity and connectivity remain somewhat intact (Hutchison, Mirsattari et al. 2010; Liu, Zhu et al. 2012; Guilfoyle, Gerum et al. 2013; Kalthoff, Po et al. 2013). It has been demonstrated that it takes nearly an hour following isoflurane discontinuation for the end tidal volumes of isoflurane to drop below 0.1% following relatively short isoflurane paradigms (Sommers, van Egmond et al. 2009). This residual isoflurane likely introduces lingering effects on both neural activity (continued neural suppression) and the vasculature (continued vasodilation) that must be considered.

Dexmedetomidine is a $\alpha_2$-adrenergic receptor agonist which selectively binds to and stimulates $\alpha_2$-adrenergic receptors after crossing the blood-brain barrier. It is also a vasoconstrictor (Asano, Koehler et al. 1997). Dexmedetomidine acts by inhibiting adenylyl cyclase activity, causing a reduction of firing rates of locus coeruleus noradrenergic neurons, thus leading to sedation (Nelson, Lu et al. 2003). Unlike many other anesthetics that deeply suppress central nervous system (CNS) activity (Rehberg,

Xiao et al. 1996), dexmedetomidine induces a neural state very similar to natural sleep (Nelson, Lu et al. 2003) while simultaneous causing muscular relaxation. The drug was previously formulated as medetomidine, which contains the active enantiomer, dexmedetomidine used in the current experiment. (In 2009, Pfizer discontinued medetomidine [Domitor] in their veterinary line and switched to dexmedetomidine [Dexdomitor]). Both drugs have nearly identical effects on the rodent; however, the dosing of dexmedetomidine is half that of medetomidine (Granholm, McKusick et al. 2007).

In previous experiments using (dex)medetomidine, our lab has observed time-dependent effects of medetomidine on functional connectivity measured with resting state fMRI, functional network spatiotemporal dynamics (Majeed, Magnuson et al. 2009; Grigg and Grady 2010), and spectral characteristics of functional time-courses. Consequently, we designed a longitudinal experimental paradigm using two anesthetic regiments, one with a short duration of isoflurane (30 minutes; comparable to typical studies using isoflurane for induction and setup (Weber, Ramos-Cabrer et al. 2006; Pawela, Biswal et al. 2009; Hutchison, Mirsattari et al. 2010)) prior to functional imaging and another with a long isoflurane duration (3 hours; comparable to studies involving complex surgical procedures such as combined electrophysiology-fMRI (Pan, Thompson et al. 2011)) prior to imaging; both paradigms are followed by the same dosage of dexmedetomidine anesthesia concurrent with a 5.75 hour imaging series.

The goals of this work are twofold; first, to evaluate possible lingering, duration dependent effects of isoflurane on functional connectivity, and secondly to evaluate evolving changes in the rat's functional state based upon long term use of

dexmedetomidine anesthesia. We found that an extended isoflurane paradigm attenuates functional activity for a longer duration as compared to a shorter isoflurane paradigm. Furthermore, we also observed a significant evolution of functional metrics as a result of long durations of dexmedetomidine use under the currently accepted and refined dexmedetomidine sedation paradigm (Pawela, Biswal et al. 2009).

## Materials and Methods

### Animal Preparation and Physiological Monitoring

All experiments were performed following guidelines set by the Emory Institutional Animal Care and Use Committee (IACUC). Eleven male Sprague–Dawley rats (200–300 g) were anesthetized with 2% isoflurane mixed with ~1:1 oxygen and room air while undergoing experimental setup. The rat was placed in the MRI cradle and the head was secured with a bite bar and ear bars. Heart rate and blood oxygen saturation percentage were recorded with a pulse oximeter placed on the rear left paw. Body temperature was monitored with a rectal thermometer and maintained at ~37° C using an adjustable warm water pad. Respiratory rate was also monitored by using a pressure-sensitive balloon placed under the rat's chest.

Once setup was complete, the rat was left to rest in the cradle under 2% isoflurane until total time under isoflurane reached 3 hours (long isoflurane - experimental group 1) or 30 minutes (short isoflurane – experimental group 2). . For the long isoflurane group, after 2 hours and 30 minutes, isoflurane was reduced to 1.5% for 30 minutes before the induction of dexmedetomidine (Dexdomitor, Pfizer, Karlsruhe, Germany). The long

isoflurane "wait period" was chosen to replicate our previous experiments where it was necessary to keep the rat under isoflurane for long periods of time while surgical procedures were performed (Pan, Thompson et al. 2011). The short isoflurane group replicates the typical setup time for a rodent to be anesthetized and prepared for scanning where no surgery or complex setup is involved. Following the wait period, the short isoflurane group was switched directly from 2% isoflurane to dexmedetomidine.

A subcutaneous bolus injection of 0.025 mg/kg dexmedetomidine was administered to the rat's upper right leg. Five minutes after the dexmedetomidine bolus, isoflurane was discontinued. Fifteen minutes post-bolus, subcutaneous infusion of 0.05 mg/kg/hr dexmedetomidine was initiated using a butterfly needle taped in place to maintain anesthetic depth for the duration of the experiment (Weber, Ramos-Cabrer et al. 2006). Approximately eighty minutes following the initial dexmedetomidine bolus, the infusion dosage was increased to 0.15 mg/kg/hr (3× initial infusion rate) for maintaining anesthetic depth (Pawela, Biswal et al. 2009). The beginning of the 3x infusion did not exactly match Pawela's protocol. In experiments where surgery was performed, it was necessary to ensure anesthetic depth, and we found that increasing the dexmedetomidine dosage at ~80 minutes was conducive to adequate sedation with no alteration functional activity (Weber, Ramos-Cabrer et al. 2006).

**Image Acquisition**

All resting state functional images were acquired on a 20 cm horizontal bore 9.4 T Bruker BioSpec magnet equipped with an actively shielded gradient coil capable of producing 20 G/cm gradient strength with a rise time of 120 μs. The BioSpec was interfaced with an AVANCE (Bruker, Billerica, MA) console. An actively decoupled

imaging setup was used including a 2cm surface coil for reception and a 7cm volume coil for RF transmission (Bruker, Billerica,MA).

A FLASH (fast low-angle shot) image was acquired in three planes, providing necessary anatomical information to properly position the single slice to be used for resting state imaging. Using the flash image a coronal slice was selected covering the primary somatosensory (SI) cortex, based on known anatomical markers. Shimming was conducted on this single slice to obtain maximum SNR and spatial homogeneity. 45 minutes after the initial dexmedetomidine bolus, the first resting state scan was collected with the following parameters: Single-shot gradient echo EPI, Repetitions = 1000, TR = 500ms, TE = 15ms, total scan time = 8 minutes 20 seconds, number of slices = 1, slice thickness = 2mm, FOV = 2.56cm × 2.56cm, matrix size = 64 × 64. Every thirty minutes this identical resting state scan was repeated until the 5.75 hour mark was reached. This paradigm constituted eleven total scans; all scans were collected in 8 of 11 rodents. One rodent was missing the initial time point and one rodent was missing two of the initial time points due to delays during setup. Also one rodent was missing the final scan and another rodent was missing the final three scans; they were removed from the scanner because of slight motion (indicating the rat may be coming out of sedation). Following the final scan, rodents were removed from the MRI scanner.

**Data Analysis**

Functional activity and spectral metrics were directly compared between the short and long isoflurane experimental groups. Functional metrics were also compared between early and late portions of the experiment within each group. All fMRI data processing and analysis was performed using code written in MATLAB (MathWorks, Natick, MA).

Two initial preprocessing steps were performed before data evaluation. First the mean value was subtracted from functional time courses followed by division by one standard deviation to normalize for comparison between rats (Majeed, Magnuson et al. 2009). Following normalization, whole brain signal regression was performed (Liu, Zhu et al. 2012).

Spectral Analysis

Following the initial preprocessing, spectral data was evaluated. A nine voxel (3x3 square) ROI from the single coronal slice imaged was chosen manually in the forepaw region of the primary somatosensory cortex (S1FL), and a functional time course was obtained for the average intensity in the ROI for the duration of the scan. Power spectra were obtained for the resulting functional time course, using the Welch method (200 second sections, 99.5% overlap, Hamming window). The resulting power spectra were averaged at each time point to create a spectrum for both experimental groups, highlighting frequencies where consistent high power is present, while reducing noise from non-relevant frequency components. Maximum power value (%/cHz), maximum power frequency location (Hz), and the center of mass for power (Hz) were calculated using spectral data between 0.05 and 0.3 Hz (chosen based on analysis of low frequency BOLD power localization from previous works) (Majeed, Magnuson et al. 2009; Magnuson, Majeed et al. 2010; Majeed, Magnuson et al. 2011). Data were divided into low-band power (0.05 – 0.149 Hz), high-band power (0.015 – 0.30 Hz), and broadband power (0.05 – 0.3Hz). For the purposes of this manuscript, when describing spectral ranges, the designations “low-band,” “high-band,” and “broad-band” power will be used. Spectral data < 0.05 Hz was not used for raw spectral analysis due to the presence of high

powered 0-0.05Hz components in some of the data sets that were not removed by detrending or global signal regression. Each set of values was plotted against dexmedetomidine sedation time to determine time sensitive systematic influences of the anesthesias.

Functional Connectivity Analysis

Functional connectivity and spatiotemporal dynamics were evaluated for each data set. Additional preprocessing was required before analysis; data was linearly de-trended followed by finite impulse response (FIR) band pass filtering between 0.01 Hz – 0.3 Hz (allowing for removal of DC artifacts and higher frequency components). The ROI selected for spectral analysis was used to obtain a time course of the filtered and detrended SI data. The functional time course of the left S1FL was then correlated with all other voxels in the image to obtain a functional connectivity map. The correlation values (*r*) from the 15 most highly correlated voxels in the hemisphere contralateral to the seed (clustered in SI) time course were averaged to generate a functional connectivity value for every rat and every scan. Correlation values were plotted against dexmedetomidine sedation times. Total low-band spectral power was plotted vs. broadband functional connectivity to determine if a relationship exists between the two. All data points for each experimental group were plotted on a scatter plot, and $R^2$ (linear regression), *r* (Pearson correlation), and p values (Unpaired, two-tailed, equal variance *t*-tests; multiple comparisons corrected) were calculated for each group.

Global signal connectivity was evaluated (using preprocessed data without global signal regression) by performing Pearson correlation between the average functional timecourse from all voxels in the brain and each individual voxel. Mean correlation was

calculated representing global similarities in functional timecourses. Global signal connectivity was plotted versus time to determine if a relationship existed.

Spatiotemporal Dynamic Analysis

A pattern-finding algorithm designed to identify reproducible spatiotemporal dynamics was applied to the filtered data (Majeed, Magnuson et al. 2009; Majeed, Magnuson et al. 2011), allowing for the visualization of patterns of low frequency activity that propagate through cortical and subcortical brain regions. A chunk of consecutive images is chosen from the resting state data set at a random starting position; sliding correlation is then performed between the image chunk and the preprocessed image series, correlation peaks are detected from the sliding correlation data, image chunks corresponding to the correlation peaks are then averaged together to create a new template. This averaged template is once again used in sliding correlation analysis; this process continues until convergence is reached. The final template, containing 11 images in this case (5.5 seconds), is then displayed on an image strip or as a movie to allow for ideal viewing of spatiotemporal dynamic patterns. This algorithm is explained in detail by Majeed et al., 2011 (Majeed, Magnuson et al. 2009; Majeed, Magnuson et al. 2011).

Templates for each scan were visualized on a blue to red color scale (colors indicate template strength, blue – low, red – high, "jet" in MATLAB); all templates were visually evaluated for the presence of spatiotemporal dynamics. Scans were grouped in a Boolean fashion as either showing or not showing the presence of spatiotemporal dynamics.

Inter- and intra- Group *t*-tests

Two sets of statistical analyses were performed, intergroup and intragroup analysis. Unpaired, two-tailed, equal variance *t*-tests were performed between the two experimental groups at each time point for all metrics discussed above (except spatiotemporal dynamics). Unpaired, two-tailed, equal variance *t*-tests were also performed within each experimental group comparing data from the first half of the imaging series (0.75 – 3.25 hours) to data from the second half of the imaging series (3.75 – 5.75 hours) to evaluate evolving properties of each metric. This division of time points was chosen because of the emergence of the ~0.18 Hz peak at this time point; in addition it represents the half-way point of functional imaging.

Multiple Regression Analysis: Resting State Metrics and Physiology

Multivariate ANOVA analysis was performed to determine if quantified functional resting state metrics were significantly coupled with variation in physiological parameters. Heart rate was obtained in 9 out of 11 rats, oxygen measurements were collected in 10 out of 11 rats, and breath rate and temperature were collected for all 11 rats. For each rat, spectral center of mass, max power, frequency location of max power, bilateral connectivity, and total low-frequency power (0.05 – 0.3 Hz) were independently evaluated vs. all physiological recordings (heart rate, breath rate, blood oxygen, and body temperature). Four P-values were obtained for each ANOVA indicating the statistical significance and interaction effects of the relationship between all physiological parameters and the evaluated functional resting state metrics (spectral center of mass, maximum spectral power, frequency location of maximum spectral power, maximum connectivity, and total spectral power between 0.05 and 0.3 Hz. Multiple regression

ANOVAs were performed for each rodent's physiological parameters and each calculated RS metric (50 total ANOVAs). Twenty sets of P-values were obtained (five functional metrics * four physiological parameters).

Physiological parameters were also evaluated individually to determine if there was a significant shift in physiological condition in the first half of scanning as compared to the second half of scanning. Student t-tests were performed comparing physiological data from the first half of the experiment (0.75 – 3.25 hours) to the same parameters from the second half of the experiment (3.75 – 5.75 hours).

Correction for Multiple Comparisons

The sequential goodness of fit (SGoF) method developed by Carvajal-Rodriguez, et al. (Carvajal-Rodriguez, de Una-Alvarez et al. 2009) was used to correct for multiple comparisons to minimize the chance that false positives would be considered significant. Seventy-seven hypotheses were tested regarding the relationship between our two experimental groups (seven functional metrics on eleven different time points). SGoF performs a binomial test based on a null hypothesis on the expected distribution of the P-value family created from the 77 student *t*-tests performed. This allows for controlling type 1 errors (the false rejection of a true null hypothesis) and minimizes the chance of false-positives being presented. SGoF was also performed on a second family of hypotheses (intra-individual comparisons) where data from the first six time points for each rat are compared to the second five time points to test for significant differences. Eight comparisons are made for both experimental groups for a total of 16 comparisons. All values described as significant in the results section have passed SGoF multiple comparison correction.

## Results

Functional connectivity, spectral content, and spatiotemporal dynamics exhibit evolving properties occurring as the length of time from isoflurane use increases and the duration of dexmedetomidine exposure increases. A summary of all inter- and intra-subject statistical comparisons can be found in Table 3 and Table 4 respectively; all values highlighted in bold are significant and have passed SGoF multiple comparison correction (Table 3: $p < 0.0319$; Table 4: $p < 0.0345$).

### Spectral Characteristic Evolution

Inter-group Analysis

Figure 6 contains the group average of spectral components obtained from time courses extracted from the right S1FL at each recorded time point for both short and long isoflurane groups. Data collection began 0.75 hours following the initial dexmedetomidine bolus. Resting state scans occurred at 30 minutes intervals until the 5.75 hour post-bolus data point is reached (11 plots represent 11 time points).

**Table 3:** Inter-group P-values of student t-tests were performed between the short and long isoflurane groups at each time point for each functional metric. The values highlighted in bold represent statistically significant differences between the groups that passed multiple comparisons testing (SGoF) which indicated significance at $p < 0.0319$. Significant differences between the groups were found in functional connectivity; maximum spectral power; low-band, high-band, and broad-band power; and global connectivity. Interestingly no significant differences were found after the 2.75 hour time point suggesting the influences of the long isoflurane duration prior to functional imaging had dissipated by the 3.25 hour time point.

| Time Point (hours) | 0.75 | 1.25 | 1.75 | 2.25 | 2.75 | 3.25 | 3.75 | 4.25 | 4.75 | 5.25 | 5.75 |
|---|---|---|---|---|---|---|---|---|---|---|---|
| Connectivity | **0.019** | 0.283 | 0.245 | 0.746 | 0.976 | 0.874 | 0.992 | 0.685 | 0.250 | 0.110 | 0.178 |
| Spectral Center of Mass | 0.035 | 0.113 | 0.490 | 0.353 | 0.682 | 0.132 | 0.666 | 0.383 | 0.365 | 0.370 | 0.420 |
| Max Power | 0.045 | **0.008** | **0.0006** | 0.079 | **0.010** | 0.114 | 0.572 | 0.348 | 0.044 | 0.412 | 0.185 |
| Max Location | 0.276 | 0.614 | 0.250 | 0.504 | 0.698 | 0.042 | 0.988 | 0.092 | 0.246 | 0.699 | 0.756 |
| Low-band Power | 0.048 | **0.0002** | **0.004** | 0.078 | **0.002** | 0.771 | 0.691 | 0.474 | 0.359 | 0.319 | 0.617 |
| High-band Power | 0.112 | **0.005** | **0.013** | 0.050 | **0.016** | 0.145 | 0.503 | 0.098 | 0.172 | 0.222 | 0.534 |
| Broadband Power | 0.052 | **0.0001** | **0.0001** | **0.0138** | **0.002** | 0.149 | 0.414 | 0.035 | 0.123 | 0.151 | 0.310 |
| Global connectivity | **0.032** | 0.041 | **0.029** | 0.051 | 0.066 | 0.159 | 0.066 | 0.66 | 0.114 | 0.141 | 0.840 |

**Table 4:** Intra-group P-values of student t-tests were performed between all functional metrics comparing the 0.75 – 3.25 hour time frame to the same metrics from the 3.75 – 5.75 hour time points. All values highlighted in bold represent statistically significant findings passing multiple comparisons correction (SGoF), p <0.0345. Long isoflurane data shows a significant evolution of functional metrics for 5/8 functional metrics while short isoflurane data indicates a significant evolution of functional metrics for 3/8 metrics.

| | Connectivity | CoM Location | Max Power | Max Location | Low-band Power (0.05 – 0.149 Hz) | High-band Power (0.15 – 0.3 Hz) | Broadband Power (0.05 – 0.3 Hz) | Global Connectivity |
|---|---|---|---|---|---|---|---|---|
| Long ISO | **0.0002** | 0.332 | **$5.57 \times 10^{-6}$** | **0.034** | **$5.84 \times 10^{-8}$** | **$2.8 \times 10^{-8}$** | **$2.23 \times 10^{-11}$** | 0.749 |
| Short ISO | 0.729 | 0.042 | **0.003** | 0.079 | 0.177 | **0.0008** | **$5.81 \times 10^{-5}$** | 0.229 |

At the 0.75 hour time point power is low across the entire spectrum; slightly higher power exists in the low frequency band (0.05 Hz – 0.149 Hz) for both experimental groups. At the second time point (1.25 hours) the short isoflurane group displays a major increase in low frequency power; low frequency power increases slightly in the long isoflurane group as well. This spectral organization continues in general through the 2.75 hour time point; while a gradual increase in the high-band frequencies (0.15 – 0.3) beginning to occur in both groups. At the 3.25 hour time point the power spectra of the two groups come close to convergence and evolve similarly throughout the final 5 time points. An interesting phenomenon begins to occur at 3.75 hours when a strong peak begins to emerge at ~0.18 Hz in both short and long isoflurane groups. By the 5.25 hour time point the ~0.18 Hz peak dominates the spectra. This peak remains dominant throughout the remaining time points for both groups.

Average power and squared error of the mean (SEM) for the low-band, high-band, and broadband spectrums are plotted in Figure 7 for both experimental groups. A statistical analysis of the qualitative evaluation described in the previous paragraph (and shown in Figure 6) comparing the groups is presented in Figure 7. For low-band total power (Figure 7- top), statistical differences exist between the short and long isoflurane groups at 1.25 hours ($p = 0.0003$), 1.75 hours ($p = 0.0036$), and 2.75 hours ($p = 0.0022$). Low-band spectral power values become more similar at 3.25 hours and finally converge at 3.75 hours. A similar trend is seen in the high-band power (Figure 7 center); however, average power values for the first time point (0.75 hours) are more similar than in the low band; following the first time point there is an ‘unzipping’ of high-band power data values until the 3.25 hour time point where the values ‘re-zip’. Statistically significant

differences were found for the same time points, 1.25 hours ($p = 0.0049$), 1.75 hours ($p = 0.0129$), and 2.75 hours ($p = 0.0164$), as seen in the low band power. Broadband power (Figure 7, bottom) reflects a combination of low-band and high-band values; naturally a similar trend is seen as in the previous two cases, although statistical differences between the short and long term isoflurane groups are also found at the 2.25 hour time point ($p = 0.0001$) in addition to the 1.25 ($p = 0.0001$), 1.75 ($p = 0.0138$) and 2.75 ($p = 0.0017$) hour time points. Qualitatively, the short isoflurane group appears to have greater power throughout all time points in the high-band and broadband ranges as compared to the long isoflurane group; however, SEM increases as the mean power increases and diminishes the statistical significance of differences between the two groups.

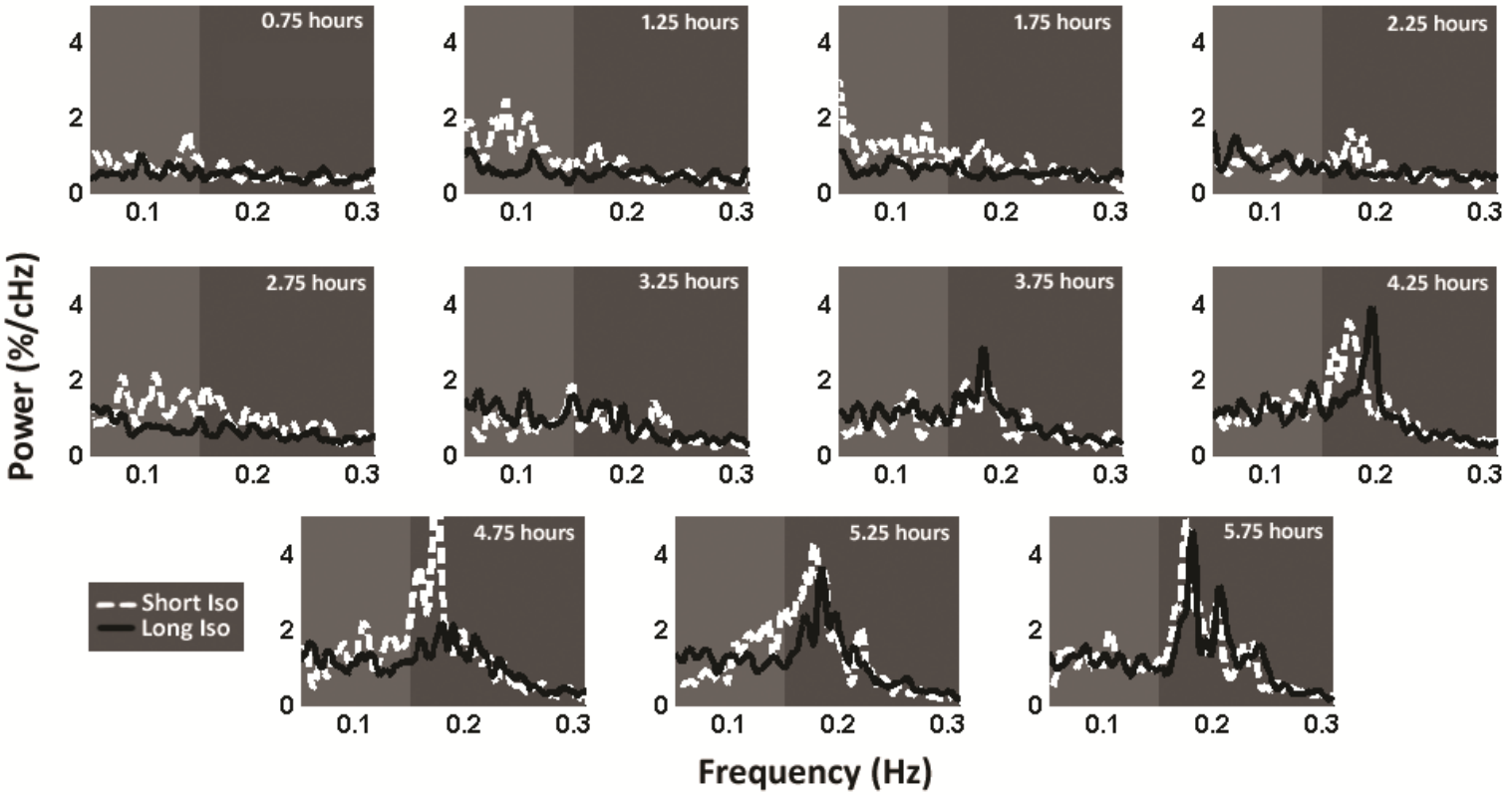


**Figure 6:** Power spectra evolution. Plots of average power spectra from the short isoflurane (30 minutes) group (4 rats – dotted line) and long isoflurane (3 hours) group (7 rats – solid line) followed by resting state imaging in 30 minute intervals under a fixed dosage of dexmedetomidine for 5.75 hours. Power spectra are derived from a time course generated from the left primary somatosensory cortex. Low-band power (0.05 – 0.149 Hz; light grey) increases at the 1.25 hour time point in the short isoflurane group and does not increase in the long isoflurane to a similar level until the 3.25 hour time point when near convergence of the two group's spectral signal occurs. At the 3.25 hour time point a strong ~0.18 Hz peak arises in both group within the high-band data (0.15 – 0.3 Hz) and dominates the power spectra for the remainder of the functional scans. Both groups indicate a clear evolution of spectral information as time under dexmedetomidine (and time since isoflurane cessation) increases.

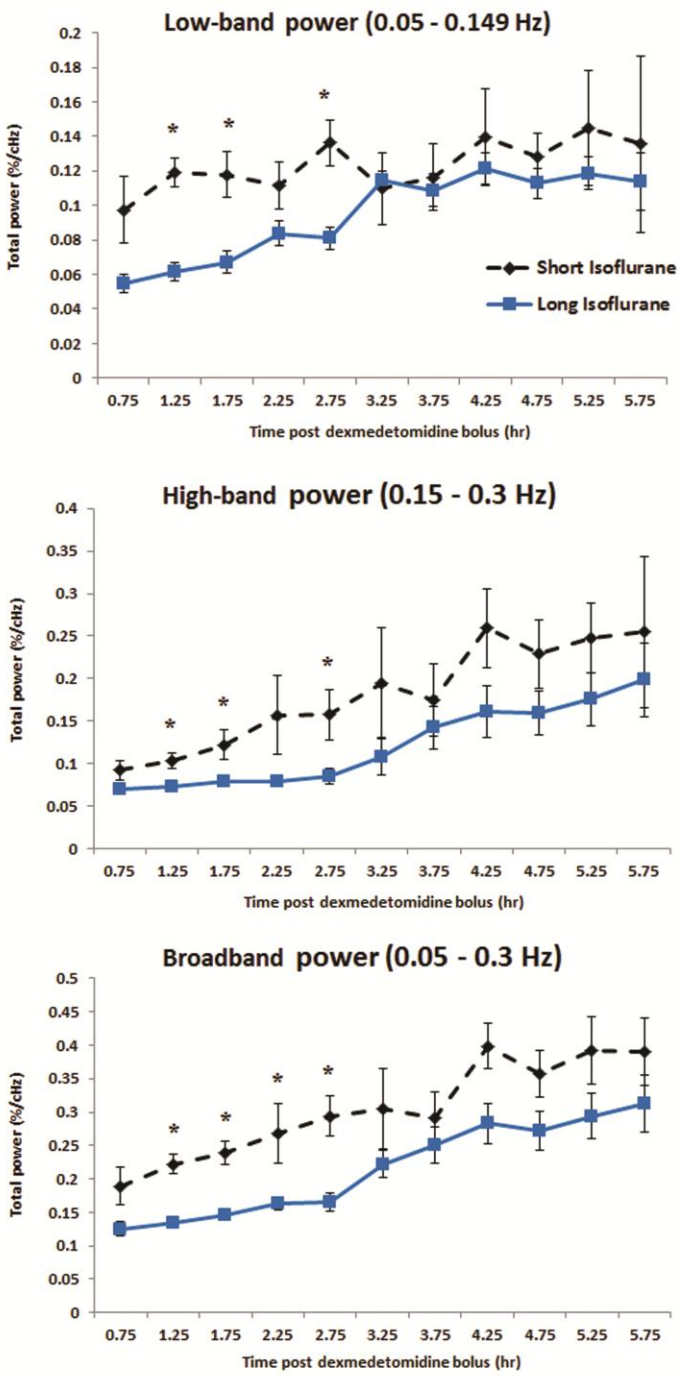


**Figure 7:** Average power evolution. Summation of low-band power (left, 0.05-0.149Hz), high-band power (middle, 0.15-0.3Hz), and broadband power (right, 0.05-0.3Hz) for both the short (dotted line) and long (solid line) isoflurane groups. Mean and SEM values for each group are plotted for each time point. Significant differences are found between the short and long isoflurane groups in the low-band power at the 1.25, 1.75, and 2.25 hour data points; in the high-band power at the 1.25, 1.75 and 2.25 hour data points; and in the broadband power at the 1.25, 1.75, 2.25 and 2.75 hour data points. Intra-group evaluations highlighting changes between early data and late data are calculated and presented in Table 4.

Peak power, peak location, center of spectral mass (CoM), and bilateral primary somatosensory (SI) functional connectivity are plotted in Figure 8 for both experimental groups. No statistically significant differences were found between the short and long isoflurane groups for center of mass calculations (Figure 8, top left) or the frequency location of the maximum spectral power (Figure 8, bottom right). Maximal power occurring in the broadband spectrum (Figure 8, bottom left) is significantly different between the short and long isoflurane groups at 1.25 ($p = 0.0078$), 1.75 ($p = 0.0006$), and 2.75 ($p = 0.0103$) hours. While mean maximum power appears greater in the short isoflurane group than the long isoflurane for most time points, SEM increases substantially as mean maximum spectral power increases resulting in overlap between the groups.

Intra-group Analysis

Functional metrics were also evaluated on an intra-group basis evaluating their evolution occurring as a result of both time since isoflurane discontinuation as well as total duration under dexmedetomidine. Early time points (0.75 – 3.25 hours) were compared to late time points (3.75 – 5.75 hours) for each functional metric. Qualitatively the short isoflurane group's low-band power shows a slight trend towards increasing power over the 5 hour recording duration; however, comparing early data to late data does not reveal a significant difference. The long isoflurane group has a more dramatic increase in low frequency power as a function of scanning time; a significant difference between early and late time points in long isoflurane low-band power is calculated ($p = 5.84e\text{-}8$).

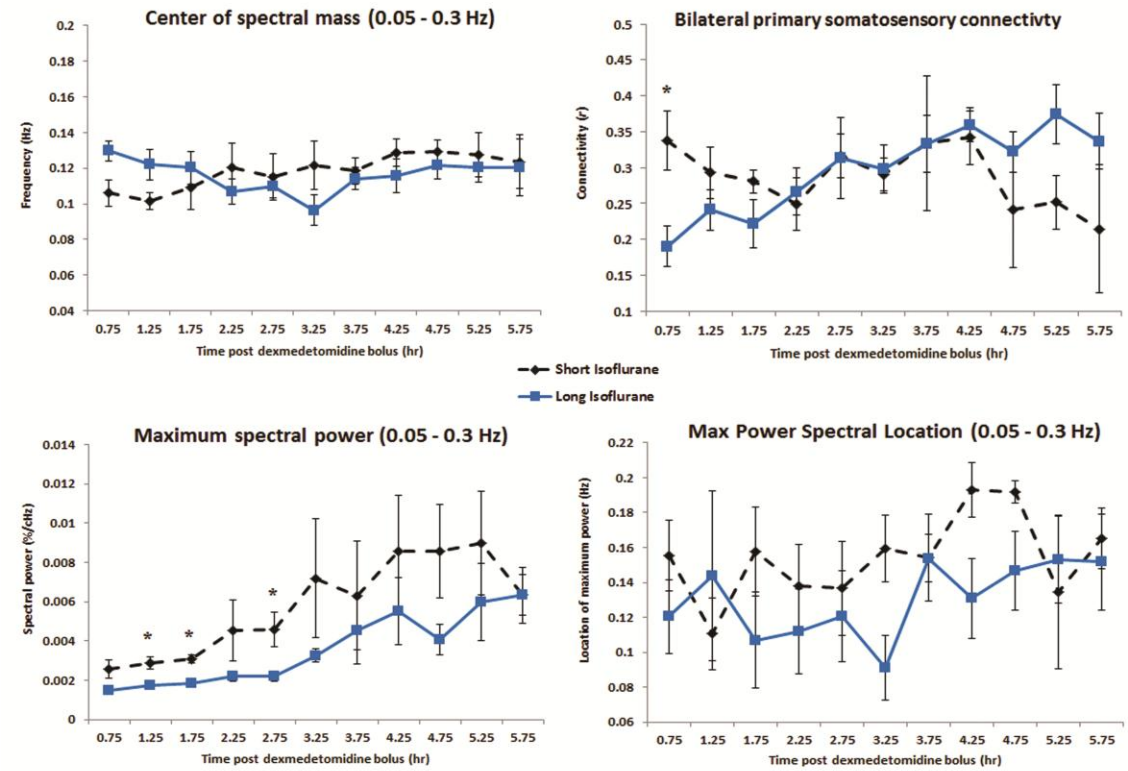


**Figure 8:** Spectral characteristic and connectivity evolution. Average group values and SEM are plotted for center of spectral mass (top left), bilateral primary somatosensory connectivity (top right), maximum spectral power (bottom left), and the location of that maximum power (bottom right) for both the short and long isoflurane groups. No significant differences are found between the two groups for spectral center of mass or for location of the max spectral power. Bilateral functional connectivity exhibits a significant difference between the groups at 0.75 hour time point followed by a convergence in connectivity data at the 2.25 hour time point. Significant differences between maximum spectral powers are found at the 1.25, 1.75 and 2.75 hour time points. Intra-group evaluations highlighting changes between early data and late data are calculated and presented in Table 4.

Short and long isoflurane high-band power display a strong increase as time under dexmedetomidine anesthesia increases with statistically significant differences in early and late data in both experimental groups (short, $p = 0.0008$; long, $p = 2.8 \times 10^{-8}$). Much of this increasing power in the high-band data is a result of the appearance of a high powered ~0.18 Hz peak in both groups occurring around the 3.75 hour time point (see Figure 6). Similarly in the broadband power, data for both short and long isoflurane

groups display a pattern of increasing power over the duration of the scanning session with both groups having highly significant differences between early and late data (short, $p = 2.23 \times 10^{-11}$; long, $p = 5.81 \times 10^{-5}$).

Intra-group analysis of center of spectral mass data reveals minor shifts over the duration of the experiment in both experimental groups (Figure 8; top left), but neither shift was significant after multiple comparisons correction. The maximum value of broadband spectral power increased significantly in both the short and long isoflurane groups over the experiment's duration; both experimental groups confirmed a statistically significant shift in data from the first half of the experiment to the second (short, $p = 5.57 \times 10^{-6}$ ; long, $p = 0.0035$). Finally, the specific frequency location of the maximum spectral power also has a general trend of shifting towards the higher frequencies as the time under dexmedetomidine increases in both experimental groups. Only the long isoflurane data exhibited a statistically significant shift in location of the maximum spectral power ($p = 0.035$).

**Seed Based Functional Connectivity**

Inter-group Analysis

Bilateral connectivity of the primary somatosensory cortex was evaluated for all rats and scans. There was a significant difference in functional connectivity (Figure 8, top right) between the short and long term isoflurane groups at only the 0.75 hour time point ($p = 0.0187$). While no other time points show a significant difference in connectivity, convergence of mean connectivity values does not occur until the 2.25 hour time point.

A visual example of functional connectivity over time is shown in Figure 9 (top). The resulting maps represent the correlation between a timecourse derived from the left primary somatosensory cortex and all other voxels within this coronal brain slice. In this example depicted in Figure 9 (long isoflurane – rat 7) functional connectivity generally increases as dexmedetomidine sedation times increases.

Connectivity between the average signal from the whole brain and each voxel in the brain was also evaluated for each rat and scan to determine anesthetic influences on whole brain connectivity. Mean global connectivity was generally stronger for all data points from the short isoflurane data as compared to the long isoflurane data; however, significant differences were only confirmed at the 0.75 ($p = 0.0319$) and 1.75 ($p = 0.0292$) hour time points.

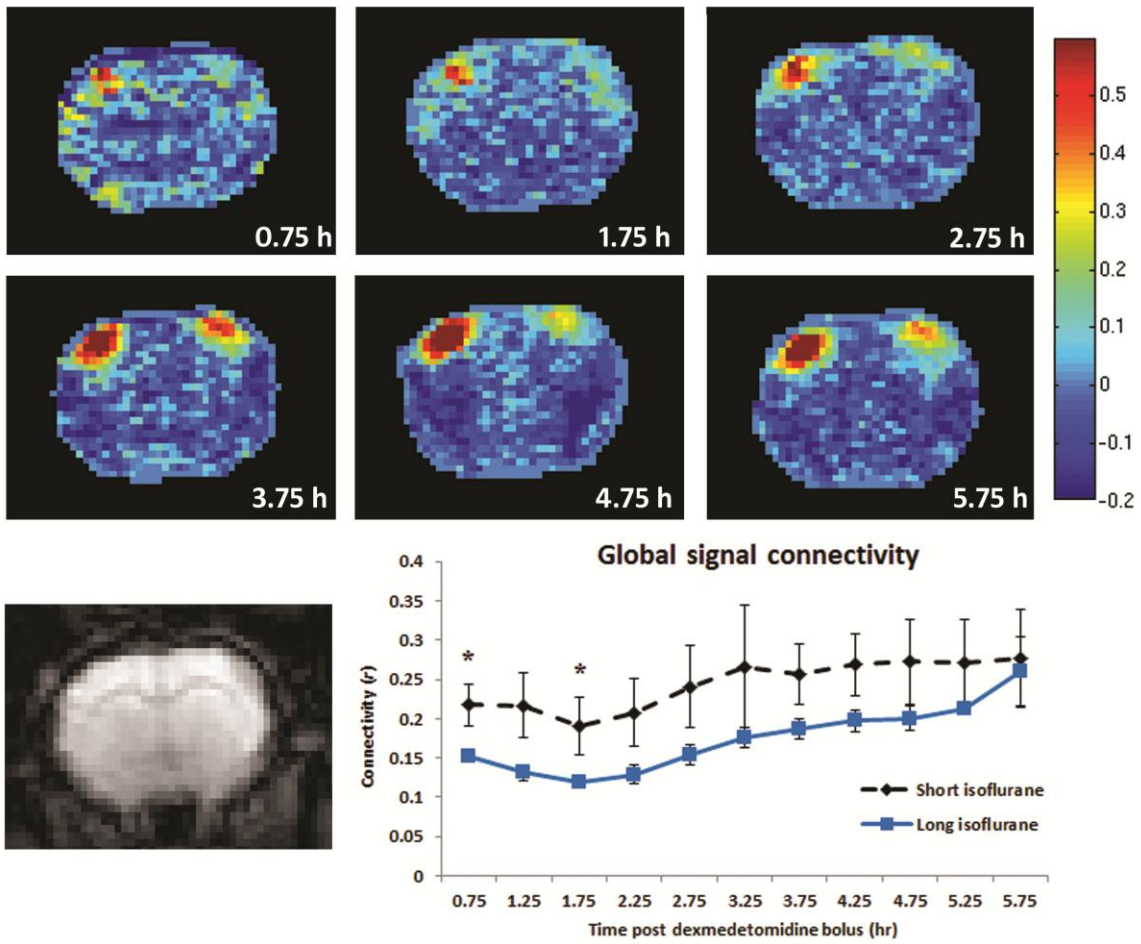


**Figure 9:** Functional connectivity spatial extent evolution. Top: Correlation maps representing functional connectivity between left SI and the rest of the coronal brain slice (coronal slice contains primary and secondary somatosensory cortices, the caudate putamen complex, and the primary motor cortices) as a function of time. The rat pictured is rat 7 from the long isoflurane group (chosen for display due to its similarity with the group correlation analysis). The strong correlation values in the left superior region represent autocorrelation with the seed time course. High correlation values in the bilaterally symmetric region on the right side of the brain represent bilateral functional connectivity. As total time under dexmedetomidine increases functional connectivity becomes more prominent, until it reaches a semi-stable state around 3.75 hours. Very little connectivity is evident before 2.75 hours. Similar trends are apparent in the group analysis of long isoflurane data as seen in the data in Figure 8. Bottom left: Single slice EPI image corresponding to functional connectivity maps above. Bottom right: Global signal connectivity is plotted as function of time for both long and short isoflurane data with no global signal regression. Significant differences in global signal connectivity between the two groups are found at the 0.75 and 1.75 hour time points.

Intra-group Analysis

Short isoflurane connectivity shifts throughout the duration of experiment but not in a monotonic fashion; SEM of recorded connectivity values increases significantly in the last 2 hours of data collection. There is no significant evolution of short isoflurane functional data over the duration of the experiment. Long isoflurane connectivity increased consistently and significantly throughout the experimental duration ($p = 0.0002$).

**Functional Connectivity's Relationship to Low-band Power**

Total low-band spectral power (0.05 – 0.149 Hz) is plotted vs. bilateral functional connectivity for both experimental groups in Figure 10. Linear regression of the short isoflurane data did not reveal linearity or significance. Long isoflurane data did indicate a linearly significant relationship between low band power and connectivity ($R^2 = 0.2635$, $p = 3.42 \times 10^{-6}$). A relationship between high-band power and functional connectivity was not significant in either experimental group. The relationship between broadband power and functional connectivity is significant in the long isoflurane data ($p = 0.0345$), but not in the short isoflurane data. A summary of these results can be found in Table 5.

**Table 5:** $R^2$, p-values, and Pearson correlation values were calculated indicating the relationship between total spectral power and functional connectivity. Significant linear relationships exist between long isoflurane data and functional connectivity in the low-band and broadband power spectra. No significant linear relationships exist between spectral power and functional connectivity in the short isoflurane data.

| | | low-band (0.05- 0.149 Hz) | high-band (0.15 – 0.3 Hz) | broadband (0.05 – 0.3 Hz) |
|---|---|---|---|---|
| Short Isoflurane | $R^2$ | 0.0002 | 0.0059 | 0.0049 |
| | p | 0.9335 | 0.6339 | 0.6646 |
| | *r* | 0.0134 | -0.0766 | -0.0698 |
| Long Isoflurane | $R^2$ | 0.2635 | 0.0066 | 0.0614 |
| | p | **$3.42 \times 10^{-6}$** | 0.4948 | **0.0345** |
| | *r* | 0.513296 | 0.08118 | 0.247817 |

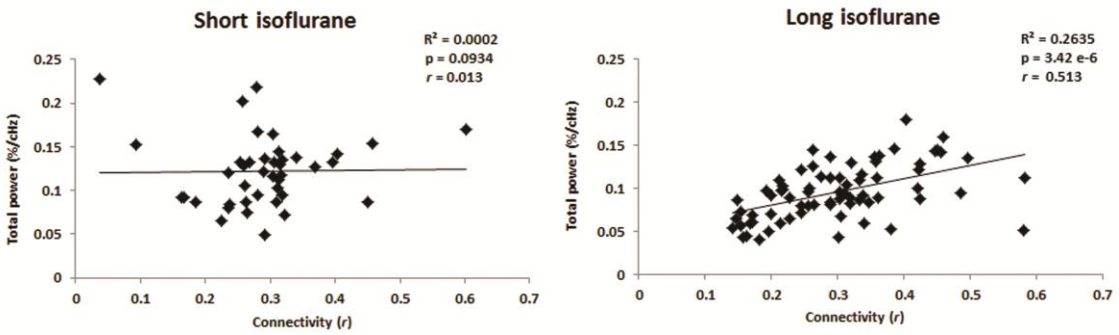


**Figure 10:** Summation of low-band power is plotted against bilateral functional connectivity for the short (left) and long (right) isoflurane groups. There is no significant relationship found between short isoflurane and functional connectivity; however, a significant linear relationship was found between the summation of low-band power and functional connectivity in the long isoflurane data.

**Spatiotemporal Dynamics**

The template resulting from spatiotemporal dynamic analysis manifests in one of two forms: largely spatially un-localized high and low correlations spread sporadically throughout the brain (Figure 11; top row – no coordinated spatiotemporal dynamics) or propagating waves of activity moving from the lateral cortex (SII) towards the medial cortex (MI) (Figure 11; bottom row – coordinated cortical spatiotemporal dynamics). The latter dynamic pattern matches the previously reported spatiotemporal pattern in the rat cortex (Majeed, Magnuson et al. 2009; Majeed, Magnuson et al. 2011).

A second output of spatiotemporal dynamic analysis is a plot of mean spatial correlation vs. the defined template. This correlation incidence analysis reveals patterns of activity which are spatially reproducible throughout the duration of the scan. Once this coordinated template is observed, it remains present throughout all subsequent scans in the study. Figure 11 shows a 4.5 second template generated from two scans occurring before the presence of strong spatiotemporal dynamics (top) and two scans occurring after the coordinated, reproducible spatiotemporal dynamics are present (bottom) in one rat (long isoflurane, rat 5). There is an obvious qualitative shift between the two states. Based on visualization, spatiotemporal dynamics are grouped as either being detectable or not detectable. The percentage of scans displaying coordinated cortical spatiotemporal dynamics is plotted for each time point and shown in Figure 12. Of note is that 50% of rats contain coordinated spatiotemporal dynamics by the 1.75 hour time point in the short isoflurane group while the 50% marker is not reached in the long isoflurane rats until the 3.25 hour time point.

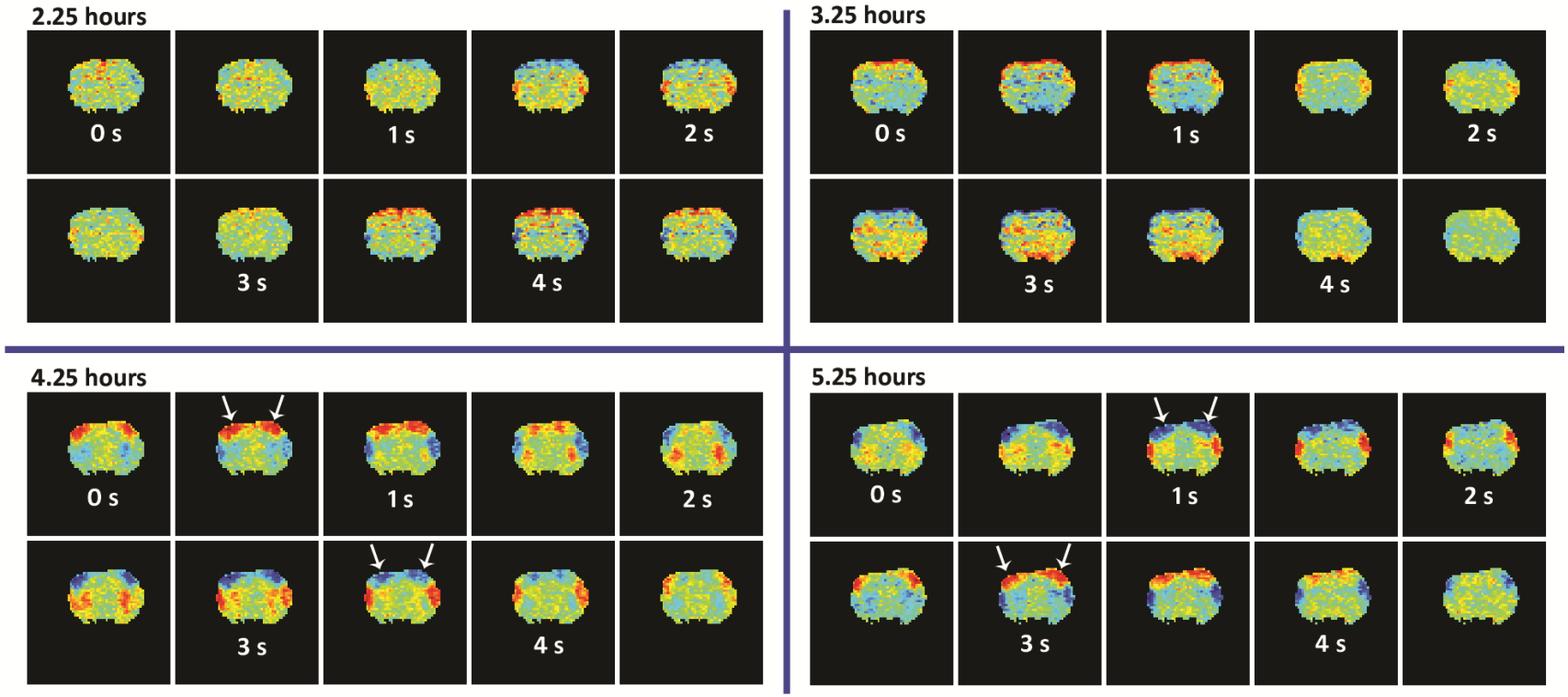


**Figure 11:** Spatiotemporal dynamic evolution. Each of the four windows contains data from a single coronal brain slice containing the primary motor and primary somatosensory cortical brain regions. Spatiotemporal dynamic templates were generated from four time points of a single rat (2.25 hours, 3.25 hours, 4.25 hours, and 5.25 hours). These templates indicate repeating patterns of hemodynamic activity occurring in space and time. Detailed information regarding the formation of spatiotemporal dynamic templates can be found in Majeed et al. (Majeed, Magnuson et al. 2009). The top row indicates the state where no visible dynamics are present, while the bottom row shows the presence of coordinated cortical spatiotemporal dynamics. For this rat (long isoflurane, rat 5; chosen for display because of its similar timing to spatiotemporal group analysis for spatiotemporal dynamic data), spatiotemporal dynamics began at 3.75 hours. High correlation values located on the edge of the brain at the 2.25 and 3.25 hour time points are likely due to slight motion or breathing effects and are present in the template as they represent the only quantified pattern in that time point data by the spatiotemporal dynamic algorithm.

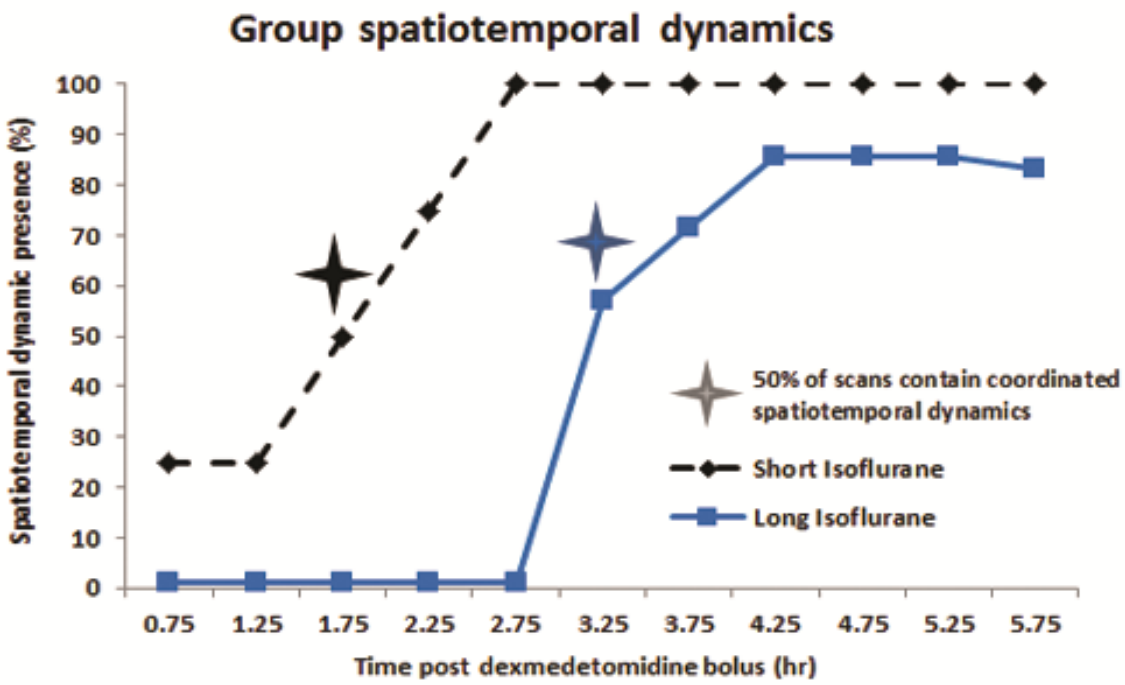


**Figure 12:** Percent of rodents with coordinated cortical spatiotemporal dynamics present for each time point recorded. Dynamics were grouped into the present and not present categories based on visual inspection of the dynamic template generated for each scan. Spatiotemporal dynamics are present in 50% of rats at the 1.75 hour time point in the short isoflurane group and 50% of rats in the long isoflurane group at the 3.25 hour time point.

**Physiological Parameters**

Heart rate, breathing rate, oxygen saturation, and body temperature over the duration of anesthesia were plotted in Figure 13. Physiological parameters all fell into acceptable ranges: Heart rate – 299 ± 2.57 beats / min; breathing rate – 79.8 ± 1.6 breaths / minute; oxygen saturation - 98.4 ± 0.08 %; body temperature - 37.2 ± 0.04 °C.

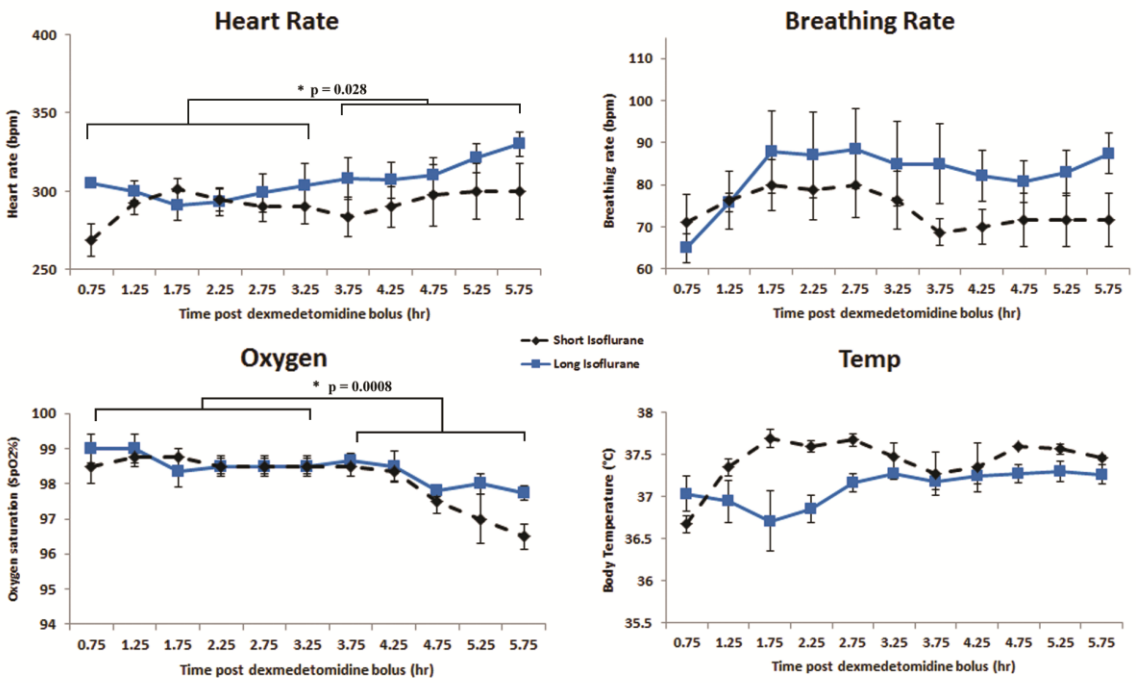


**Figure 13:** Physiological parameters are plotted as a function of total time under dexmedetomidine. Short isoflurane data is indicated by a black line while long isoflurane data is represented by a solid line. Significance was tested comparing data from the 0.75 – 3.25 hour time frame to data from the 3.75 – 5.75 hour time frame for the average of both experimental groups. There were significant differences in the group data for heart rate ($p = 0.028$) and oxygenation ($p = 0.0008$). While there are some slight modulations in the physiological data, all recorded values fell into physiologically acceptable ranges. The y-scale represents generally accepted physiological ranges for Sprague-Dawley rats under this anesthetic protocol. There were no significant differences calculated between the physiological metrics in the two groups.

There were no sudden variations in physiological parameters throughout the duration of anesthesia use, but there were sustained drifts in physiological parameters for all four metrics. Dividing physiological data into the 0.75 – 3.25 hour range and the 3.75 – 5.75 hour range, heart rate and oxygenation indicated a significant change in their physiological parameters over anesthetic duration (P-values shown in Figure 13). There was no significant change for breathing rate. Despite significant changes as a result of

anesthetic duration, all physiological parameters were maintained in expected and acceptable ranges for the entire length of the functional studies.

**Multivariate ANOVA Analysis: Resting State Metrics and Physiology**

55 (eleven rats x five functional metrics) multivariate ANOVA regression analyses were performed between four physiological metrics (heart rate, breath rate, oxygenation, and temperature) and five functional metrics (center or mass, maximum power, max location, functional connectivity, and band power) for all rats. 205 P-values (55 ANOVAs x 4 physiological parameters minus rats where specific physiology was not collected, see ANOVA section of methods) were obtained; and multiple comparisons correction was performed on the results. Three significant p-values were calculated indicating there is a statistically relevant relationship between that physiological parameter and the measured resting state metric. Heart rate is coupled with center of mass measurement in one out of eleven rats; temperature levels are significantly coupled with center of mass in one out of eleven rats and total bandpower in one out of eleven rats. No significant results were obtained for maximum power, location of that power peak, or for functional connectivity values relating to any recorded physiology based on the ANOVA analysis.

## Discussion and Conclusion

To determine the effects of an anesthesia regimen consisting of isoflurane and prolonged dexmedetomidine use we evaluate spectral components of functional BOLD activity, seed based functional connectivity, and the presence of spatiotemporal dynamics

over a five hour period of resting state fMRI scanning (0.75 – 5.75 hours post dexmedetomidine bolus). Two experimental groups were used to compare and contrast the effects of increased periods of isoflurane use prior to functional imaging and possible effects of extended durations of dexmedetomidine use. The first experimental group was anesthetized using a short period of isoflurane, 30 minutes, followed by 5.75 hours of dexmedetomidine anesthesia. The second experimental group's anesthesia regimen began with a long period under isoflurane to mimic surgical preparation, 3 hours, followed by the standard dexmedetomidine dosing for 5.75 hours. There were several significant differences between functional metrics in our two experimental groups within the first 2.75 hours of scanning; following that time point, no significant differences were found between the two groups. Both groups exhibited an evolution of the analyzed functional metrics as time under dexmedetomidine anesthesia (and time since use of isoflurane) increased. This process was more dramatic in the long isoflurane group as compared to the short isoflurane group.

Recent studies have examined the differential effects of isoflurane and dexmedetomidine on resting state functional connectivity (Hutchison, Mirsattari et al. 2010; Liu, Zhu et al. 2012; Kalthoff, Po et al. 2013). Kaltoff et al. focus on each anesthetic state separately, functional imagine is performed either under 1.5% isoflurane or standard dexmedetomidine (Kalthoff, Po et al. 2013). They reveal the marked decrease in functional connectivity and reliable generation of functional networks when isoflurane is used as compared to medetomidine. Liu et al. identify effects of variable doses of isoflurane of functional activity and discovered that under low levels of isoflurane functional networks remain intact; however, as isoflurane levels are increased, spatial

specificity of functional networks is greatly reduced (Liu, Zhu et al. 2011). In the current work we contribute an important missing link combining independent anesthetic approaches by performing two "typical" isoflurane/dexmedetomidine anesthetic protocols and evaluating the evolution of the BOLD fluctuations over time.

The primary findings of this study suggest increased durations of isoflurane use prior to functional imaging using dexmedetomidine anesthesia result in pronounced lingering effects of isoflurane that do not allow normal functional activity for multiple hours. Functional metrics analyzed from the long isoflurane data do not match those of the short isoflurane data until ~3.25 hours following the cessation of isoflurane. Short isoflurane usage prior to functional imaging exhibits early signs of functional activity depression, but they diminish quickly allowing for robust functional activity and connectivity as early at 1.25 hours following the cessation of isoflurane. Once the effects of isoflurane diminish there is a secondary effect presumably arising from the use of dexmedetomidine anesthesia that manifests as evolving functional metrics as time under dexmedetomidine increases. Experimenters using isoflurane/dexmedetomidine anesthetic regiment for functional imaging paradigms should consider isoflurane sedation length prior to functional imaging when evaluating data. They should also be aware of evolving states of functional activity, specifically the increase of high-band power and the appearance of strong ~0.18 Hz spectral peak that occur under the currently accepted method for dexmedetomidine sedation (Weber, Ramos-Cabrer et al. 2006). These findings are particularly relevant since most researchers use low-pass cutoffs of 0.08 or 0.1 Hz, based on early findings in human functional connectivity. These low frequencies do not appear to encompass the full range of the BOLD fluctuations in the anesthetized

rat, and due to the temporal evolution of the signal, functional connectivity measured at later times in the scan may appear artificially low as most of the BOLD power is above the standard cutoff frequencies.

Parsing the effects of isoflurane from the effects of extended use of dexmedetomidine is a difficult task considering overlapping variables in our experimental groups and the known lingering effects and interactions of both anesthesias; however, we can reasonably assume there are effects of each from our experimental results. Short isoflurane data has consistent low-band power throughout the duration of the experiment while long isoflurane data begins low and does not reach the power level of short isoflurane data until the 3.25 hour time point. Similarly functional connectivity in the short isoflurane data is relatively consistent throughout the duration of the experiment (although there is decreased mean and increased variation in the final hour of experimentation) while long isoflurane functional connectivity begins low and converges with the long isoflurane data around the 2.25 hour time point. Evaluating the presence of highly coordinated patterns of spatiotemporal activity in each group reveals spatiotemporal dynamics are present, on average, 1.5 hours sooner in the short isoflurane data than the long isoflurane data. A final piece of the puzzle untangling the effects of isoflurane from dexmedetomidine lies in the relationship between low-band power and functional connectivity which indicates there is no relationship in the short isoflurane data but a linear relationship in the long isoflurane data. The linear relationship between connectivity and total power in the long isoflurane data suggests a depressed functional state in the early portion of the experiment, manifesting as reduced low-band spectral power and functional connectivity that "returns to normal" as time post isoflurane use

progresses and functional metrics converge with the short isoflurane data at ~2.75 hours. This relationship is not found in the short isoflurane data suggesting that functional connectivity is minimally disrupted by the use of isoflurane prior to imaging. Each of these occurrences suggests short and long isoflurane data display differing functional activities which we can only be attributed to the difference in isoflurane anesthetic duration.

The second portion of the story involving parsing the isoflurane effects for dexmedetomidine effects lies in the similarities between the two groups. Both groups show a time locked evolution of high-band and broadband spectral power. Similarly both groups show the presence of a strong ~0.18 Hz peak appearing at the 3.75 hour time point following the cessation of isoflurane. Based on the known differential effects of isoflurane on the functional parameters we infer that this time locked functional evolution may be attributed to the effects of the dexmedetomidine either on the vascular capacity or the neural activity.

We have gained two primary insights regarding the combined use of dexmedetomidine and isoflurane: 1.) there are significant repercussions of increased durations of isoflurane use prior to dexmedetomidine on functional activity and 2.) as the effects of isoflurane subside, there are secondary functional activity effects that seemingly can only be attributed to long term dexmedetomidine use.

There was a significant difference in recorded physiological metrics between the pre- and post- 3.75 hour time points (corresponding to both the halfway point of the experiment and emergence of the ~0.18 Hz peak) for heart rate and oxygenation;

however, all measurements fell into normal physiological ranges (see physiological parameters section of results) throughout the experiment. While the variance of most physiological parameters was relatively consistent over the duration of the resting state scans, oxygenation exhibited a sudden decrease of mean signal and increased variance for the final 3 data points for both experimental groups. Interestingly most of the functional metrics recorded exhibited their greatest variance in the final three data points. Blood oxygenation is a primary influencer of the BOLD signal, and it is possible that the increased variance of the oxygenation was directly related to increased variance in the functional metrics. There were no significant physiological differences between the short and long isoflurane groups for any of the recorded time points.

Multiple regression ANOVA analysis was performed to evaluate the relationship between physiology and functional activity and revealed that body temperature shows a significant relationship with spectral center of mass as well as total bandpower calculations in one out of eleven rats. Heart rate is significantly related to the center of mass metric in one out of eleven rats. Physiological parameters show no significant correlation with the maximum spectral power, frequency location of that peak, or functional connectivity. It is not surprising that heart rate may have an influence on center of mass calculations. Based on our 2 Hz sampling rate, aliasing of the cardiac signal into the 0.01 – 0.3 Hz spectral range will occur during low heart rates (~260 bpm) and higher heart rates (~340 bpm). In these cases, heart rate has a subtle but significant impact on the center of mass of low frequency spectral power as a result of signal aliasing. It is important to note that both experimental groups were subject to similar

physiological evolutions, thus the differences between the two groups remain intact despite possible physiological influences.

Volatile anesthetics (e.g. isoflurane and halothane) are conventionally used for initial anesthetization before dexmedetomidine administration. The behavioral effects of volatile anesthetics typically wear off quickly when administration is discontinued; however, these agents are also potent vasodilators and the effects on the vasculature may persist after behavior has returned to baseline (Ohata, Iida et al. 1999). Dexmedetomidine is a vasoconstrictor and may inhibit the cerebrovascular dilation induced by isoflurane. The inverse effects on vascular walls due to the change in anesthetics may cause unstable responses in neurovascular coupling during a certain period after the anesthetic switch (Nasrallah, Tan et al. 2012). It is likely that the evolution of the ~0.18 Hz BOLD peak is related to modulations in vascular tone. In 2010 our lab reported a study comparing functional connectivity measured with BOLD and cerebral blood volume (CBV) contrast (Magnuson, Majeed et al. 2010); these results are discussed in Chapter 2 of this thesis. Interestingly a ~0.2 Hz peak presents dominantly in the low frequency spectrum for the CBV-weighted images, well before the 3.75 hour critical time point discussed in this paper for the BOLD signal peak emergence. BOLD is a composite measure of CBF, CBV, and $CMRO_2$, while an independent measure of CBV is almost entirely vascular. We infer from previous work that the CBV component of BOLD is largely associated with the ~0.18 Hz peak (Magnuson, Majeed et al. 2010). Because of the timing of the emergence of this peak, 3.75 hours following isoflurane use and the beginning of dexmedetomidine use, we assume dexmedetomidine is the primary

culprit as opposed to isoflurane whose dosing is variable between groups and appears to wear off by the ~3.25 hour time point.

While we have grouped the presence of spatiotemporal dynamics in a Boolean fashion, quantitative analysis of the templates (unpublished work) suggest that there is a period of time where the dynamics are in an in-between state; the dynamics are beginning to occur, yet we cannot clearly visually detect them. For the purpose of this paper, visual determination of an on or off current dynamic state is adequate for evaluating normal and depressed functional sates.

Ideally anesthetized rodents should be in a condition as close to the "normal functioning" awake state as possible; however, defining normal activity is not an easy task. In this work we have discovered that lingering effects of isoflurane have a significant effect on functional activity and persist after cessation of isoflurane at a length corresponding to the initial isoflurane anesthetic length. Similarly we have uncovered an interesting phenomenon of a strong ~0.18Hz peak which dominates the low frequency spectrum beginning 3.75 hours into the scanning period that should be explored in more depth.

This work focuses on the anesthetic protocols presented by Pawela and Weber, specifically the influences of the length of time under isoflurane prior to the switch to dexmedetomidine (Weber, Ramos-Cabrer et al. 2006; Pawela, Biswal et al. 2009). Secondly our results show an evolution of functional activity independent of the isoflurane use and are likely a result of prolonged dexmedetomidine usage. Potentially confounding factors could be addressed with pharmacological intervention, change in

dexmedetomidine dosage, or using an anesthesia other than isoflurane for induction; however, that is the topic of further work. Researchers using isoflurane induction followed by dexmedetomidine in the rat model should utilize caution in interpreting functional data acquired in the first hour after isoflurane is discontinued when using short isoflurane lengths (< 30 minutes) and as long as 3.25 hours when using longer durations (3 hours) of isoflurane prior to the switch to dexmedetomidine. When making comparisons between subjects, it is imperative that data has experienced similar anesthetic paradigms at the time of functional recording.

# CHAPTER 4

# EFFECTS OF COMPLETE SEVERING OF THE CORPUS CALLOSUM ON COHERENT ELECTRICAL AND HEMODYNAMIC INTERHEMISPHERIC FUNCTIONAL BRAIN NETWORKS IN THE RODENT MODEL

## Why the Split-brain Model for Probing Functional Brain Networks?

Coordinated spontaneous oscillations in functional networks have been well characterized and confirmed across modalities and models including EEG (Mantini, Perrucci et al. 2007; He, Snyder et al. 2008; Hlinka, Alexakis et al. 2010), fMRI (Biswal, Yetkin et al. 1995; Keilholz, Silva et al. 2006; Vincent, Patel et al. 2007; Fox, Zhang et al. 2009; Chang and Glover 2010; Magnuson, Majeed et al. 2010), MEG (de Pasquale, Della Penna et al. 2010; Liu, Fukunaga et al. 2010; Brookes, Hale et al. 2011), voltage sensitive dye (VSD) (Carlson and Coulter 2008; Mohajerani, McVea et al. 2010) and multimodal approaches (Nir, Fisch et al. 2007; Srinivasan, Winter et al. 2007; Xu, Olivas et al. 2010 Shmuel, 2008 #156; Pan, Thompson et al. 2011). These functional networks are thought to reflect coordinated neural activity between spatially distinct cooperating brain areas that facilitate efficient processing (Fox, Snyder et al. 2005) specifically on complex tasks requiring bilateralization (van der Knaap and van der Ham 2011). Functional networks in monkeys and humans examined with fMRI are primarily localized to the ultra-low (< 0.1 Hz) frequency range (Biswal, Yetkin et al. 1995; Cordes, Haughton et al. 2000; Hampson, Peterson et al. 2002; Fox, Zhang et al. 2009; Majeed,

Magnuson et al. 2009), while neural and MEG functional network correlates are found throughout the 0 – 100 Hz range (He, Snyder et al. 2008). The relationship between coordinated blood oxygen level dependent (BOLD) activity and the correlated electrical activity seems largely dependent on the network being examined (Mantini, Perrucci et al. 2007). Pan et al.'s simultaneous fMRI-electrophysiological work reveals a direct correlation between low frequency BOLD oscillations and the power envelope of broadband neural activity in the same frequencies (0.01 – 0.25 Hz) (Pan 2013). While we have a firm understanding of the "whats" as it relates to classifying functional networks, we must focus on the "hows" and "whys" with the purpose of providing order to the complexities of the working brain. Elucidating mechanisms by which functional networks operate is a vital step towards this goal.

Functional networks commonly contain bilaterally symmetric anatomical components suggesting the possible role of callosal pathways in mediating functional networks. Callosotomies were performed before 1940 to treat patients with intractable epilepsy (Van Wagenen 1940); the results indicated that the procedure seemed to reduce epileptic seizures in many cases. Behavioral implications of the split brain model have since been evaluated in models including cats (Myers 1956; Myers and Sperry 1958), monkeys (Gazzaniga 1966), and humans (Brazdil, Brichta et al. 1997; Johnston, Vaishnavi et al. 2008) revealing the importance of the corpus callosum for bi-hemispheric exchange of motor, sensory, gnostic, and perceptual information (Paul, Brown et al. 2007). Generalizing the current body of work reveals that for simple tasks the split brain is capable of performing normally; however, as the complexity of the task increases, requiring recruitment of both hemispheres, performance is severely impacted

(Banich and Belger 1990; Belger and Banich 1998; Brown, Jeeves et al. 1999; Weissman 2000). The corpus callosum's role in providing a route of communication between the hemispheres is apparent from these works.

The corpus callosum is a dense collection of myelinated and unmyelintated axons, 1.9e8 in humans (Tomasch 1954) and 1.2e7 in rats (Gravel, Sasseville et al. 1990), providing homotopic and hetero-homotopic projections linking the two hemispheres of the brain. From a physiological perspective there is contention as to the pathway by which the corpus callosum mediates functional connectivity. One school of thought suggests an inhibitory role of the corpus callosum (Cook 1984; Banich and Belger 1990) while the more widely accepted theory advocates an excitatory role of the corpus callosum (Dorion, Chantome et al. 2000; Rattenborg, Amlaner et al. 2000); however both theories allow for selective lateralization (or unilateral hemispheric domination) of cortical activation as a function of the callosal pathways (van der Knaap and van der Ham 2011).

Bilateral functional connectivity has been assessed in the split brain human model using fMRI; in all cases epileptic patients were evaluated. Johnston et al. collected resting state fMRI before and after a complete sectioning of the corpus callosum, revealing a prominent reduction in interhemispheric functional connectivity while intrahemispheric connectivity remained relatively intact during the immediate post-operative period (Johnston, Vaishnavi et al. 2008). A similar study by Pizoli et al. evaluating connectivity before and after a two-thirds corpus callosotomy that interestingly resulted in improved BOLD and EEG bilateral functional connectivity (from highly uncoordinated and

sporadic to coordinated and near normal) evaluated one day post and four months post-surgery respectively (Pizoli, Shah et al. 2011).

Montplasier et al. evaluated EEG bilateral functional connectivity during stage II and REM sleep before and after partial callosotomies in two patients (Montplaisir, Nielsen et al. 1990). The work indicated significant reductions in bilateral coherence across frequency bands that accurately reflected the degree of anatomical sectioning. This anatomical-connectivity relationship was confirmed in another EEG study evaluating three epileptic patients pre- and post-surgery revealing profound decreases in bilateral connectivity following the sectioning (Brazdil, Brichta et al. 1997). Conversely Corsi-Cabrera and colleagues presented EEG analysis of a single patient with a partial callosotomy before and after surgery and distinguished only minor, non-significant changes in bilateral connectivity (Corsi-Cabrera, Trias et al. 1995). Later work by the same group indicated a decrease in bilateral EEG coherence following callosal sectioning; however, connectivity was still present and fluctuated depending on the wakeful state (Corsi-Cabrera, Ondarza et al. 2006).

The results of the human split-brain studies in epileptic patients are equally interesting and incongruent, highlighting the need for controlled studies in healthy subjects where experimental variabilities are reduced, while the number of subjects is increased. In the present study we expand on the current body of functional network and split brain work by evaluating bilateral functional connectivity in the somato-motor network of the split brain rat model using consecutive fMRI and electrophysiological recordings. The focus therefore shifts singularly to the role of the corpus callosum in

modulating functional networks as opposed to the copious variability associated with clinically and functionally complicated epileptic patients.

While fcMRI shows promise as a clinically useful tool, researchers still do not fully understand the physiological or functional basis of coherent slow wave oscillations. This work provides two important insights. We explore the neural correlates of functional connectivity MRI by directly comparing bilateral fMRI connectivity to the analogous electrophysiological bilateral connectivity in the split brain rodent model. This experiment provides a unique platform to evaluate the coupling between electrophysiological and BOLD signals on the network level. Secondly we further probe the role of the corpus callosum, the primary interhemispheric neural pathway, in facilitating functional connectivity using multimodal functional recordings.

## Methods

### Animal Preparation and Physiological Monitoring During Callosotomy Surgery

All experiments were performed following the guidelines set by the Institutional Animal Care and Use Committee (IACUC) at Emory University. Ten male Sprague-Dawley rats (200-300 g) were initially anesthetized in an anesthetic chamber filled with a mixture of isoflurane and oxygen. Rats were divided into two groups; five rats were in the full callosotomy group and five rats were in the "sham" callosotomy group. Once the rat was anesthetized, he was moved to a stereotaxic head holder (Harvard Apparatus) and secured with a bite bar and ear bars. The rat was supplied with 2 – 2.5 % isoflurane (depending on anesthetic needs, physiology determined) mixed with oxygen, while

undergoing initial experimental setup and the succeeding surgery. Body temperature was monitored and maintained at ~ 36° C for the duration of the surgery to keep vasodilation to a minimum. The right femoral artery with catheterized to allow for monitoring of blood pressure.

Fur was removed from the top of the rodent's head using an electric shaver followed by the use of a liquid hair removal product to remove the remaining hair. Optical ointment was applied to each eye to prevent corneal drying throughout the duration of the experiment. All rats were checked for response to a toe pinch before beginning surgery. An incision was made along rostral-caudal midline (bregma +5mm through -10mm) through the skin and muscle to expose the skull. Skin and muscle was carefully retracted to reveal skull areas containing the bregma and bilateral primary somatosensory areas, 4mm lateral and 1mm rostral from bregma. A low temperature cauterizer was used to stop any bleeding from the skull.

**Cranial Window**

The next step was to create a cranial window for performing the callosotomy. Using a fine-tipped drill (Omni-Drill35; World Precision Instruments) a rectangular section of the skull was shaved until the dura was reached. Drilling was performed while viewing the skull through a 5x binocular microscope. The cranial window extended in the rostral-caudal direction from +2mm to -5mm from the bregma, and laterally the window extended from 0 mm toward the right side of the skull to +2 mm from bregma (Figure 14). Once the dura was visible it was carefully pierced and sliced along the entire rostral-caudal cranial window using a 27 gauge needle; care was taken to avoid slicing vessels.

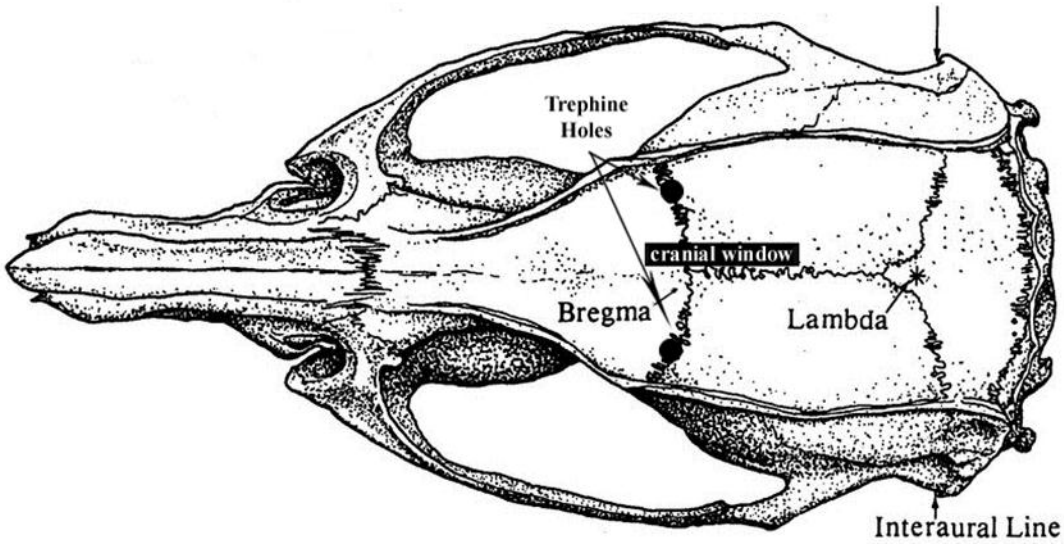


**Figure 14:** Rat skull structure indicating the cranial window and trephine holes.

**Callosotomy**

A knife was fashioned using 316 stainless steel wire with an outer diameter of 0.33 mm. 40mm of wire was used for creation of the knife with 3mm at one end bent using forceps to a 90° angle. A 5x binocular microscope was used to view the 3mm edge of the knife. Using a fine grained triangular hand file steel was removed at a 45° angle on opposite sides of the knife to form a sharpened 'V' on the leading edge of the knife. Similarly material was filed away from the back edge of the knife to form a second V, leaving a diamond shaped section of wire 5mm in length perpendicular to a 35mm section of undisturbed wire.

Once the wire was sharpened, the 35mm edge of the knife was lightly covered in Superglue® and inserted into a section of a 23 gauge needle, with the sharp needle portion removed. 6mm of the wire, adjacent to the 90° bend, was left protruding from the

needle while the other 29mm was encapsulated by the needle. The purpose of this was to reinforce the long section of the knife which would be attached to a micromanipulator resulting in a minimization of deflection during the cutting process described below.

The wire knife was attached to the long arm of a micromanipulator integrated with the head holder system (Harvard Aparatus). The knife was positioned such that the end of the short side of the knife was facing in the rostral-caudal plane with the free tip pointing caudally. The manipulator was tilted to an angle of 10° such that the tip of the free end of the knife was pointing slightly upward. The 10° angle was implemented such that the cutting edge of the knife was parallel to the direction of the corpus callosum. The knife was positioned rostral-caudally to +2mm from bregma and 1mm laterally to the right of bregma (for one full callosotomy rat, the corpus callosum was sliced on the left side) and lowered to the brain surface. The micromanipulator was moved in one of two manners to create either a full callosotomy or a sham callosotomy, making up the two experimental groups.

**Full Callosotomy**

The manipulator arm was moved in the following manner from the surface of the brain beginning @ +2mm rostral and +1mm laterally right of the bregma with a 10° rostral tilt: 1.) 4.82mm into the brain (ventral) 2.) 1mm out (dorsal) 3.) 1mm caudal 4.) 0.5mm dorsal 5.) 1mm caudal 6.) 0.5mm dorsal 7.) 1mm caudal 8.) 0.5mm dorsal 9.) 1mm caudal 10.) 0.5mm dorsal 11.) 2.41mm caudal 12.) 0.35mm ventral 13.) removed dorsally. The surgical process is depicted in 7 steps in Figure 15.

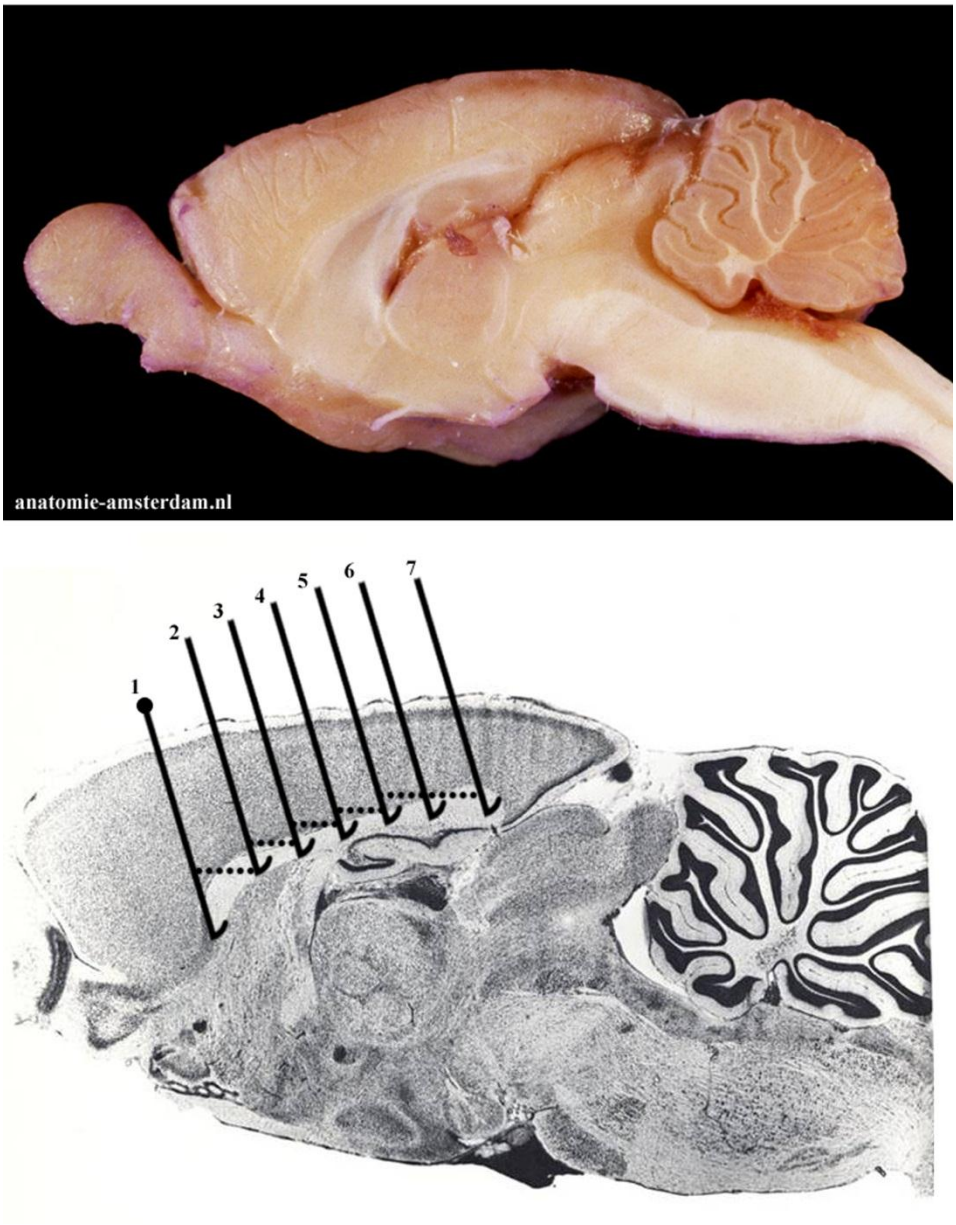


**Figure 15:** Fresh sagittal tissue slice clearly displaying the corpus callosum (top). The bottom window indicates the seven surgical steps that result in severing of the corpus callosum.

**Sham Callosotomy**

Beginning at +2mm rostral and +1mm laterally right of the bregma, in order to create a sham callosotomy, the micromanipulator was adjusted nearly identically to the

full callosotomy model. The only difference was at step 1 (described in the previous paragraph), the manipulator was adjusted ventrally 3.1mm as opposed to 4.82mm to avoid reaching to the depth of the corpus callosum. 0.5 mm of "buffer space" was built in to the sham paradigm to account for slight variability in brain size to ensure the corpus callosum was not affected. All other manipulations are identical to the full callosotomy paradigm and occur in the same order.

Following the callosotomy or sham callosotomy, light pressure was applied using gauze until bleeding ceased. A map of the rat's vascular structure is presented in Figure 16. Vascular disruption was centralized to the right superior cerebral vein. Mineral oil was used to fill the cranial window, providing a barrier against excessive drying of surface brain tissue. The rat was then removed from the head holder and placed into an anesthetic chamber lightly filled with isoflurane to allow transfer to the imaging suite.

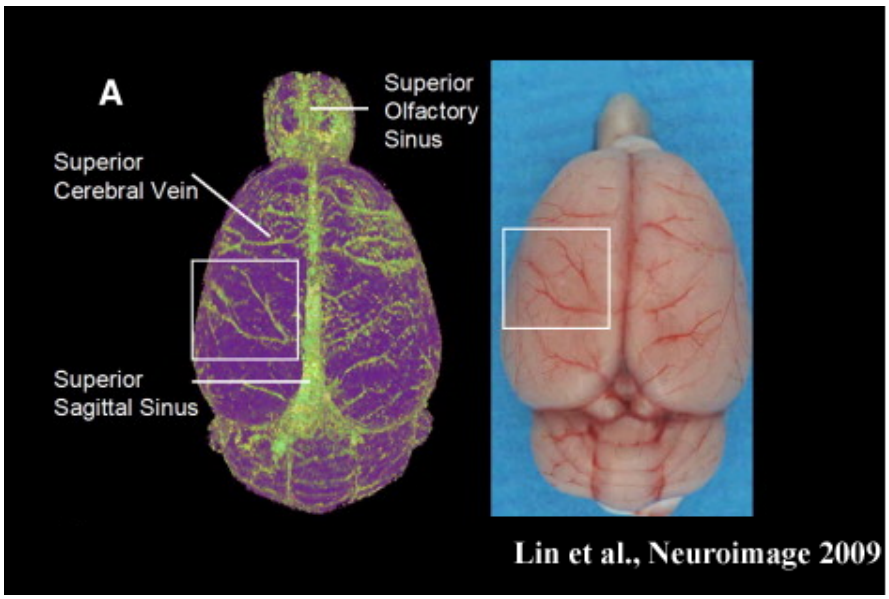


**Figure 16:** Rat vascular structure. Modified from Lin et al. (Lin, Lin et al. 2009).

**fMRI setup**

The rat was transferred from the anesthetic chamber to a plastic MRI cradle (Bruker, Billerica, MA), where his head was fixed in place using a bite bar and ear bars. Isoflurane was continued at 2% throughout the duration of the fMRI setup with slight modulations based on physiological state. Heart rate and oxygen saturation were monitored and recording using a pulse oximeter placed on the left rear forepaw. Body temperature was monitored and recording using a rectal thermometer; temperature was maintained at ~37° C using an adjustable temperature warm water circulation system. Respiratory rate was monitored using a pressure-sensitive balloon placed directly under the rat's chest. Colgate toothpaste was applied onto the skull surface to mimic the properties of the previously removed muscle. Major distortions are present in the EPI images from susceptibility artifacts induced due to the brain/air interface; the toothpaste alleviates these artifacts (Lewin J.S 1995). Following application of the toothpaste, eye ointment was reapplied and a 2cm Bruker surface receive coil was taped to the coil directly above the rat's head.

Once setup was complete a subcutaneous bolus of 0.025 mg/kg of dexmedetomidine (Dexdomitor, Pfizer, Karlsruhe, Germany) was delivered to the rat's upper right leg; isoflurane was discontinued 5 minutes after the dexmedetomidine bolus. Total time under isoflurane was approximately 4 hours at the time of the switch to dexmedetomidine (total time under anesthesia was matched between the full and sham groups). Dexmedetomidine is used as an alternative to isoflurane for functional imaging because it causes less burst suppression and a sedated effect (Nelson, Lu et al. 2003) as opposed to a highly anesthetized state (Nakao, Itoh et al. 2001). Fifteen minutes post-

bolus a subcutaneous infusion of 0.05 mg/kg/hr dexmedetomidine was initiated; the drug was delivered through a 27 gauge butterfly needle inserted subcutaneous and attached to the rat's upper right leg. ~90 minutes following the initial bolus, dexmedetomidine was increased to 3x the original infusion dose for maintenance of anesthetic depth (Weber, Ramos-Cabrer et al. 2006; Pawela, Biswal et al. 2009).

**Image Acquisition**

All MRI images were acquired using a 20cm horizontal bore 9.4 T Bruker BioSpec magnet equipped with an actively shielded gradient coil with 20 G/cm gradient strength and rise time of 120 μs. The Bruker BioSpec was controlled using an AVANCE console (Bruker, Billerica, MA). An actively decoupled cross-coil imaging setup was used which included a 7cm volume coil for RF transmission and a Bruker built 2cm surface coil for signal reception (Bruker, Billerica, MA).

Initially automatic adjustment of shimming, basic frequency, transmit power, and receiver gain was performed; following these adjustments a FLASH image was acquired in three planes. Based on the FLASH image a single 2 mm slice was positioned over the primary somatosensory cortex (SI) based on known anatomical markers. A high resolution rapid acquisition with relaxation enhancement (RARE) image (TR = 5s, TE = 17.5, Averages = 4, Resolution = 100 μm in-plane) was acquired in over 20 0.5mm slices positioned perpendicularly to the length of the callosotomy to obtain an image displaying the efficacy of the surgery and possible influences to surrounding anatomy.

Following the RARE acquisition, shimming was performed on the single slice of interest to obtain maximum SNR and spatial homogeneity. Approximately one hour

(Full- 1.1 ± 0.06 hours Sham- 1.2 ± 0.12 hours) following the dexmedetomidine bolus and cessation of isoflurane use, the first resting state functional image was acquired with the following parameters: single-shot gradient echo EPI, Repetitions = 1000, TR = 500ms, TE = 15ms, total scan time = 8 minutes 20 seconds, number of slices = 1, slice thickness = 2mm, FOV = 2.56cm × 2.56cm, matrix size = 64 × 64. A resting state scan with the listed parameters was collected every 15 minutes for 2 hours; eight total resting state images are obtained. Following the final resting state scan, isoflurane was turned back on at ~2% mixed 1:1 with oxygen and room air. The rat was removed from the scanner and the MRI cradle, dexmedetomidine was discontinued and isoflurane anesthesia was once again induced. The rat was returned to the mobile anesthetic chamber and transported to the procedure room for further surgery and electrophysiological recording.

**Trephine Holes and Electrophysiology**

The rat was once again placed in the stereotaxic head holder. Toothpaste was removed from the skull and the area was thoroughly cleaned cleaned. Two holes are opened, one on the left side and one on the right side of the skull 4mm lateral and 1mm rostral to the bregma using a fine tipped drill (Omni-Drill35; World Precision Instruments) while viewing through a 5x binocular microscope. Skull bone was shaved down slowly and carefully until the dura was revealed. Each hole measured ~1.5 mm in diameter. Surface brain vessels are visually identified, and the tip of a 27 gauge needle is used to pierce the dura away from the vessels to allow for insertion of the microelectrodes. Microelectrodes were fabricated from borosilicate using a micropipette

puller (PE-2, NARISHIGE), to form a tip ~10 µM in diameter, allowing for local field potential recordings.

The electrodes were filled with a sodium chloride solution resulting in an impedance of 1-5 MΩ measured at 1 KHz. Two separate stereotaxic arms were used to hold the electrode over the holes; the electrodes were angled 30 degrees laterally and lowered to a depth of ~1mm directly into the primary somatosensory cortex. The recorded electrode signal was checked for noise and signal inflection direction. The signal ground was inserted under the skin of the caudal portion of the surgically opened area (several ground locations were tested, and this area provided the most consistent reduction in background noise).

Following electrode insertion, a bolus of 0.025 mg/kg of dexmedetomidine was once again delivered to the rat's upper right leg. Five minutes post bolus, isoflurane was discontinued. Fifteen minutes after the bolus, an infusion of 0.05 mg/kg/hr dexmedetomidine was started and delivered through a subcutaneously inserted butterfly needled attached to the upper right leg.

Approximately 45 minutes following the switch to dexmedetomidine (Full - 0.7 ± 0.2 hours; Sham- 0.7 ± 0.2 hours), eight resting state recordings of right and left primary somatosensory activity were obtained. Sampling was acquired at a rate of 12 KHz and five minutes of data was obtained for each scan. Scans occurred in 10 minute intervals until eight scans were collected.

Following the final resting state electrophysiology scan, electrodes were removed from the brain, dexmedetomidine was discontinued and the rat was returned to the isoflurane filled anesthesia chamber.

**Histology**

Perfusion was performed on the first three rats from each experimental group using 4% formaldehyde and phosphate buffered saline. Brains were removed and then allowed to saturate for 24 hours in a mixture of formalin and 15% sucrose; brains were then moved to a solution of 30% sucrose and formalin for an additional 24 hours. Following this saturation period, brains were frozen and sliced in 250 µM coronal slices using a microtome perpendicularly to the length of the corpus callosum. 4x microscope images were acquired and histological evaluation was performed to confirm experimental success (severing or non-severing of the corpus callosum). Histological classification was then matched with the corresponding RARE MRI images. Five MRI researchers familiar with rat brain anatomy performed blinded classification of experimental methods (sham or full callosotomy) using only the RARE MRI data to determine if accurate evaluation of experimental success was possible without the need for histology.

**Data Analysis**

Comparisons were made between the sham callosotomy and full callosotomy experimental groups by evaluating band limited and broadband electrophysiological bilateral connectivity, fMRI seed based bilateral connectivity, and whole brain spatiotemporal dynamic activity in the fMRI data. All data was processed and evaluated using code written in MATLAB (MathWorks, Natcik, MA).

fMRI

Each resting state scan was 8 minutes and 20 seconds and was prepared with 20 dummy scans, allowing for transient signal intensity fluctuations to dissipate before acquiring data. Preprocessing was the first step in preparing data for analysis. Whole brain signal was regressed from all data sets followed by quadratic detrending. A bandpass filter was then applied using a finite impulse response filter between frequencies of 0.01 – 0.3 Hz with a 100 second filter window length (1/ minimum evaluated frequency). Following filtering data were normalized to unit variance by subtracting the mean and dividing by one standard deviation for all image voxels, allowing for comparison to be made between rats. Data sets were masked to excluded information from tissue outside of the brain.

Seed regions of interest (ROI) were selected manually in the primary somatosensory cortex (SI), secondary somatosensory cortex (SII), and the caudate/putamen (CP) complex in the opposite hemisphere from the callosotomy procedure. Normalized cross correlation was calculated between functional timecourses generated from the seed region and all other voxels in the brain. Connectivity values ($r$) from the 15 most correlated voxels from contralaterally analogous region were transformed to Z-scores and averaged, representing bilateral functional connectivity strength. Average values for SI, SII, and CP bilateral connectivity were calculated for both experimental groups. Two-tailed, unpaired $t$-tests were performed between the sham and full callosotomy groups for each seed time course. Change in shared variance was calculated between the two groups [$(r^2_{sham} - r^2_{full}) / r^2_{sham}$] (Johnston, Vaishnavi et al. 2008).

A pattern finding algorithm first implemented by Majeed et al. was used to evaluate the presence of reproducible patterns of low frequency spatiotemporal dynamic activity manifesting as waves of high and low coordinated activity propagating through the cortex (Majeed, Magnuson et al. 2009; Majeed, Magnuson et al. 2011). The algorithm functions by selecting a chunk of consecutive images of specified length (5 seconds; 10 repetitions) chosen at a random start point in the data set. Sliding correlation was performed between the image chunk and the entire preprocessed image series. Time points of high correlation between the original chunk and the image series are averaged together to create a new template that represents a repeating spatial and temporal pattern of functional activity. Sliding correlation was then performed with the new template and the original data set, and time segments of high correlation are once again averaged. This process repeats until convergence of the template occurs. The resulting template reveals the presence or non-presence of spatiotemporal activity patterns. Templates are visualized on a blue to red color scale (blue – low, red-high, Matlab colorbar "jet") representing the strength of the finalized template. Final spatiotemporal dynamics templates are categorized into one of three groups: no dynamics, bilaterally symmetric dynamics, or unilateral dynamics. Detailed explanation of this algorithm and the underlying theory can be found in the Majeed et al. papers (Majeed, Magnuson et al. 2009; Majeed, Magnuson et al. 2011).

Electrophysiology

Band-limited power (BLP) timecourses were created for six well characterized electrophysiological frequency bands: delta (1-4 Hz), theta (4-8 Hz), alpha (8-14 Hz), low-beta (14-25 Hz), high-beta (25-40 Hz), and gamma (40-100 Hz). To calculate BLP

power, a specified window length (delta and theta – 2 seconds; beta and gamma – 0.5 seconds) was used to generate a representative spectrogram by performing an FFT of the raw timecourse. Mean power within the band of interest was calculated. The window was then shifted in 0.5 second intervals and mean BLP was calculated for each window shift until the entire electrophysiological run had been evaluated. Windows for delta and theta band were overlapped by 75%; no overlap occurred for the theta, beta, or gamma band calculations. Raw time courses were also directly filtered between the broadband ranges of 0 - 100Hz.

Following BLP calculations and broadband power filtering, Pearson correlation was calculated between data from the left and right electrodes (positioned in bilateral SI) using all six BLP timecourses and the broadband filtered data sets from each rat. Resulting correlation values were z-transformed and finally two-tailed, unpaired, student t-tests were performed between z-scores in each band between the sham and full callosotomy groups. Change in shared variance was calculated between the two experimental groups for each band.

Multiple Comparisons

Bonferroni correction was used to correct for possible Type I errors (false positives considered significant). Two families were evaluated: BOLD comparisons and electrophysiological comparisons. There were three P-values in the BOLD family and eight 7-values in the BOLD family. All values described as significant in the work have based Bonferroni multiple comparison correction.

## Results

In this work we evaluate BOLD and electrophysiological bilateral functional connectivity in rats with either a complete sectioning of the corpus callosum or a sham surgery in which the corpus callosum was left intact. Group averages of temperature, heart rate, breathing rate, and oxygenation can be found in Table 6.

**Table 6:** Physiological measurements. Temperature, breath rate, heart rate, and $Sp0_2$% were calculated for both the sham and full callosotomy groups. Mean and SEM values are presented for each group.

| | Temperature (°C) | Breath Rate (bpm) | Heart Rate (bpm) | Oxygenation ($Sp0_2$%) |
|---|---|---|---|---|
| **Sham** | 37.01 ± 0.22 | 72 ± 8.79 | 315.63 ± 12.18 | 98.44 ± 0.89 |
| **Full** | 37.37 ± 0.17 | 73.98 ± 4.81 | 335.50 ± 7.29 | 99.33 ± 0.16 |

### Experimental Classification

Histological evaluation of the effectiveness of the surgical procedure was carried out for the first three rats from each group. Surgeries were successful for all six rats resulting in minor variations in cut depth (± 0.2 mm) with relation to the corpus callosum over the rostral caudal plane; however, for all six rodents the corpus callosum was either fully severed or remained intact. Five MRI researchers familiar with MRI data examined high resolution RARE images (blinded to the histological findings) and were able to classify the images into the correct experimental group (matching histology) with 98.7% accuracy (148/150 correct). An example of the matched RARE images and the

corresponding histology are shown in the top row of Figure 17. Accurate surgical procedures were confirmed based on RARE images in the final 4 rats where histology was not performed. Slices from the five sham rats (Figure 17 - left) and six full callosotomy rats (Figure 17 - right) reveal the success of both experimental procedures.

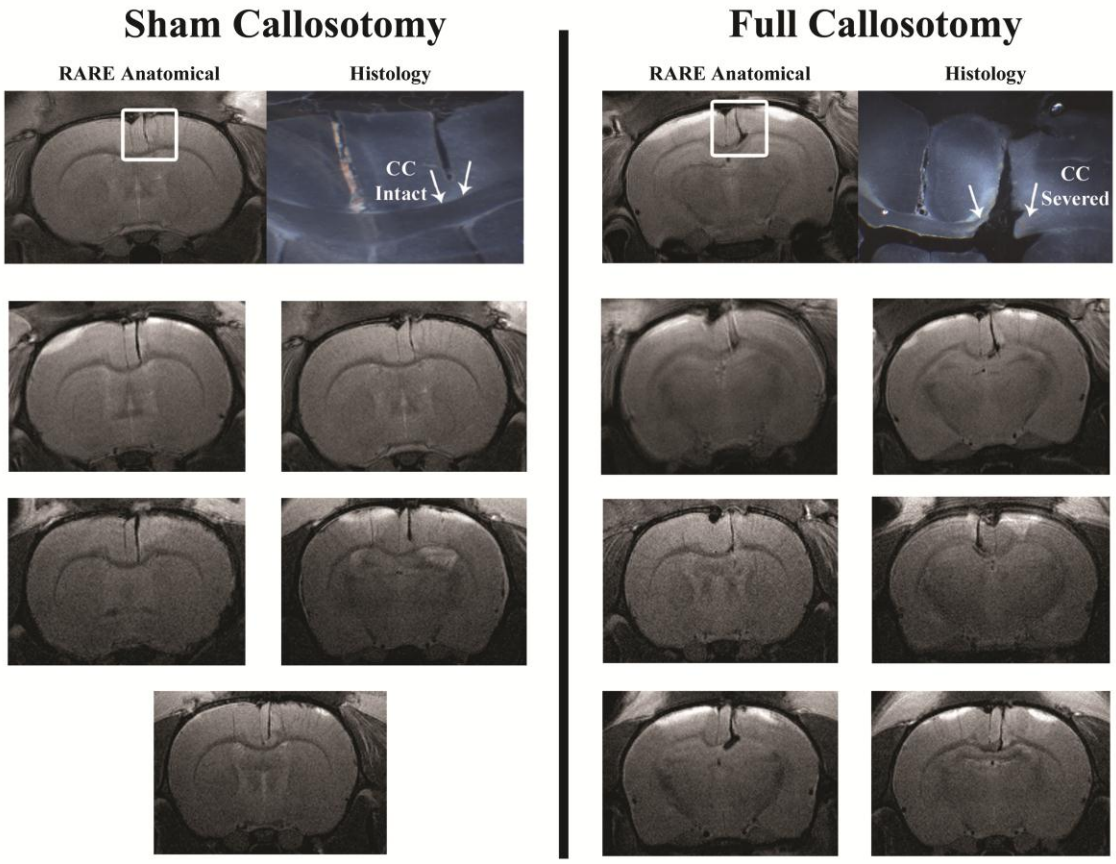


**Figure 17:** RARE images and histology. Single slice RARE MRI (matching functional recording slice) data is shown for all five rats in the sham callosotomy group and all six rats in the full callosotomy group. A single matched RARE-histological confirmation is also shown for both experimental groups. These images confirm a clear distinction and success of two experimental groups; one where a full callosotomy is performed and another where equal gray matter is severed, but the corpus callosum remains intact.

Data Exclusion

All eleven rats were used for evaluation of the fMRI data; however, data from entire rats were excluded from the electrophysiological analysis. An incorrect amplifier setting resulted in complete saturation of a single electrode in one rat, and no data was recorded for that electrode; electrophysiological data from this rat was not used. Additionally, a rat was excluded from both the sham and full callosotomy results based on persistent data anomalies. All bilateral correlation values for all bands are plotted for both experimental groups in Figure 18. Included data is shown in solid gray while the excluded data is shown in a striped red color. More than 10% of data points recorded for both excluded rats resulted in a value greater than 2 standard deviations from the band-limited mean. Interestingly, the raw data time courses from the two excluded rats exhibited opposing baseline polarities, while all included rats timecourses shared a directional baseline polarity. Visual examination of all raw data sets resulted in the removal of two additional scans from one rat as major artifacts were present in data from both electrodes resembling a jostling of the electrode wires.

fMRI

ROI positioning and the resulting correlation maps are shown in Figure 19 for the sham and full callosotomy groups. The connectivity maps in Figure 19 are from individual rats, but illustrate approximately the group averages for each ROI. Figure 20 indicates average connectivity values for the sham and full callosotomy groups at each evaluated ROI; error bars represent squared error of the mean (SEM). Connectivity between bilateral low pass filtered (0.01 – 0.3 Hz) BOLD data revealed higher mean connectivity values in the sham group for primary and secondary somatosensory cortices

as well as the caudate putamen complex as compared to the full callosotomy group. Statistically significant differences in functional connectivity were found between the sham and full callosotomy group for all three seed regions evaluated. Shared variance was reduced after a full callosotomy as compared to the sham callosotomy by 51.7%, 41.7%, and 43.9% in SI, SII, and CP respectively. A summary of group means, SEMs, p-values of statistical comparisons, and decreases in shared variance can be found in Table 7.

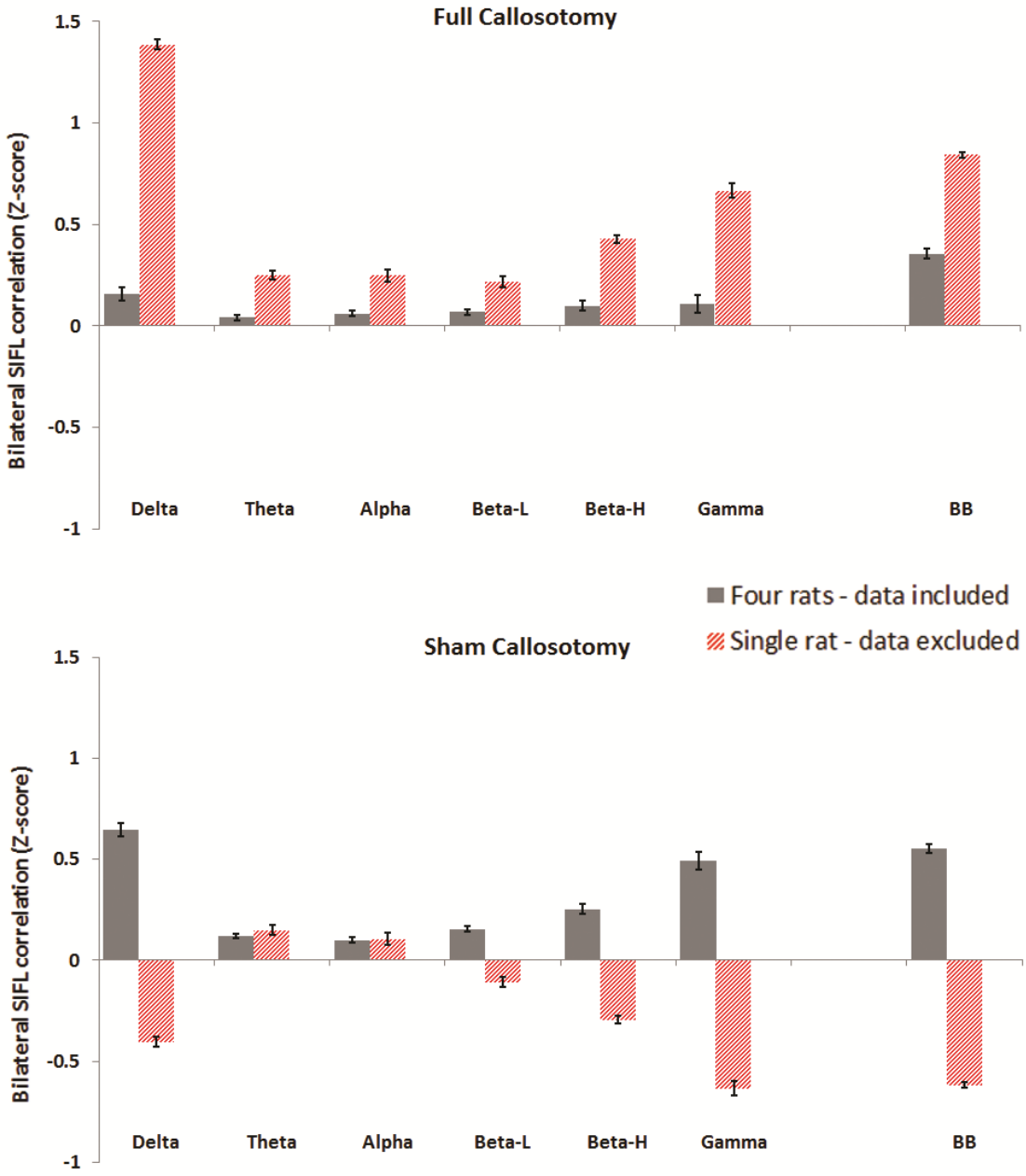


**Figure 18:** Z-scores representing bilateral electrophysiological correlation from all rats and all frequency bands (sham-top, full-bottom). Solid gray bars indicate data from the four rats from each group from which electrophysiological data was included; the striped red bars represent the single rat in each group where electrophysiological data was exclude. In the excluded data > 10% of calculated bilateral connectivity values fell > 2 standard deviations from the band specific mean.

**Table 7:** Bilateral connectivity and statistics. Mean and SEM are presented for BOLD and electrophysiological bilateral functional connectivity data. P-values and decrease in shared variance are calculated between the sham and full callosotomy groups for each seed region (BOLD) and across all BLP frequency bands (electrophysiology). Decrease in shared variance between sham and full callosotomy groups is similar for BOLD SI data and the corresponding broadband BOLD SI connectivity data.

| | Sham Callosotomy (*r*) | Full Callosotomy (*r*) | Decrease in Shared Variance | P-Value |
|---|---|---|---|---|
| **BOLD** | | | | |
| SI | 0.1605 ± .021 | 0.1116 ± .009 | 51.7% | **0.0133** |
| SII | 0.1471 ± .014 | 0.1123 ± .008 | 41.7% | **0.0203** |
| CP | 0.193 ± .022 | 0.1445 ± .012 | 43.9% | **0.0278** |
| **Electrophysiology** | | | | |
| Delta | 0.5613 ± .015 | 0.2802 ± .028 | 75.1% | **$1.61 \times 10^{-17}$** |
| Theta | 0.1180 ± .011 | 0.0585 ± .008 | 75.4% | **$2.39 \times 10^{-5}$** |
| Alpha | 0.1021 ± .014 | 0.0730 ± .010 | 48.9% | 0.0460 |
| Beta-L | 0.1534 ± .012 | 0.0730 ± .011 | 77.4% | **$2.54 \times 10^{-5}$** |
| Beta-H | 0.2420 ± .014 | 0.1243 ± .022 | 73.6% | **$4.61 \times 10^{-6}$** |
| Gamma | 0.4542 ± .012 | 0.2068 ± .041 | 79.3% | **$1.07 \times 10^{-11}$** |
| Broadband | 0.4847 ± .016 | 0.3370 ± .018 | 51.7% | **$1.02 \times 10^{-6}$** |

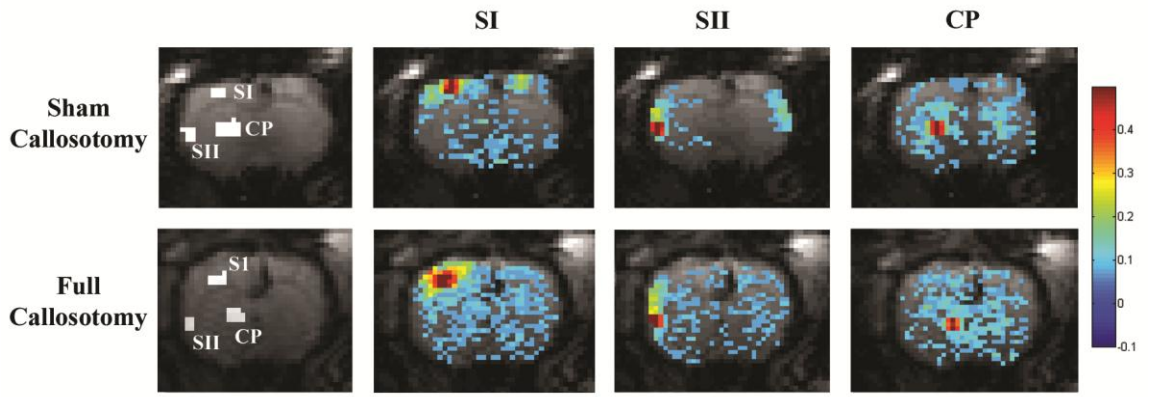


**Figure 19:** BOLD functional connectivity. Pearson correlation functional connectivity maps are overlaid on corresponding EPI images for one rat from each experimental group. Correlation maps from each rat closely match mean group values and were chosen for that purpose. Manually selected representative ROIs are shown for both rats. Significantly higher spatially specific bilateral functional connectivity is observed in the sham callosotomy rodent and compared to the full callosotomy rodent.

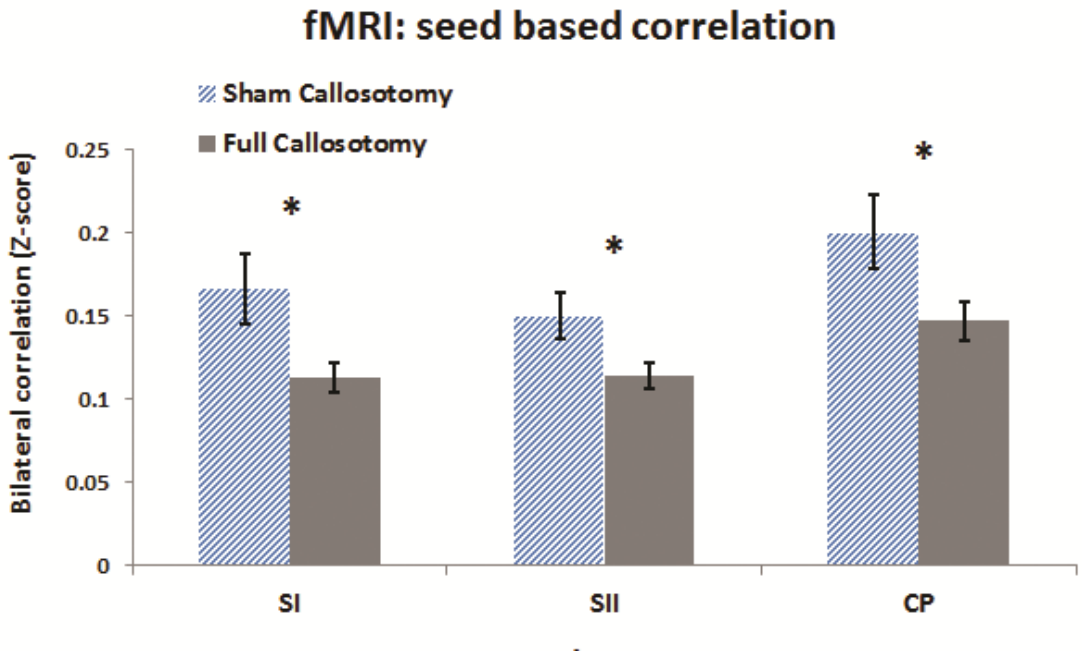


**Figure 20:** fMRI low frequency (0.01 – 0.3 Hz) bilateral functional connectivity in three seed regions. Significant differences in bilateral functional connectivity are calculated between the sham and full callostomy groups for the primary and secondary somatosensory cortices as well as for the caudate/putamen complex. Correlation strength is universally stronger in the sham callosotomy group.

Spatiotemporal dynamic templates were generated for all rats. Resulting spatiotemporal dynamic templates were categorized by visual inspection into three groups presented in Figure 21: bilateral, unilateral, or no spatiotemporal dynamics. A dynamic pattern was only confirmed when the movement of a high or low correlated cluster could visually be observed "travelling" in an organized manner across the cortex from one frame to the next. Waves of activity typically traveled from lateral cortical regions (SII), through central cortical regions (SI) and finally into the motor cortex and midline before beginning again in the lateral cortex. A summary of the spatiotemporal dynamic categorization for rats in both experimental groups can be found in Table 8. The full callosotomy rodents never exhibited the presence of bilateral spatiotemporal dynamics; however, there were high occurrences of unilaterally propagating waves (48.9% of scans) which have rarely been observed in previous experiments using healthy, non-surgically altered rats. Bilateral waves of activity were present 20% of the time in the sham callosotomy group; however, most commonly, no spatiotemporal dynamics were present.

**Table 8:** Spatiotemporal dynamic categorization. Spatiotemporal dynamic templates were generated for both experimental group; the resulting templates were categorized as exhibiting bilateral, unilateral, or no dynamic behavior (see Figure 21). There were no bilateral dynamics present in any of the full callosotomy data; however, a novel unilateral spatiotemporal dynamic pattern was observed for the majority of spatiotemporal dynamic templates in the full callosotomy data.

| Dynamic State: | Bilateral | Unilateral | None |
|---|---|---|---|
| **Sham** | 22.2% | 2.8% | 72.2% |
| **Full** | 0.0% | 48.9% | 51.1% |

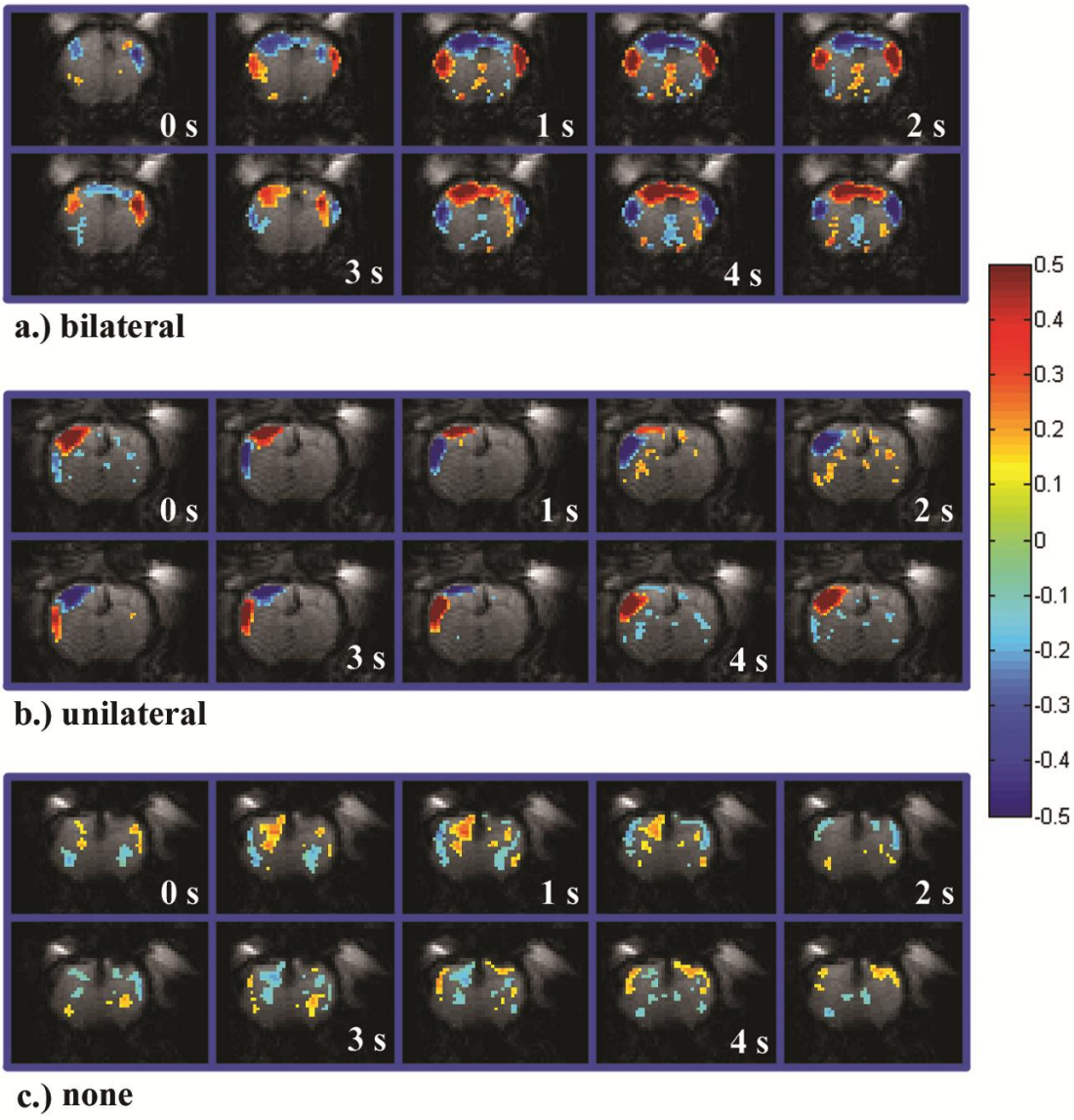


**Figure 21:** Spatiotemporal dynamic templates generated according to Majeed et al. paradigm (Majeed, Magnuson et al. 2011). Spatiotemporal dynamics were clearly categorized into three groups, bilateral dynamics (top), unilateral dynamics (middle), or no dynamics (bottom). Unilateral dynamics are unique to these callosotomy data and have not been seen previously in non-callostomized rodents. Percentage of rats from each experimental group that were classified into each of these dynamics categorizations can be found in Table 8.

**Electrophysiology**

Bilateral connectivity of band limited electrophysiological power was assessed in delta, theta, alpha, low beta, high beta, and gamma band frequency ranges. Direct bilateral correlation of filtered broadband activity was also assessed. Figure 22 illustrates the results of analysis. The sham callosotomy data exhibited universally higher functional connectivity for all evaluated bands. Statistically significant differences between the two were calculated for delta, theta, low beta, high beta, gamma, and broadband ranges. A summary of all electrophysiological connectivity results can be found in Table 2. There was a reduction of shared variance of 51.7% in the broadband correlation data in the full callosotomy group as compared to the sham callosotomy group. This reduction in shared variance was equal to the analogous calculation performed between bilateral primary somatosensory BOLD data.

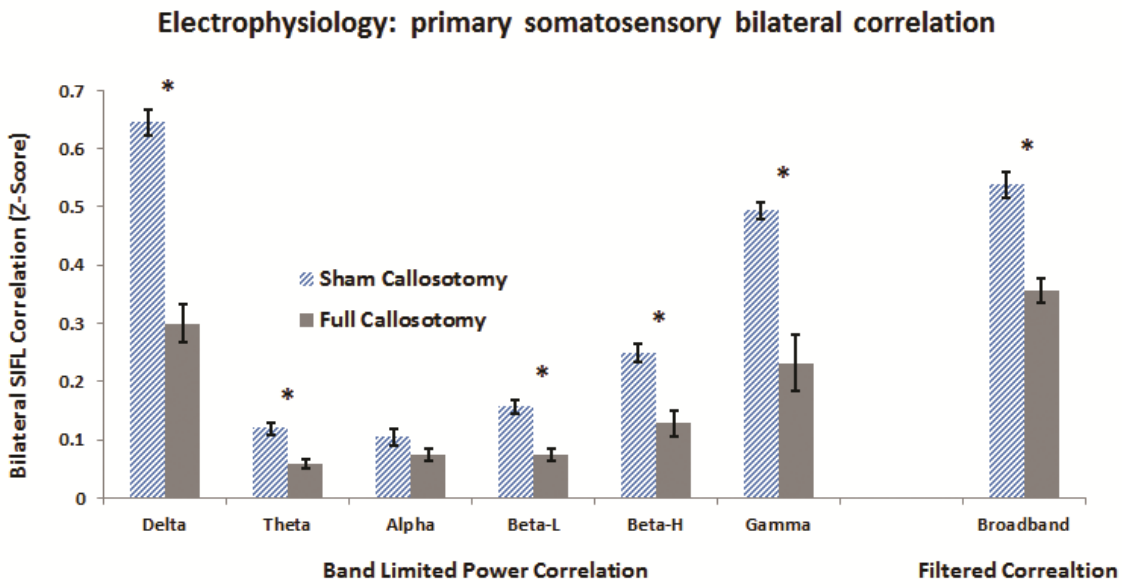


**Figure 22:** Electrophysiological band limited power functional connectivity between bilateral primary somatosensory regions. Mean Pearson connectivity is universally higher for the sham callosotomy rodents as compared to the full callosotomy, and significant differences between the groups are found in delta, theta, low beta, high beta, gamma, and broadband data. The most strongly significant differences were found in the delta and gamma band data.

## Discussion

Surgeries were performed in two groups of rodents resulting in either a complete sectioning of the corpus callosum or a sham sectioning (gray matter was severed, but not the corpus callosum). Electrophysiological and BOLD fMRI were used to assess bilateral connectivity following these surgeries. A universal reduction in bilateral functional connectivity was apparent in BOLD and electrophysiological data in the full callosotomy groups. The significance of these findings are twofold: for the first time the effects of the split brain model on functional network integrity has been evaluated in a previously healthy rodent population, secondly the split brain model provides an ideal platform for

evaluating the interconnectedness of BOLD and neural activity by determining the similarity of effects on each modality as a results of the interventional surgery.

Anesthesia is another area of potential confound; both the isoflurane used for long period of time prior to functional imaging and the concurrent use of dexmedetomidine while imaging surely influence ongoing functional activity. In Chapter 2 of this thesis, we reveal longitudinal, lingering influences of long durations of isoflurane prior to functional imaging that may take up to several hours to dissipate depending on the preceding length of isoflurane use. Waiting for absolute dissipation of the functional effects of isoflurane was not feasible due to the length of the procedures in their current form. In lieu of waiting, we were careful to maintain equidistant spacing between the cessation of isoflurane and functional recordings in both groups (see fMRI and electrophysiology subsections of methods), thereby limiting possible biasing effects of anesthetic influences. The resulting fMRI connectivity in the current study, even within the sham group, was lower than normally seen (~0.3 – 0.55 depending upon the imaging and processing techniques) in healthy non-callotomized rats (He, Snyder et al. 2008; Zhao, Zhao et al. 2008; Magnuson, Majeed et al. 2010; Williams, Magnuson et al. 2010; Kalthoff, Po et al. 2013) and was likely due to compounding influences of vascular perturbations and lingering isoflurane effects. Furthermore it is clear from Figure 19 that highly specific BOLD bilateral correlation is found in sham callosotomy data while the full callosotomy data connectivity seemingly reflects less spatially specific residual correlation. Also of interest is the strong electrical connectivity (once again dependent upon hardware parameters and processing techniques) found in the sham callosotomy data. This is likely due to recording occurring long after the initial surgical isoflurane

period (multiple hours) and the neural activity being significantly less affected by possible vascular damage.

Minor surgical variability was apparent in our RARE MRI images as well as histology in the depth of the sham callosotomies (apparent in Figure 17). 0.5 mm of buffer space was built into the sham callosotomy group to insure the corpus callosum was not affected by the surgical procedure. While zero variation in surgical depth of the sham cut would have been ideal, the resulting surgical outcomes were clearly categorized into two groups: severed corpus callosum and intact corpus callosum and served our purposes in this work.

All rodents were included in BOLD analysis as fMRI setup is relatively easy and consistent; however, in the electrophysiological data, one rodent contained hardware setup errors and was discarded, and two additional rodents (one from each group) were discarded due to drastic data anomalies. >10% of bilateral connectivity values throughout the electrophysiological bands felt outside of 2 standard deviations for the anomalous rats. For all other rats combined there were only 2 anomalous data values out of 702 total data points. It is clear from the data in Figure 18 that data from the anomalous rats fell into separated groupings as compared to data from the other four rats in each group. Raw data from both excluded rats exhibited a peculiar DC bias between the two electrodes, possibly the result of collecting data from too shallow of cortical depth, manifesting as inverse contributions from spiking activity. Specifically in the sham callosotomy group the excluded values appear to be approximately an inverse of the mean values for each group.

Gamma and delta band BLP connectivity are thought to be most closely reflective of ultra-low frequency fMRI networks (Leopold, Murayama et al. 2003; Lu, Zuo et al. 2007; Scholvinck, Maier et al. 2010). In the work presented here bilateral delta BLP connectivity showed the greatest statistical difference between the sham and full callosotomy experimental groups, while the next most significant difference between the groups occurred in gamma BLP connectivity.

Doron et al., in studying an interhemispheric coordination model using lexical visual stimuli, encounter the transient manner in which functional networks activate and deactivate highlighting the need for non-static evaluations of functional networks to obtain novel insights into sensitive spatiotemporal information that was not previously obtainable (Doron, Bassett et al. 2012). We address this dynamic evaluative need in our work by performing spatiotemporal dynamic template analysis that was first offered by Majeed et al. (Majeed, Magnuson et al. 2009). While our static evaluation revealed little to no connectivity in the full callosotomy model, the robust presence of unilateral spatiotemporal dynamics activity were indicated (Figure 6b). This unilateral pattern is a spatiotemporal template variation that is rarely observed in previous experimental groups suggesting its relationship to the surgical paradigm. While this pattern was also observed on a single occasion in the sham callosotomy group, the unilateral pattern appears to primarily be a correlate of the full callosotomy group. The unilateral nature of these dynamics suggests further that information necessary for bilateral coordination is not being exchanged between the hemispheres. The continuation of unilateral spatiotemporal patterns (that closely match the one sided counterpart from the bilateral spatiotemporal dynamics) suggests the possibility that these dynamics are driven by subcortical inputs,

but the bilateral coordination of these dynamics are mediated by the now severed corpus callosum. This subcortical influence theory is supported by Uddin et al.'s work who found strong residual bilateral connectivity in a patient with entirely removed commissural pathways (albeit 45 years following the callosotomy allowing ample time for functional rearrangement); they conclude the cortical networks are coordinated, at least in part, by subcortical mechanisms (Uddin, Mooshagian et al. 2008).

To summarize, we present a robust finding indicating the corpus callosum's role in facilitating bilateral functional connectivity in the rodent model. BOLD and electrophysiological data indicate significantly less bilateral functional connectivity in the experimental group where the corpus callosum was fully severed as compared to the sham callosotomy group. Furthermore bilateral primary somatosensory connectivity was affected to a similar degree in both BOLD and electrophysiological data suggesting significant interconnectedness between the measured signals.

# CHAPTER 5

# QUANTIFYING SPATIOTEMPORAL DYNAMIC WAVES USING A BOOTSTRAPPING AND STATISTICAL PARADIGM

## Spatiotemporal Dynamic Analysis in its Current Form

### The Need for Dynamic Analysis

Until recently, evaluation of large scale functional networks has been performed in a spatially and temporally static manner. Seed based functional connectivity is performed by acquiring one timecourse from a single location, followed by a Pearson correlation between that time course and other timecourses of interest. This result in dynamic information from all time periods of the resting state period (minutes long) being compressed to a single correlation value; time sensitive events (seconds long) and relationships are lost. In essence, from seed based correlation, we only obtain a picture of the brain's relationship to one specific location, and copious information regarding the dynamic processes that make up that seed based connectivity or lack of connectivity are lost. In 2009, Majeed et al. (Majeed, Magnuson et al. 2009) presented a spatiotemporal dynamic paradigm (that we have used previously in analysis for this thesis) that alleviated many of the seed based limitations and provided a qualitative view of spatial and temporally relevant events that underlie coordination between specific brain regions. Since Majeed's work, spatiotemporal dynamic analysis using alternate paradigms have been proposed (Chang and Glover 2010; Grigg and Grady 2010; Hutchison, Womelsdorf et al. 2012; Liu and Duyn 2013).

### The Need for Quantification of the Current Spatiotemporal Dynamic Paradigm

While the technique presented by Majeed et al. is robust and provides ideal visualization of space and time sensitive events, there is a major limitation which arises from the spatially continuous output generated from the algorithm. Majeed's spatiotemporal dynamic algorithm includes all brain areas during analysis to probe for potential relationships, but for the majority of a resting state scan, most brain areas are not exhibiting a coordinated spatiotemporal relationship with other areas (or are represented by a secondary, unrelated spatiotemporal pattern). This results in a continuous output with highly variable "strength of correlation" values, which makes thresholding arbitrary and difficult, and leads to a final pattern that, while qualitatively dense with information, cannot be easily quantified. In this chapter we present a randomization technique to generate a threshold based on statistical significance. We apply this proposed spatiotemporal dynamic quantification paradigm to anesthesia time dependence data presented in Chapter 3.

## Methods

### Preprocessing and Spatiotemporal Template Generation

The Whole brain signal was regressed from resting state BOLD data followed by linear detrending and filtering the data between 0.01 – 0.3 Hz using a FIR filter. Spatial blurring was performed using a 3x3 Gaussian kernel. Data sets were then masked to remove background noise, skull, and muscle to only include the brain area.

For each rat and scan spatiotemporal dynamic templates were generated using the Majeed et al. algorithm. A chunk of consecutive images is chosen from the resting state data set at a random starting position; sliding correlation is then performed between the image chunk and the preprocessed image series (evaluating spatial and temporal properties of correlation), correlation is calculated between the initial chunk and all other chunks of equal size using sliding correlation analysis. Correlation analysis reveals the image chunks which correlate most strongly with the initial chunk; these image segments are averaged together to create a new template. The averaged template is then used for a second round of sliding window correlation to find image chunks that share the strongest connectivity with the revised image chunk; this process continues until convergence is reached.

**Data Randomization and Statistics**

Preprocessed data from each rat is phase randomized by circularly shifting all voxel timecourses in the image a random distance. In this manner spatial relevance is retained; however, real phase locked signal relationships occurring throughout the brain will be lost. Spatiotemporal dynamic templates are then generated for the phase randomized data. One thousand iterations of this process are performed, until 1000 random-phase spatiotemporal templates are available. A 2-tailed null distribution was generated at each voxel using calculated voxel values from the phase randomized template. P-values were calculated by comparing the actual voxel template value from the non-randomized data to the cumulative distribution function of the generated null distribution. Strict Bonferroni correction was implemented followed by rejection of

spatial clusters less than 25 voxels (based on smallest anatomical component in rodent cortex; secondary somatosensory cortex).

## Results

Figure 25 (top) shows the formation of a spatiotemporal dynamic template using the Majeed et al. algorithm. Quantification is difficult due to the continuous nature of template values, and the arbitrariness of a cutoff considering the variability in template strengths between scans and rats. Figure 25 (bottom) illustrates the statistically limited amplitude values from the template, overlayed on the mean EPI image, which shows only the voxel values that are statistically different from the phase randomized null distribution. Three metrics of quantified dynamic outputs were calculated: total count of statistically significant voxels, mean amplitude values from statistically thresholded voxels, and the summation of mean amplitude values from statistically thresholded voxels. Static bilateral functional connectivity was compared to each of these metrics. This comparison between spatiotemporal dynamic quantification and traditional seed based functional connectivity reveals a statistically significant linear relationship for voxel count ($p = 8.7x10^{-7}$), mean voxel amplitude ($p = 0.005$), and summation of voxel amplitudes ($p = 6.0\ x10^{-6}$). Figure 26 shows the count of statistically significant voxels vs. connectivity for 7 rats from the anesthesia time dependence work (Chapter 3). Finally, Figure 27 indicates the relationship between the average functional connectivity scores and average voxels passing the statistically significant quantification threshold in rats undergoing a callosotomy or sham callosotomy.

A seed was placed in the bilateral somatosensory cortex, and the timecourses generated from spatiotemporal dynamics passing through that static point were plotted

(Figure 28). Correlation based on the spatiotemporal dynamics with no other relevant functional information reveals strong bilateral similarity.

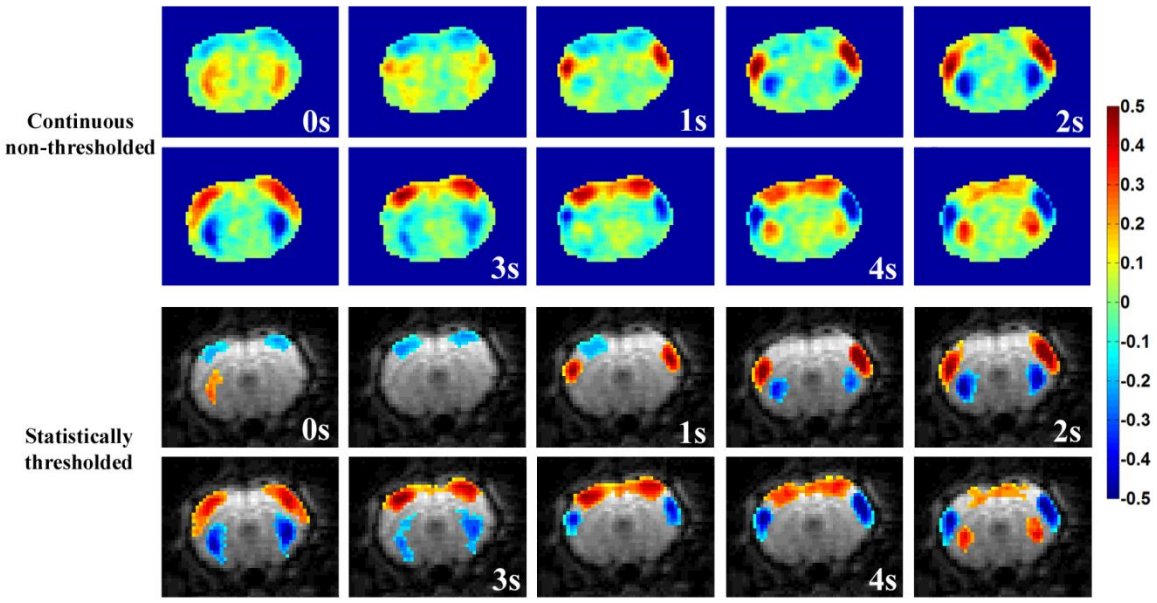


**Figure 25:** Spatiotemporal dynamic templates generated from the original Majeed et al. paradigm (top). Statistically thresholded dynamics allowing for quantification (bottom) of spatiotemporal dynamics.

## Discussion

Spatiotemporal dynamic analysis is a novel approach for exploring functional activity, providing a more complete and information dense representation of the complex processes occurring over the duration of a functional scan. Quantification is necessary to allow for inter-subject comparisons. The tight coupling between the quantified dynamics and the static measure of functional connectivity suggests they are directly influencing one another or are a product of the same source.

If the only functional information present in an fMRI data set were these observed spatiotemporal dynamic patters, strong bilateral functional connectivity would result using seed based correlation. While we cannot make any claims regarding the causality of the relationship between static connectivity and dynamic patterns, there is clearly a relationship between the two. Logically it seems much more likely that dynamics are driving static connectivity as opposed to a more convoluted relationship of static connectivity driving the dynamic processes.

Spatiotemporal quantification clearly indicates significant voxels in the caudate putamen complex, indicating that the dynamic processes found traversing the cortex also extend into the subcortical structures. When the cortex is experiencing high amplitude pattern correlations, the caudate/putamen complex is typically experiencing low amplitude correlations. One explanation for this oscillation in high and low spatial activation involves whole brain energy consumption. Theoretically only a certain portion of the brain can be highly active at any one time based on limited energy availability; to counteract this increased energy consumption necessary for the high level of bilaterally symmetric activation, another portion of the brain must consequently be functionally depressed.

Quantifying spatiotemporal dynamic patterns converts the original qualitative pattern finding algorithm into a powerful tool for comparing dynamic information between subjects. This tool is a substantial step towards harnessing the copious information available from dynamic analysis of brain function.

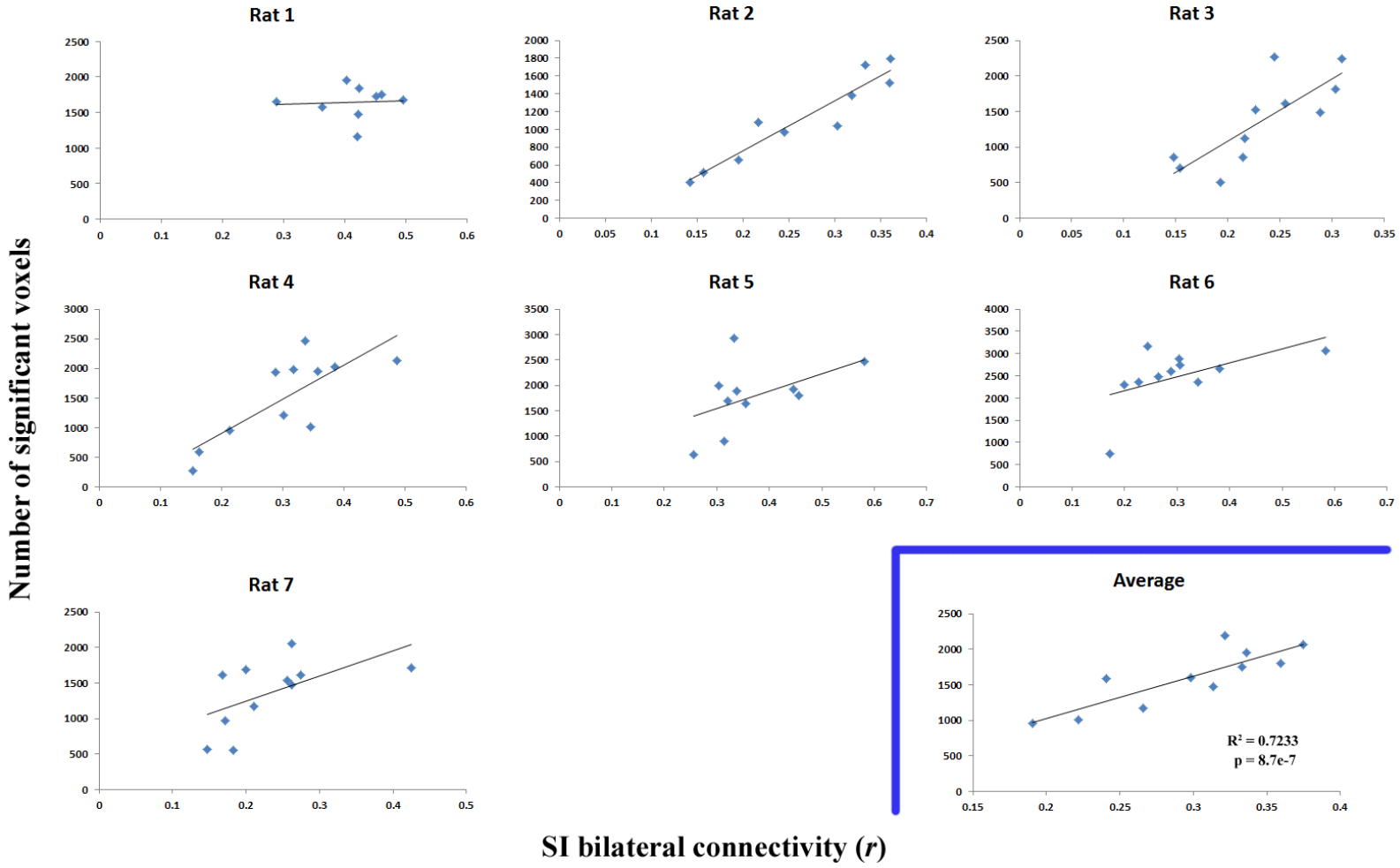


**Figure 26:** Traditional functional connectivity plotted versus quantified spatiotemporal dynamics for seven rats collected from the anesthesia data presented in Chapter 4. Averaged values from all seven rats are shown at bottom right.

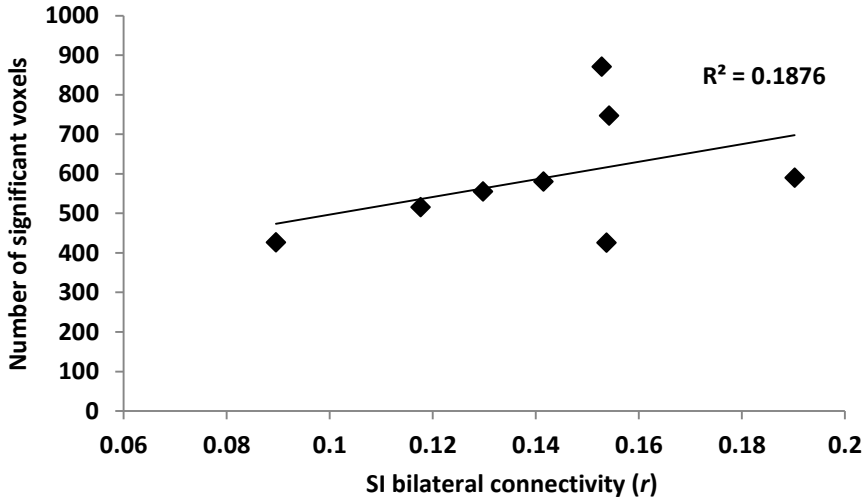


**Figure 27:** Functional connectivity is plotted versus quantified spatiotemporal dynamics for the 11 rats that underwent either a callosotomy or sham callosotomy.

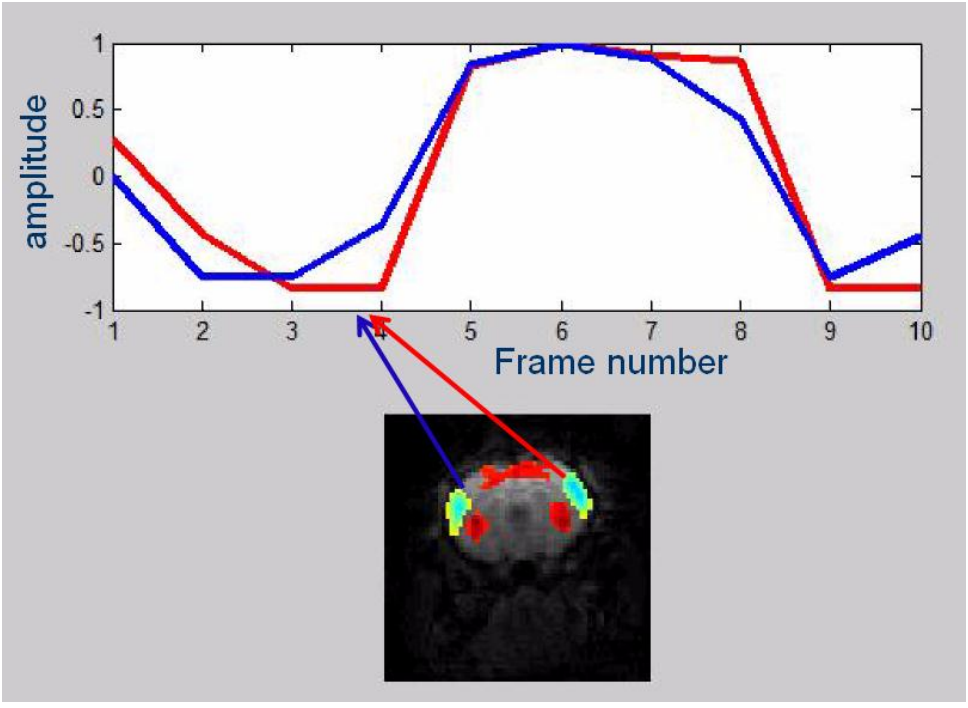


**Figure 28:** Timecourses are generated from a seed region placed in the primary somatosensory cortex based solely on dynamic information passing through these regions. Strong functional similarity is apparent in the bilaterally symmetric timecourses.

# CONCLUSION

Understanding the structural and functional architecture of large scale brain networks is a critical step to grasping the complexities of the working mind. From the seemingly simplistic finding by Biswal et al. of temporally synchronous activity between spatially distant brain regions, brain research has undergone a major paradigm shift. Nearly every complex process our brains perform requires the coordination and communication of brain regions. We have quantified and defined these networks throughout the brain, across modalities, and on many different temporal scales; yet we still have not grasped the driving forces underlying this robust phenomenon.

The callosotomy model provides a unique platform to evaluate the neuroanatomical impact on functional network integrity. Our robust findings with a bi-modal experimental paradigm indicate that the corpus callosum facilitates bilateral functional connectivity in the rodent model. The corpus callosum's effect on connectivity remains controversial due to the inhomogeneous findings in humans; this thesis work serves to largely alleviate the currently confounding results. Furthermore, bilateral primary somatosensory connectivity was affected to a similar degree in both BOLD and electrophysiological data suggesting the likely interconnectedness between the measured signals, which is a relationship still under investigation.

Connectivity between bilateral cortical structures was significantly reduced in the callosotomy model as compared to the sham callosotomy model. This finding was not unexpected as there are direct axonal projections connecting analogous contralateral cortical anatomy. Interestingly the caudate/putamen complex, a subcortical structure, also

indicated a significant reduction in connectivity in the callosotomy model as compared to the sham callosotomy model, despite a lack of direct cortical projections between the two hemispheres. In order for the corpus callosum to influence subcortical connectivity in such a manner, information must be transferred across several synaptic pathways to reach the contralateral hemisphere. Following a full callosotomy, spatiotemporal dynamic patterns often presented only unilaterally, suggesting that information necessary for bilateral coordination is not being exchanged between the hemispheres. The continued presence of dynamic waves of activity despite the severed corpus callosum suggests dynamics are likely driven by subcortical inputs; however, the bilateral coordination of these dynamics is mediated by the now severed corpus callosum.

Apart from the central thrust of this work, we provide several additional valuable contributions to the brain research community. We clearly characterize potential functional consequences of time-dependent variability in a commonly used anesthetic regiment and propose an ideal time window in which functional recording should take place. We compared and contrasted, for the first time, functional network activity assessed using CBV to recordings in the same rat using traditional BOLD imaging. These findings have been published and represent a unique and beneficial contribution to the field. We have also created a novel tool to allow for the quantification of spatiotemporal dynamics. Each provides a means for quantifying data that was previously non-quantifiable. The strong linearity between the quantified dynamics and the historically accepted measure of static functional connectivity suggests the significance of dynamics in defining functional networks, which is a continuing area of research.

Future work exploring the origin and functions of brain networks is vast. While the current work has indicated the corpus callosum's role in mediating functional networks, the driving origin of the synchronous signal has not been uncovered. Probing deep brain neurons in the thalamus, midbrain, or brainstem may reveal links between stimulation and synchronous network activity which would suggest a potential origin. Modulation of functional networks using methods such as trans-cranial direct current stimulation, mindfulness training paradigms, or pharmacological pathways could prove to be clinically useful tools for many disease states. We evaluated the largest cortical spatiotemporal network in the brain; however, spatiotemporal networks on smaller scales likely exist as well which should be explored. One possibility for this exploration would be developing mathematical algorithms that can harness and compare the time and frequency relationships that exist between all of the voxels in fMRI data; methods such as wavelet analysis may be ideal for this formidable task.

This thesis work represents a substantial contribution to fMRI and general brain research by providing significant evidence suggesting the corpus callosum's role in mediating activity in functionally connected networks.

# REFERENCES


Alnajjar, F., Y. Yamashita, et al. (2013). "The hierarchical and functional connectivity of higher-order cognitive mechanisms: neurorobotic model to investigate the stability and flexibility of working memory." Front Neurorobot 7: 2.

Antunes, L. M., H. D. Golledge, et al. (2003). "Comparison of electroencephalogram activity and auditory evoked responses during isoflurane and halothane anaesthesia in the rat." Vet Anaesth Analg 30(1): 15-23.

Asano, Y., R. C. Koehler, et al. (1997). "Pial arteriolar constriction to alpha 2-adrenergic agonist dexmedetomidine in the rat." Am J Physiol 272(6 Pt 2): H2547-2556.

Austin, V. C., A. M. Blamire, et al. (2005). "Confounding effects of anesthesia on functional activation in rodent brain: a study of halothane and alpha-chloralose anesthesia." Neuroimage 24(1): 92-100.

Banich, M. T. and A. Belger (1990). "Interhemispheric Interaction - How Do the Hemispheres Divide-and-Conquer a Task." Cortex 26(1): 77-94.

Belger, A. and M. T. Banich (1998). "Costs and benefits of integrating information between the cerebral hemispheres: A computational perspective." Neuropsychology 12(3): 380-398.

Biswal, B., A. G. Hudetz, et al. (1997). "Hypercapnia reversibly suppresses low-frequency fluctuations in the human motor cortex during rest using echo-planar MRI." J Cereb Blood Flow Metab 17(3): 301-308.

Biswal, B., F. Z. Yetkin, et al. (1995). "Functional connectivity in the motor cortex of resting human brain using echo-planar MRI." Magn Reson Med 34(4): 537-541.

Boly, M., E. Balteau, et al. (2007). "Baseline brain activity fluctuations predict somatosensory perception in humans." Proc Natl Acad Sci U S A 104(29): 12187-12192.

Brazdil, M., J. Brichta, et al. (1997). "Interhemispheric EEG coherence after corpus callosotomy." European Journal of Neurology 4(4): 419-425.

Brett, M., I. S. Johnsrude, et al. (2002). "The problem of functional localization in the human brain." Nat Rev Neurosci 3(3): 243-249.

Brookes, M. J., J. R. Hale, et al. (2011). "Measuring functional connectivity using MEG: methodology and comparison with fcMRI." Neuroimage 56(3): 1082-1104.

Brown, W. S., M. A. Jeeves, et al. (1999). "Bilateral field advantage and evoked potential interhemispheric transmission in commissurotomy and callosal agenesis." Neuropsychologia 37(10): 1165-1180.

Bullmore, E. T., S. Rabe-Hesketh, et al. (1996). "Functional magnetic resonance image analysis of a large-scale neurocognitive network." Neuroimage 4(1): 16-33.

Buxton, R. B., E. C. Wong, et al. (1998). "Dynamics of blood flow and oxygenation changes during brain activation: the balloon model." Magn Reson Med 39(6): 855-864.

Carlson, G. C. and D. A. Coulter (2008). "In vitro functional imaging in brain slices using fast voltage-sensitive dye imaging combined with whole-cell patch recording." Nat Protoc 3(2): 249-255.

Carmichael, D. W., J. S. Thornton, et al. (2010). "Feasibility of simultaneous intracranial EEG-fMRI in humans: a safety study." Neuroimage 49(1): 379-390.

Carvajal-Rodriguez, A., J. de Una-Alvarez, et al. (2009). "A new multitest correction (SGoF) that increases its statistical power when increasing the number of tests." BMC Bioinformatics 10: 209.

Chang, C. and G. H. Glover (2010). "Time-frequency dynamics of resting-state brain connectivity measured with fMRI." Neuroimage 50(1): 81-98.

Cook, N. D. (1984). "Homotopic callosal inhibition." Brain Lang 23(1): 116-125.

Cordes, D., V. M. Haughton, et al. (2000). "Mapping functionally related regions of brain with functional connectivity MR imaging." AJNR Am J Neuroradiol 21(9): 1636-1644.

Corsi-Cabrera, M., R. Ondarza, et al. (2006). "Role of corpus callosum in interhemispheric coherent activity during sleep." Clin Neurophysiol 117(8): 1826-1835.

Corsi-Cabrera, M., G. Trias, et al. (1995). "EEG interhemispheric correlation after callosotomy: one case study." Percept Mot Skills 80(2): 504-506.

Cullen, K. R., D. G. Gee, et al. (2009). "A preliminary study of functional connectivity in comorbid adolescent depression." Neurosci Lett 460(3): 227-231.

Damoiseaux, J. S. and M. D. Greicius (2009). "Greater than the sum of its parts: a review of studies combining structural connectivity and resting-state functional connectivity." Brain Struct Funct 213(6): 525-533.

de Pasquale, F., S. Della Penna, et al. (2010). "Temporal dynamics of spontaneous MEG activity in brain networks." Proc Natl Acad Sci U S A 107(13): 6040-6045.

Dorion, A. A., M. Chantome, et al. (2000). "Hemispheric asymmetry and corpus callosum morphometry: a magnetic resonance imaging study." Neuroscience Research 36(1): 9-13.

Doron, K. W., D. S. Bassett, et al. (2012). "Dynamic network structure of interhemispheric coordination." Proc Natl Acad Sci U S A 109(46): 18661-18668.

Drew, P. J., J. H. Duyn, et al. (2008). "Finding coherence in spontaneous oscillations." Nat Neurosci 11(9): 991-993.

Eichele, T., S. Debener, et al. (2008). "Prediction of human errors by maladaptive changes in event-related brain networks." Proc Natl Acad Sci U S A 105(16): 6173-6178.

Fairhall, S. L., I. Indovina, et al. (2009). "The brain network underlying serial visual search: comparing overt and covert spatial orienting, for activations and for effective connectivity." Cereb Cortex 19(12): 2946-2958.

Ferron, J. F., D. Kroeger, et al. (2009). "Cortical inhibition during burst suppression induced with isoflurane anesthesia." J Neurosci 29(31): 9850-9860.

Fox, M. D., M. Corbetta, et al. (2006). "Spontaneous neuronal activity distinguishes human dorsal and ventral attention systems." Proc Natl Acad Sci U S A 103(26): 10046-10051.

Fox, M. D., A. Z. Snyder, et al. (2005). "The human brain is intrinsically organized into dynamic, anticorrelated functional networks." Proc Natl Acad Sci U S A 102(27): 9673-9678.

Fox, M. D., D. Zhang, et al. (2009). "The global signal and observed anticorrelated resting state brain networks." J Neurophysiol 101(6): 3270-3283.

Garrity, A. G., G. D. Pearlson, et al. (2007). "Aberrant "default mode" functional connectivity in schizophrenia." Am J Psychiatry 164(3): 450-457.

Gazzaniga, M. S. (1966). "Visuomotor integration in split-brain monkeys with other cerebral lesions." Exp Neurol 16(3): 289-298.

Golanov, E. V., S. Yamamoto, et al. (1994). "Spontaneous waves of cerebral blood flow associated with a pattern of electrocortical activity." Am J Physiol 266(1 Pt 2): R204-214.

Grady, C. L., M. L. Furey, et al. (2001). "Altered brain functional connectivity and impaired short-term memory in Alzheimer's disease." Brain 124(Pt 4): 739-756.

Granholm, M., B. C. McKusick, et al. (2007). "Evaluation of the clinical efficacy and safety of intramuscular and intravenous doses of dexmedetomidine and medetomidine in dogs and their reversal with atipamezole." Vet Rec 160(26): 891-897.

Gravel, C., R. Sasseville, et al. (1990). "Maturation of the Corpus-Callosum of the Rat .2. Influence of Thyroid-Hormones on the Number and Maturation of Axons." Journal of Comparative Neurology 291(1): 147-161.

Greicius, M. D., B. H. Flores, et al. (2007). "Resting-state functional connectivity in major depression: abnormally increased contributions from subgenual cingulate cortex and thalamus." Biol Psychiatry 62(5): 429-437.

Grigg, O. and C. L. Grady (2010). "Task-related effects on the temporal and spatial dynamics of resting-state functional connectivity in the default network." PLoS One 5(10): e13311.

Gruetter, R. (1993). "Automatic, localized in vivo adjustment of all first- and second-order shim coils." Magn Reson Med 29(6): 804-811.

Guilfoyle, D. N., S. V. Gerum, et al. (2013). "Functional connectivity fMRI in mouse brain at 7T using isoflurane." J Neurosci Methods.

Haider, B. and D. A. McCormick (2009). "Rapid neocortical dynamics: cellular and network mechanisms." Neuron 62(2): 171-189.

Hampson, M., B. S. Peterson, et al. (2002). "Detection of functional connectivity using temporal correlations in MR images." Hum Brain Mapp 15(4): 247-262.

He, B. J., A. Z. Snyder, et al. (2008). "Electrophysiological correlates of the brain's intrinsic large-scale functional architecture." Proc Natl Acad Sci U S A 105(41): 16039-16044.

Hesselmann, G., C. A. Kell, et al. (2008). "Spontaneous local variations in ongoing neural activity bias perceptual decisions." Proc Natl Acad Sci U S A 105(31): 10984-10989.

Hlinka, J., C. Alexakis, et al. (2010). "Slow EEG pattern predicts reduced intrinsic functional connectivity in the default mode network: an inter-subject analysis." Neuroimage 53(1): 239-246.

Honey, C. J., O. Sporns, et al. (2009). "Predicting human resting-state functional connectivity from structural connectivity." Proc Natl Acad Sci U S A 106(6): 2035-2040.

Hoptman, M. J., D. D'Angelo, et al. (2010). "Amygdalofrontal functional disconnectivity and aggression in schizophrenia." Schizophr Bull 36(5): 1020-1028.

Huber, D. E., X. Tian, et al. (2008). "The dynamics of integration and separation: ERP, MEG, and neural network studies of immediate repetition effects." J Exp Psychol Hum Percept Perform 34(6): 1389-1416.

Hutchison, R. M., S. M. Mirsattari, et al. (2010). "Functional networks in the anesthetized rat brain revealed by independent component analysis of resting-state FMRI." J Neurophysiol 103(6): 3398-3406.

Hutchison, R. M., T. Womelsdorf, et al. (2012). "Resting-state networks show dynamic functional connectivity in awake humans and anesthetized macaques." Hum Brain Mapp.

Johnston, J. M., S. N. Vaishnavi, et al. (2008). "Loss of resting interhemispheric functional connectivity after complete section of the corpus callosum." J Neurosci 28(25): 6453-6458.

Kalthoff, D., C. Po, et al. (2013). "Reliability and spatial specificity of rat brain sensorimotor functional connectivity networks are superior under sedation compared with general anesthesia." NMR Biomed.

Keilholz, S. D., A. C. Silva, et al. (2004). "Functional MRI of the rodent somatosensory pathway using multislice echo planar imaging." Magn Reson Med 52(1): 89-99.

Keilholz, S. D., A. C. Silva, et al. (2006). "BOLD and CBV-weighted functional magnetic resonance imaging of the rat somatosensory system." Magn Reson Med 55(2): 316-324.

Kelly, A. M., L. Q. Uddin, et al. (2008). "Competition between functional brain networks mediates behavioral variability." Neuroimage 39(1): 527-537.

Kim, S. K., K. C. Wang, et al. (2008). "Epilepsy surgery in children: outcomes and complications." J Neurosurg Pediatr 1(4): 277-283.

Leocani, L. and G. Comi (1999). "EEG coherence in pathological conditions." Journal of Clinical Neurophysiology 16(6): 548-555.

Leopold, D. A., Y. Murayama, et al. (2003). "Very slow activity fluctuations in monkey visual cortex: implications for functional brain imaging." Cereb Cortex 13(4): 422-433.

Lewin J.S, W. D., Durek J.L. (1995). "Susceptibility-induced artifacts in functional Mr-imaging." Radiology 197: 219.

Li, S. J., B. Biswal, et al. (2000). "Cocaine administration decreases functional connectivity in human primary visual and motor cortex as detected by functional MRI." Magn Reson Med 43(1): 45-51.

Lin, C. Y., M. H. Lin, et al. (2009). "In vivo cerebromicrovasculatural visualization using 3D DeltaR2-based microscopy of magnetic resonance angiography (3DDeltaR2-mMRA)." Neuroimage 45(3): 824-831.

Liu, X. and J. H. Duyn (2013). "Time-varying functional network information extracted from brief instances of spontaneous brain activity." Proc Natl Acad Sci U S A.

Liu, X., X. H. Zhu, et al. (2011). "Neural origin of spontaneous hemodynamic fluctuations in rats under burst-suppression anesthesia condition." Cereb Cortex 21(2): 374-384.

Liu, X., X. H. Zhu, et al. (2012). "The Change of Functional Connectivity Specificity in Rats Under Various Anesthesia Levels and its Neural Origin." Brain Topogr.

Liu, Y., C. Yu, et al. (2007). "Whole brain functional connectivity in the early blind." Brain 130(Pt 8): 2085-2096.

Liu, Z., M. Fukunaga, et al. (2010). "Large-scale spontaneous fluctuations and correlations in brain electrical activity observed with magnetoencephalography." Neuroimage 51(1): 102-111.

Logothetis, N. K., J. Pauls, et al. (2001). "Neurophysiological investigation of the basis of the fMRI signal." Nature 412(6843): 150-157.

Lowe, M. J., B. J. Mock, et al. (1998). "Functional connectivity in single and multislice echoplanar imaging using resting-state fluctuations." Neuroimage 7(2): 119-132.

Lowe, M. J., M. D. Phillips, et al. (2002). "Multiple sclerosis: low-frequency temporal blood oxygen level-dependent fluctuations indicate reduced functional connectivity initial results." Radiology 224(1): 184-192.

Lu, H., C. A. Scholl, et al. (2007). "Quantifying the blood oxygenation level dependent effect in cerebral blood volume-weighted functional MRI at 9.4T." Magn Reson Med 58(3): 616-621.

Lu, H., Y. Zuo, et al. (2007). "Synchronized delta oscillations correlate with the resting-state functional MRI signal." Proc Natl Acad Sci U S A 104(46): 18265-18269.

Magnuson, M., W. Majeed, et al. (2010). "Functional connectivity in blood oxygenation level-dependent and cerebral blood volume-weighted resting state functional magnetic resonance imaging in the rat brain." J Magn Reson Imaging 32(3): 584-592.

Majeed, W., M. Magnuson, et al. (2011). "Spatiotemporal dynamics of low frequency BOLD fluctuations in rats and humans." Neuroimage 54(2): 1140-1150.

Majeed, W., M. Magnuson, et al. (2009). "Spatiotemporal dynamics of low frequency fluctuations in BOLD fMRI of the rat." J Magn Reson Imaging 30(2): 384-393.

Mandeville, J. B. and J. J. Marota (1999). "Vascular filters of functional MRI: spatial localization using BOLD and CBV contrast." Magn Reson Med 42(3): 591-598.

Mantini, D., M. G. Perrucci, et al. (2007). "Electrophysiological signatures of resting state networks in the human brain." Proc Natl Acad Sci U S A 104(32): 13170-13175.

Mayhew, J. E., S. Askew, et al. (1996). "Cerebral vasomotion: a 0.1-Hz oscillation in reflected light imaging of neural activity." Neuroimage 4(3 Pt 1): 183-193.

Mohajerani, M. H., D. A. McVea, et al. (2010). "Mirrored bilateral slow-wave cortical activity within local circuits revealed by fast bihemispheric voltage-sensitive dye imaging in anesthetized and awake mice." J Neurosci 30(10): 3745-3751.

Montplaisir, J., T. Nielsen, et al. (1990). "Interhemispheric EEG coherence before and after partial callosotomy." Clin Electroencephalogr 21(1): 42-47.

Myers, R. E. (1956). "Function of Corpus Callosum in Interocular Transfer." Brain 79(2): 358-363.

Myers, R. E. and R. W. Sperry (1958). "Interhemispheric Communication through the Corpus Callosum - Mnemonic Carry-over between the Hemispheres." Archives of Neurology and Psychiatry 80(3): 298-303.

Nakao, Y., Y. Itoh, et al. (2001). "Effects of anesthesia on functional activation of cerebral blood flow and metabolism." Proc Natl Acad Sci U S A 98(13): 7593-7598.

Nasrallah, F. A., J. Tan, et al. (2012). "Pharmacological modulation of functional connectivity: alpha2-adrenergic receptor agonist alters synchrony but not neural activation." Neuroimage 60(1): 436-446.

Nelson, L. E., J. Lu, et al. (2003). "The alpha2-adrenoceptor agonist dexmedetomidine converges on an endogenous sleep-promoting pathway to exert its sedative effects." Anesthesiology 98(2): 428-436.

Nielsen, T., J. Montplaisir, et al. (1993). "Decreased interhemispheric EEG coherence during sleep in agenesis of the corpus callosum." Eur Neurol 33(2): 173-176.

Nir, Y., L. Fisch, et al. (2007). "Coupling between neuronal firing rate, gamma LFP, and BOLD fMRI is related to interneuronal correlations." Curr Biol 17(15): 1275-1285.

Nir, Y., R. Mukamel, et al. (2008). "Interhemispheric correlations of slow spontaneous neuronal fluctuations revealed in human sensory cortex." Nat Neurosci 11(9): 1100-1108.

Ogawa, S., T. M. Lee, et al. (1990). "Brain magnetic resonance imaging with contrast dependent on blood oxygenation." Proc Natl Acad Sci U S A 87(24): 9868-9872.

Ohata, H., H. Iida, et al. (1999). "Intravenous dexmedetomidine inhibits cerebrovascular dilation induced by isoflurane and sevoflurane in dogs." Anesth Analg 89(2): 370-377.

Osol, G. and W. Halpern (1988). "Spontaneous vasomotion in pressurized cerebral arteries from genetically hypertensive rats." Am J Physiol 254(1 Pt 2): H28-33.

Ostergaard, L., R. M. Weisskoff, et al. (1996). "High resolution measurement of cerebral blood flow using intravascular tracer bolus passages. Part I: Mathematical approach and statistical analysis." Magn Reson Med 36(5): 715-725.

Pan, W. J., G. Thompson, et al. (2011). "Broadband local field potentials correlate with spontaneous fluctuations in functional magnetic resonance imaging signals in the rat somatosensory cortex under isoflurane anesthesia." Brain Connect 1(2): 119-131.

Pan, W. J., Thompson, G.J, Magnuson, M.E., Jaeger, D., Keilholz S.D. (2013). "Tight Coupling in 'resting state' spontaneous fluctuations between the fMRI BOLD signal and intracortical infraslow potentials in the rat." Neruoimage In-press.

Paul, L. K., W. S. Brown, et al. (2007). "Agenesis of the corpus callosum: genetic, developmental and functional aspects of connectivity." Nat Rev Neurosci 8(4): 287-299.

Pawela, C. P., B. B. Biswal, et al. (2008). "Resting-state functional connectivity of the rat brain." Magn Reson Med 59(5): 1021-1029.

Pawela, C. P., B. B. Biswal, et al. (2009). "A protocol for use of medetomidine anesthesia in rats for extended studies using task-induced BOLD contrast and resting-state functional connectivity." Neuroimage 46(4): 1137-1147.

Paxinos G, W., C. (2005). The rat brain in stereotaxic coordinates: fifth edition. Sand Diego, Academic Press.

Pizoli, C. E., M. N. Shah, et al. (2011). "Resting-state activity in development and maintenance of normal brain function." Proc Natl Acad Sci U S A 108(28): 11638-11643.

Raichle, M. E., A. M. MacLeod, et al. (2001). "A default mode of brain function." Proc Natl Acad Sci U S A 98(2): 676-682.

Raichle, M. E. and M. A. Mintun (2006). "Brain work and brain imaging." Annu Rev Neurosci 29: 449-476.

Rattenborg, N. C., C. J. Amlaner, et al. (2000). "Behavioral, neurophysiological and evolutionary perspectives on unihemispheric sleep." Neurosci Biobehav Rev 24(8): 817-842.

Rehberg, B., Y. H. Xiao, et al. (1996). "Central nervous system sodium channels are significantly suppressed at clinical concentrations of volatile anesthetics." Anesthesiology 84(5): 1223-1233; discussion 1227A.

Sadaghiani, S., G. Hesselmann, et al. (2009). "Distributed and antagonistic contributions of ongoing activity fluctuations to auditory stimulus detection." J Neurosci 29(42): 13410-13417.

Scholvinck, M. L., A. Maier, et al. (2010). "Neural basis of global resting-state fMRI activity." Proc Natl Acad Sci U S A 107(22): 10238-10243.

Seeley, W. W., V. Menon, et al. (2007). "Dissociable intrinsic connectivity networks for salience processing and executive control." J Neurosci 27(9): 2349-2356.

Shmuel A, A., M., Oeltermann, A., Logotheis NK (2007). "Spontaneous fluctuations in functional MRI signal reflect fluctuations in the underlying neuronal activity." Neuroimage: 13th Annual meeting of the oranization for human brain mapping. 36(S58).

Shmuel, A. and D. A. Leopold (2008). "Neuronal correlates of spontaneous fluctuations in fMRI signals in monkey visual cortex: Implications for functional connectivity at rest." Hum Brain Mapp 29(7): 751-761.

Sirotin, Y. B. and A. Das (2009). "Anticipatory haemodynamic signals in sensory cortex not predicted by local neuronal activity." Nature 457(7228): 475-479.

Sommers, M. G., J. van Egmond, et al. (2009). "Isoflurane anesthesia is a valuable alternative for alpha-chloralose anesthesia in the forepaw stimulation model in rats." NMR Biomed 22(4): 414-418.

Srinivasan, R., W. R. Winter, et al. (2007). "EEG and MEG coherence: measures of functional connectivity at distinct spatial scales of neocortical dynamics." J Neurosci Methods 166(1): 41-52.

Strupp, J. (1996). "A GUI based fMRI analysis software package." Neuroimage: 2nd Annual meeting of the oranization for human brain mapping 3(S607).

Thompson, G. J., M. E. Magnuson, et al. (2012). "Short-time windows of correlation between large-scale functional brain networks predict vigilance intraindividually and interindividually." Hum Brain Mapp.

Tomasch, J. (1954). "Size, Distribution, and Number of Fibres in the Human Corpus Callosum." Anatomical Record 119(1): 119-135.

Tomasi, D. and N. D. Volkow (2012). "Language network: segregation, laterality and connectivity." Mol Psychiatry 17(8): 759.

Uddin, L. Q., E. Mooshagian, et al. (2008). "Residual functional connectivity in the split-brain revealed with resting-state functional MRI." Neuroreport 19(7): 703-709.

van Bruggen, N., E. Busch, et al. (1998). "High-resolution functional magnetic resonance imaging of the rat brain: mapping changes in cerebral blood volume using iron oxide contrast media." J Cereb Blood Flow Metab 18(11): 1178-1183.

van den Heuvel, M. P., C. J. Stam, et al. (2009). "Efficiency of functional brain networks and intellectual performance." J Neurosci 29(23): 7619-7624.

van der Knaap, L. J. and I. J. van der Ham (2011). "How does the corpus callosum mediate interhemispheric transfer? A review." Behav Brain Res 223(1): 211-221.

Van Wagenen, W. P. a. H. R. Y. (1940). "Surgical division of commissural pathways in the corpus callosum: relation to spread of an epileptic attack." Archives of Neruology and Psychiatry 44: 740-759.

Vern, B. A., B. J. Leheta, et al. (1997). "Interhemispheric synchrony of slow oscillations of cortical blood volume and cytochrome aa3 redox state in unanesthetized rabbits." Brain Res 775(1-2): 233-239.

Villalobos, M. E., A. Mizuno, et al. (2005). "Reduced functional connectivity between V1 and inferior frontal cortex associated with visuomotor performance in autism." Neuroimage 25(3): 916-925.

Vincent, J. L., G. H. Patel, et al. (2007). "Intrinsic functional architecture in the anaesthetized monkey brain." Nature 447(7140): 83-86.

Wang, K., M. Liang, et al. (2007). "Altered functional connectivity in early Alzheimer's disease: a resting-state fMRI study." Hum Brain Mapp 28(10): 967-978.

Weber, R., P. Ramos-Cabrer, et al. (2006). "A fully noninvasive and robust experimental protocol for longitudinal fMRI studies in the rat." Neuroimage 29(4): 1303-1310.

Weissman, D. H., K. C. Roberts, et al. (2006). "The neural bases of momentary lapses in attention." Nat Neurosci 9(7): 971-978.

Weissman, K. H. a. B. M. T. (2000). "The cerebral hemispheres cooperate to perform complex but not simple tasks." Neuropsychology 14(1): 41-59.

Williams, K. A., M. Magnuson, et al. (2010). "Comparison of alpha-chloralose, medetomidine and isoflurane anesthesia for functional connectivity mapping in the rat." Magn Reson Imaging 28(7): 995-1003.

Xiong, J., L. M. Parsons, et al. (1999). "Interregional connectivity to primary motor cortex revealed using MRI resting state images." Hum Brain Mapp 8(2-3): 151-156.

Xiong, J., S. Rao, et al. (2000). "Intersubject variability in cortical activations during a complex language task." Neuroimage 12(3): 326-339.

Xu, X., N. D. Olivas, et al. (2010). "High precision and fast functional mapping of cortical circuitry through a novel combination of voltage sensitive dye imaging and laser scanning photostimulation." J Neurophysiol 103(4): 2301-2312.

Zhao, F., P. Wang, et al. (2005). "Spatial specificity of cerebral blood volume-weighted fMRI responses at columnar resolution." Neuroimage 27(2): 416-424.

Zhao, F., T. Zhao, et al. (2008). "BOLD study of stimulation-induced neural activity and resting-state connectivity in medetomidine-sedated rat." Neuroimage 39(1): 248-260.